TECHNISCHE UNIVERSITÄT WIEN

Vienna University of Technology

DISSERTATION

The Synthesis, Characterization, and Reactivity of New Iron PNP Pincer Complexes

Ausgeführt zum Zweck der Erlangung des akademischen Grades eines Doktors der

technischen Naturwissenschaften unter der Leitung von

Ao. Prof. Dr. Karl Kirchner

Institut für Angewandte Synthesechemie 163

Eingereicht an der Technischen Universität Wien

von

DI Bernhard Bichler

Matr. Nr. 0327067

Spörlingasse 3/8

1060 Wien

_____   _____
Datum   Unterschrift (Student)

Abstract

The first part of this work focuses on the synthesis of PNP pincer ligands based on the 2,6-diaminopyridine scaffold. These feature amine spacers (NH or NR) between the phosphine donors and the aromatic pyridine backbone. The preparation of the ligands is achieved by the reaction of 2,6-diaminopyridine with 2 equivs of chlorophosphines PR_2Cl in the presence of a base (NEt_3 and/or n-BuLi). It is worthy of mentioning that the bulky bis-adamantylchloro phosphine, PAd_2Cl, was synthesized for the first time with PCl_3 and adamantane. New ligands with a modified aromatic backbone were prepared the respective 2,6-diaminopyridine. Furthermore, PNP ligands with NR linkers could be synthesized by a two-step phosphorylation procedure.

In the second part the coordination abilities of PNP-Ph ligands were studied. Treatment of anhydrous $FeCl_2$ with 2 equivs of PNP-Ph afforded the diamagnetic cationic complex [Fe(κ^3-P,N,P-PNP-Ph)(κ^2-P,N-PNP-Ph)Cl]$^+$ with two PNP ligands coordinated, one of them in the unusual κ^2-P,N-bonding mode. This reaction was independent of the stoichiometry. Introducing the sterically more demanding N-methylated ligand PNP^{Me}-Ph afforded the related complex [Fe(κ^3-P,N,P-PNP^{Me}-Ph)(κ^2-P,N-PN^{HMe})Cl]$^+$ rather than the pentacoordinated [Fe(κ^3-P,N,P-PNP^{Me}-Ph)Cl$_2$]. This reaction was accompanied by P-N bond cleavage thereby forming the new κ^2-P,N-bound N-diphenylphosphino-N,N'-methyl-2,6-diaminopyridine ligand. Complexes featuring a κ^2-P,N-bound ligand undergo facile rearrangement to give the dicationic complex [Fe(κ^3-P,N,P-PNP-Ph)$_2$]$^{2+}$. The reactivity of [Fe(κ^3-P,N,P-PNP-Ph)(κ^2-P,N-PNP-Ph)Cl]$^+$ towards CO was investigated. Depending on the counterion (Cl$^-$ vs BF$_4^-$) mono and bis CO complexes of the types cis-[Fe(κ^3-P,N,P-PNP)(CO)Cl$_2$] (with Cl$^-$) and [Fe(κ^3-P,N,P-PNP)(CO)$_2$Cl]$^+$ (with BF$_4^-$) were formed. In the course of this process the labile κ^3-P,N-bound ligand was liberated. For comparison, [Fe(κ^3-P,N,P-PNP-Ph)(κ^2-P,N-PN-Ph)Cl]$^+$ with the bidentate ligand PN-Ph ligand was prepared which did not react with CO. The CO complexes [Fe(κ^3-P,N,P-PNP)(CO)Cl$_2$] and [Fe(κ^3-P,N,P-PNP)(CO)$_2$Cl]$^+$ could be synthesized directly by mixing anhydrous $FeCl_2$ with 1 equiv of PNP ligand under a CO atmosphere. Treatment of the mono-CO complexes with a silver salt led to the formation of the bis-CO complex [Fe(κ^3-P,N,P-PNP)(CO)$_2$Cl]$^+$. The mono-CO complexes show reversible CO coordination. Upon heating cis-[Fe(κ^3-P,N,P-PNP)(CO)Cl$_2$] under vacuum the CO ligand can be easily removed thereby forming the pentacoordinated complex [Fe(κ^3-P,N,P-PNP)Cl$_2$].

The bis-carbonyl Fe(II) complex $trans$-[Fe(PNP-iPr)(CO)$_2$Cl]$^+$ was found to react with Zn as reducing agent under a dihydrogen atmosphere to yield the Fe(II) hydride complex cis-

[Fe(PNP-*i*Pr)(CO)$_2$H]$^+$ in 97% isolated yield. A crucial step in this reaction is the reduction of the acidic NH protons of the PNP-*i*Pr ligand to afford H$_2$ and the coordinatively unsaturated intermediate [Fe(PNP^H-*i*Pr)(CO)$_2$]$^+$ bearing a dearomatized pyridine moiety. This species is able to bind and heterolytically cleave H$_2$ to give [Fe(PNP-*i*Pr)(CO)$_2$H]$^+$. The mechanism of this reaction is supported by DFT/B3LYP calculations.

The last part focuses on the synthesis and characterization of Fe(0) and Fe(I) complexes. Treating of complexes [Fe(PNP)Cl$_2$] with an excess of NaHg or KC$_8$ in the presence of carbon monoxide leads to the formation of Fe(0) complexes [Fe(PNP)(CO)$_2$]. X-ray crystallographic studies revealed that these complexes adopt either a trigonal bipyramidal or a square pyramidal geometry depending on the PR$_2$ moieties. Unusual is the bending of the carbonyl ligands. In some cases the Fe-C-O angle deviates significantly from 180° (10-15°). Fe(I) complexes were obtained by treating [Fe(κ^3-*P,N,P*-PNP)(CO)Cl$_2$] with KO*t*Bu, albeit in yields <50%. These reactions take place only with PNP ligands bearing NH-linkers. All complexes with N-alkylated or N-arylated linkers form Fe(0) complexes instead. An alternative synthesis for Fe(I) complexes was developed via oxidation of Fe(0) complexes [Fe(κ^3-*P,N,P*-PNP)(CO)$_2$] with the ferrocenium cation [FeCp$_2$]$^+$ (as PF$_6$$^-$ salt). However, this reaction was limited to complexes with NH linkers, while those with NR-linkers resulted in the formation of Fe(II) fluoro complexes of the type *cis*-[Fe(κ^3-*P,N,P*-PNP)(CO)$_2$F]PF$_6$. The F$^-$ source is the PF$_6$$^-$ counteranion. Finally, these results show that complexes with NH linker undergo one electron transfer reactions (Fe(0)/Fe(I)), while those with NR-linkers undergo two electron transfer processes (Fe(0)/Fe(II)).

Kurzfassung

Der erste Teil der vorliegenden Arbeit beschäftigt sich mit der Synthese von PNP Pincer Liganden basierend auf das 2,6-Diaminopyridin Gerüst. Diese Liganden wurden durch Umsetzung von 2,6-Diaminopyridin mit verschiedenen Chlorophosphinenen, PR_2Cl, in Gegenwart einer Base (NEt_3 und/oder *n*-BuLi) synthetisiert. Besonders zu erwähnen ist das sterisch anspruchsvolle Di-Adamantylphosphinchlorid, Ad_2PCl, welches erstmals durch Reaktion von PCl_3 mit Adamantan hergestellt werden konnte. Neue ring-modifizierte PNP Liganden konnten durch Einführung von ringsubstituierten 2,6-Diaminopyridinderivaten synthetisiert werden. N-alkylierte Liganden waren durch stufenweise Phosphorylierung zugänglich.

Im zweiten Teil, wurde das Reaktionsverhalten von PNP-Ph Liganden untersucht. Durch Umsetzung von wasserfreiem $FeCl_2$ mit PNP-Ph bildete sich der kationische Komplex $[Fe(\kappa^3\text{-}P,N,P\text{-PNP-Ph})(\kappa^2\text{-}P,N\text{-PNP-Ph})Cl]^+$, wobei einer der PNP Liganden in dem ungewöhnlichen $\kappa^2\text{-}P,N$ Bindungsmode gebunden ist. Diese Reaktion konnte auch durch Kontrolle der Stöchiometrie nicht verhindert werden und der erwartete Komplex $[Fe(\kappa^3\text{-}P,N,P\text{-PNP-Ph})Cl_2]$ wurde nicht gebildet. Um die Koordination eines zweiten Liganden zu verhindern wurde der sterisch anspruchsvollere Ligand PNP^{Me}-Ph verwendet. Dieser reagierte zu dem verwandten Komplex $[Fe(\kappa^3\text{-}P,N,P\text{-PNP}^{Me}\text{-Ph})(\kappa^2\text{-}P,N\text{-PN}^{HMe})Cl]^+$, wobei die P-N Bindung eines PNP Liganden gespalten wurde. In Lösung lagerte sich der Komplex $[Fe(\kappa^3\text{-}P,N,P\text{-PNP-Ph})(\kappa^2\text{-}P,N\text{-PNP-Ph})Cl]^+$ langsam zum dikationischen Komplex $[Fe(\kappa^3\text{-}P,N,P\text{-PNP-Ph})_2]^{2+}$ um. Die Reaktivität dieser Komplexe gegenüber CO wurde untersucht. In Abhängigkeit vom Gegenion (Cl^- oder BF_4^-), bilden sich mono und bis-CO Komplexe vom Typ $[Fe(\kappa^3\text{-}P,N,P\text{-PNP})(CO)Cl_2]$ (mit Cl^-) und $[Fe(\kappa^3\text{-}P,N,P\text{-PNP})(CO)_2Cl]^+$ (mit BF_4^-) wobei dabei der labile $\kappa^3\text{-}P,N$-gebunde Ligand abgespalten wird. Zum Vergleich wurde auch der Komplex $[Fe(\kappa^3\text{-}P,N,P\text{-PNP-Ph})(\kappa^2\text{-}P,N\text{-PN-Ph})Cl]^+$ mit dem zwei-zähnigen PN-Ph Ligand synthetisiert. Dieser reagierte nicht mit CO. Die Carbonylverbindungen *cis*-$[Fe(\kappa^3\text{-}P,N,P\text{-PNP})(CO)Cl_2]$ und *trans*-$[Fe(\kappa^3\text{-}P,N,P\text{-PNP})(CO)_2Cl]^+$ konnten auch direkt hergestellt werden, indem man wasserfreies $FeCl_2$ mit dem jeweiligen PNP Liganden (1 äquiv) unter CO Atmosphäre durchführt.

Überdies wurde die Reaktivität des Komplexes *trans*-$[Fe(PNP\text{-}iPr)(CO)_2Cl]^+$ in Gegenwart von Zn als Reduktionsmittel unter Wasserstoffatmosphäre näher untersucht. Dabei konnte der Hydridkomplex *cis*-$[Fe(PNP\text{-}iPr)(CO)_2H]^+$ erhalten werden. Der Mechanismus dieser komplexen Reaktion wurde im Detail mit Deuteriummarkierungsexperimenten aufgeklärt und mithilfe von DFT Berechnungen bestätigt.

Der letzte Teil der Arbeit beschäftigt sich mit der Synthese und Charakterisierung von Eisenkomplexen in den niedrigen Oxidationsstufen Fe(0) und Fe(I). Diese Reaktionen sind überraschenderweise stark abhängig von den beiden Amino-Linkern (NH *vs* NR) der den Pyridinring mit den PR_2 Gruppen verbindet. Die Reduktion von [Fe(κ^3-*P,N,P*-PNP)Cl$_2$] mit starken Reduktionsmittel wie Na/Hg oder KC$_8$ ergab die Fe(0) Verbindungen [Fe(κ^3-*P,N,P*-PNP)(CO)$_2$]. Röntgenstrukturen der Fe(0) Komplexe zeigen in Abhängigkeit von den PR_2 Gruppen am PNP Ligand enweder eine trigonal bipyramidale oder eine qudratisch pyramidale Geometrie. Ungewöhnlich sind in einigen Fällen die Fe-C-O Bindungswinkel, welche signifikannt von 180° abweichen (10-15°). Fe(I) Verbindungen konnten auch durch die Umsetzung von [Fe(κ^3-*P,N,P*-PNP)(CO)Cl$_2$] mit KO*t*Bu hergestellt werden, wobei die Ausbeuten allerdings nur bei maximal 50% lagen. Diese Reaktion findet nur mit NH-Linkern statt. Alle Komplexe mit N-alkylierten Linkern bilden die entsprechenden Fe(0) Komplexe. Eine alternative Synthesemethode stellt die Oxidation der Fe(0) Verbindungen mit dem Ferrocenium Cation [FeCp$_2$]$^+$ (als PF$_6^-$ Salz) dar. Auch diese Reaktion fand nur mit Verbindungen welche NH Linker besitzen. Mit NR-Linkern wurden Fe(II) Fluorokomplexe vom Typ *cis*-[Fe(κ^3-*P,N,P*-PNP)(CO)$_2$F]PF$_6$ erhalten, wobei als F$^-$-Quelle das PF$_6^-$ Anion fungierte. Abschließend kann gesagt werden, dass Komplexe mit NH Linker selektiv nur Einelektronenübergänge (Fe(0)/Fe(I)), und Komplexe mit NR-Linkern nur Zweielektronenübergänge (Fe(0)/Fe(II)) eingehen.

Acknowledgments

First I would like to thank Prof. Karl Kirchner to give me the opportunity to work in his research group and the supervision on this interesting topic. Further I thank him for performing various DFT calculations and the interesting discussions about my research.

I would like to thank Berthold Stöger and Prof Kurt Mereiter for performing single crystal diffraction.

I would like to thank Dr. Michael Puchberger for performing Deuterium and low temperature NMR experiments.

I would like to thank Ernst Pittenauer for measuring ESI-MS of my compounds.

I would like to thank Prof. Luis Veiros for performing DFT calculations.

I would like to thank Liliana Ferreira for SQUID and Mössbauer measurements.

I would like to thank Esther for helping me with the CV measurements.

I would like to thank my colleagues Afrooz, Sara, Christian, Mathias, Matthias, Nikolaus, Özgur and Sathy, especially Mathias and Matthias for providing me with precursors and ligands.

I would like to thank my bachelor students Hermann and Wolfgang.

Thanks to the neighboring working groups for the coffee breaks.

I would like to thank all my friends, for going out with me and having fun, David and Hermann for going on climbing trips with me and the guys from "Die Skilehrer-WG" for the countless hours in the snow.

Finally, special thanks to my family, my parents, my two sisters and my two nephews Maximilian and Mathias for the great support.

Table of content

1. Introduction

The synthesis of well-defined catalysts is a very important topic in organometallic and organic chemistry for the development and improvement of a variety of different reactions. In recent years so called pincer complexes gained considerable interest. Pincer ligands are tridentate PNP ligands in which the central pyridine-based ring donor contains -CH_2PR_2 substituents in the two ortho positions are the most widely utilized ligands in transition metal chemistry (e.g., Fe, Ru, Rh, Ir, Pd, Pt).[1–21] In an effort to create tridentate PNP pincer-type ligands in which both the steric, electronic, and stereochemical properties can be easily varied, we have described the synthesis of a series of modularly designed PNP ligands based on N-heterocyclic diamines and R_2PCl which contain both bulky and electron-rich dialkyl phosphines as well as various P-O bond containing achiral and chiral phosphine units.[22] In these PNP ligands the central pyridine ring contains -$NR'PR_2$ (R' = H, alkyl, aryl; R = alkyl, aryl) substituents in the two ortho positions. This methodology was first developed for the synthesis of N,N'-bis(diphenylphosphino)-2,6-diaminopyridine (PNP-Ph).[23,24]

The importance of pincer chemistry is readily apparent from Figure 1 where publications per year dealing with the topic "pincer chemistry" according to Scifinder® are displayed (2014: stand of 28.07.2014).
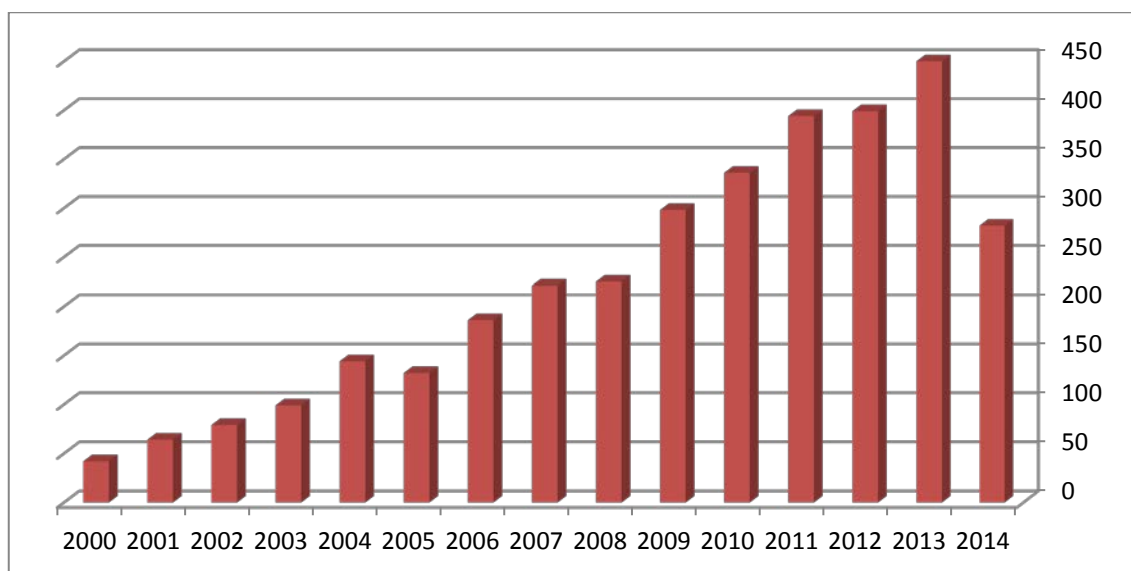

Figure 1: Publications per year dealing with pincer chemistry

With these types of PNP ligands, we thus far studied their reactivity towards different transition metal fragments which has been resulting in the preparation of a range of new pincer transition metal complexes, including several new square-planar Ni(II), Pd(II), and Pt(II) PNP complexes,[25] various iron complexes acting as CO sensors[26–28] and catalysts for the

coupling of aromatic aldehydes with ethyldiazoacetate,[29,30] several pentacoordinated nickel complexesm[31] and molybdenum and tungsten complexes halocarbonyl complexes of the types $[Mo(PNP)(CO)_3X]^+$ (X = I, Br, Cl), $[Mo(PNP)(CO)_2X_2]$ (X = I, Br, Cl, F), and $[Mo(PNP)(CO)X_2]$ (X = I, Br, Cl).[25,32,33]

In recent years, non-precious PNP pincer complexes, in particular with iron, gained a lot of interest in catalysis with the goal to replace precious metals such as palladium, rhodium, ruthenium and iridium (for example in the hydrogenation of ketones and CO_2 and C-H activation reactions).[34] Iron is of importance due to its low costs, high natural abundance and low toxicity.[35] Therefore the research of new well-defined iron catalysts is still ongoing and the number of publications is rising. Moreover, the reactivity of iron complexes towards small molecules like H_2, N_2, CO_2 and CO is an important topic in organometallic chemistry. The reactivity of CO towards iron complexes is of interest to study the electronic features that may allow activating more challenging substrates like H_2, N_2 or alkenes to develop new catalytic systems (hydrogenation, nitrogen fixation). Transforming small molecules into more complex chemicals is important to develop a more sustainable chemistry. In the case of iron carbon monoxide is a very important molecule (e.g., Fischer-Tropsch synthesis). Also in nature CO coordination to iron plays an important role. The best known system is the strong CO bonding to the Fe(II) heme group in red blood cells. Further it was discovered that the active sites of iron hydrogenases have a Fe-CO moiety. The study of iron carbonyl complexes can provide insights in the electronic features and may allow the coordination and functionalization of more challenging substrates like dinitrogen such as in the iron (or transition metal) catalyzed nitrogen fixation.

Carbon monoxide is often used as a model ligand to understand the bonding and coordination properties of transition metals to small molecules. Therefore the interactions of specific ligands with specific metal centers in different oxidation states and spin states are examined. Further CO is a mimic to N_2 and it could help to understand the reactivity in nitrogen fixation.

CO has unique coordination properties like one of the largest field splitting of ligand field energy levels; coordination is usually followed by spin state change from a high spin state to a low spin sate, from S = 2 or S = 1 to S = 0. High spin coordinatively unsaturated Fe(II) exhibit a wide range of reactivity towards CO, the binding can be very strong und irreversible, weak and reversible or even impossible due to kinetically or thermodynamically disfavored spin state changes.

The spin state of a transition metal complex, according to simple crystal field theory, of a given geometry is determined by the energy difference between the orbital splitting difference (ΔE, HUMO-LUMO gap) and the electron pairing energy (PE, the energy required to pair two electrons in the same orbital). When electrons are distributed between two or more orbitals with comparable energy difference ΔE to the PE different spin states can be observed. If $\Delta E > PE$ the complex has a low spin configuration, while $\Delta E < PE$ the high spin configuration is preferred.

The prediction of spin states changes for each electronic configuration as a function of geometry and coordination number is easy. The ligand field strength increases with coordination number and the ligand field splitting is smaller in first row transition metals than in the second or third row. Therefore coordinativley unsaturated iron complexes will favor the high spin configuration.

Different spin state configurations have different energies, so a spin state change during a reaction that involves an open shell system as starting material, product or intermediate will affect the thermodynamics or kinetics of the reaction. In a reaction where a kinetic effect results as a barrier that may hinders the crossing between the spin state surfaces the general terms "spin-blocked" or "spin forbidden" are used.

Spin sate changes occur at the minimum energy crossing point (MECP). This corresponds to the lowest energy points where both the energy and the geometry of the molecule is the same in the two surfaces. When the MECP is reached the system has the possibility of hopping from one surface to the other, the "spin-forbidden" reaction takes place.[36,37]

Figure 2 shows general energy profiles for the reaction of a coordinatively unsaturated ML_n 16e$^-$ complex with CO affording a saturated complex ML_nCO (18e$^-$) with possible spin crossovers.
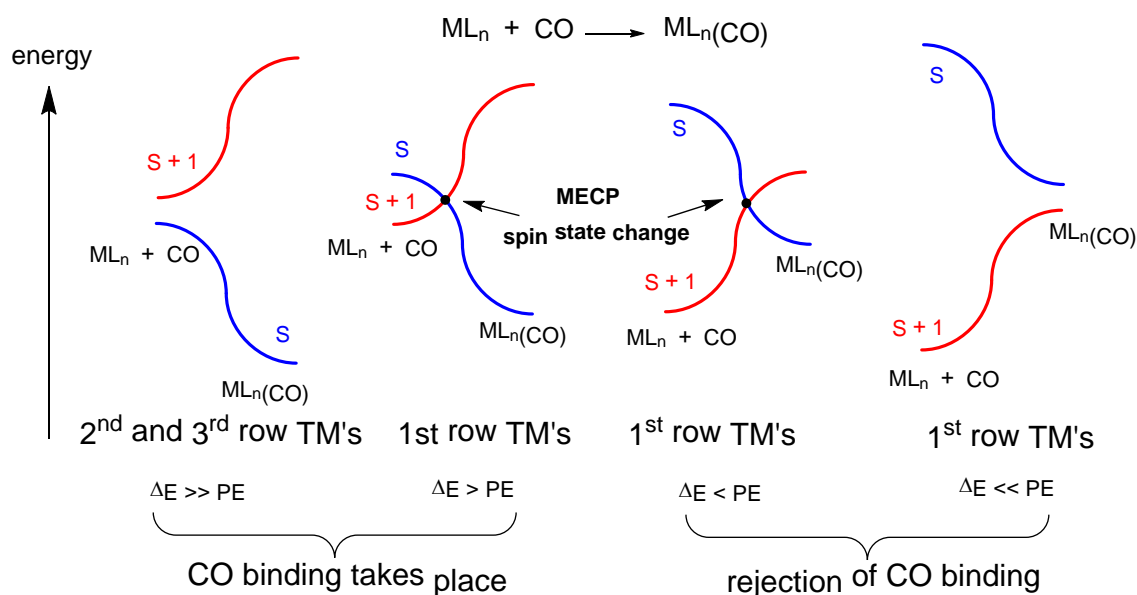
Figure 2: Energy profiles of the addition of CO to a coordinatively unsaturated complex in different spin states

When $\Delta E \gg PE$ the carbonylation reaction follows the same spin state surface S and the saturated CO complex is more stable in the same low spin configuration (Figure 2). Is the ML_n unsaturated complex in a high spin configuration and the product in low spin state, a spin state change (spin crossover) is necessary for CO addition. The spin state change occurs at the MECP (Figure 2) when $\Delta E > PE$; the reaction is exothermic. When the MECP is too high in energy the reaction may not proceed, it is "spin-blocked".

However this does not occur when $\Delta E < PE$, the reaction becomes thermodynamically disfavored and the complex remains in the unsaturated high spin configuration (Figure 2). CO addition will not take place; the energy required of pairing two electrons is higher than the energy gained from the M-CO bond. If the pairing energy is much higher CO addition will be completely rejected.

The reactivity towards CO of coordinativley unsaturated iron complexes was recently reviewed by our working group.[38] Interestingly many iron catalysts bear CO as a co-ligand especially for hydrogenation reactions. Some examples are shown in Figure 3. This indicates that the carbonyl ligand is of importance for the catalytic activity presumably for the maintenance of a low spin state.
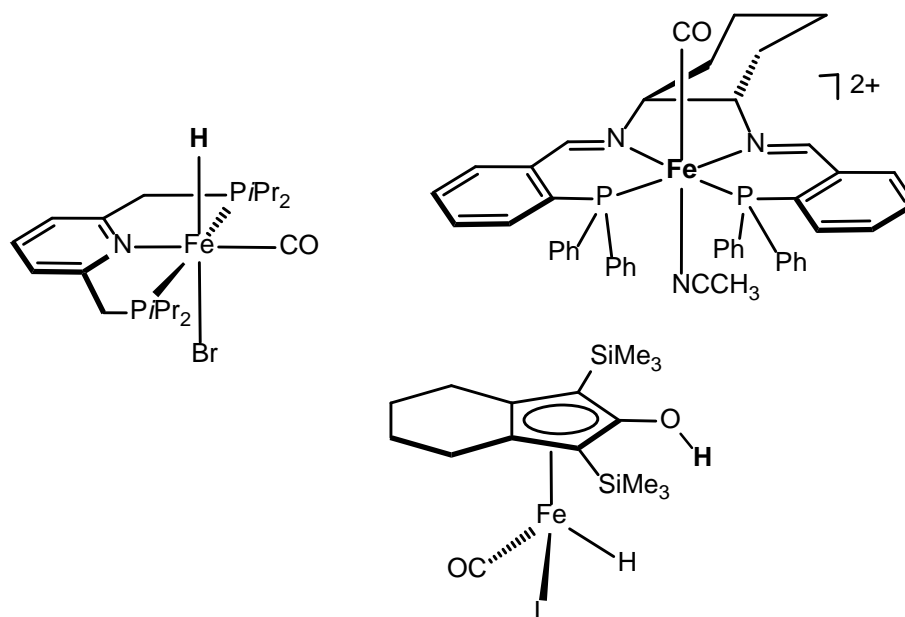
Figure 3: Recent Examples of Hydrogenation catalysts with CO as coligand

Accordingly, the objective of this work is the synthesis and reactivity of new iron PNP pincer complexes in various oxidation states. Of particular interest is their reactivity towards CO. Some of these complexes will contain new substituted 2,6-diaminopyridine scaffolds as well as new N-alkylated and N-arylated linkers. All complexes will characterized by various standard methods ranging from ^{1}H, ^{13}C{^{1}H}, ^{31}P{^{1}H} NMR, IR, Mössbauer, SQUID, and X-ray crystallography. Mechanistic investigations will be supplemented by DFT/B3LYP calculations.

2. General part

2.1 Pincer ligands

Pincer ligands are widely used in transition metal chemistry and catalysis and gained increasing interests due to their extreme stability, reactivity and broad versatility. The word pincer is derived from the tool. The first pincer complex was reported by Shaw in 1976 featuring a C-M bond with two phosphine groups.[39] In the last 30 years pincer chemistry has developed a range of different applications like C-C bond forming reactions, small molecule activation to use the compounds as hydrogenation catalysts or chemical sensors and switches.

Nowadays they are described as tridentate, meridionally coordinated ligands and can be neutral or charged. These ligands are categorized by the nature of the donor atoms and are given common abbreviation like EXE. A typical arrangement of a pincer complex is shown in Figure 4.
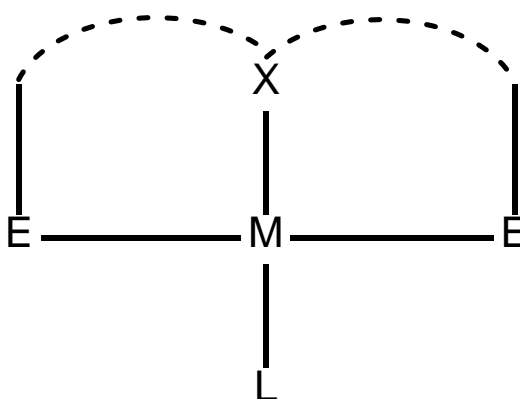

Figure 4: General structure of an **EXE** pincer complex; **E, X:** donor atoms, **L:** coligand

A wide variety of donor groups can be applied to design a pincer ligand to fine-tune steric and electronic properties. The center atom X usually is X = N, C when using aromatic or aliphatic backbones, but also X = O or S were reported.[40,41] The donors **E** typically are phosphines or amines but also N-heterocyclic carbenes (NHC), selenoethers and arsines are used. The donor groups do not need to be identical and many systems with different donor atoms have been reported. Some different pincer ligands are shown in Figure 5.
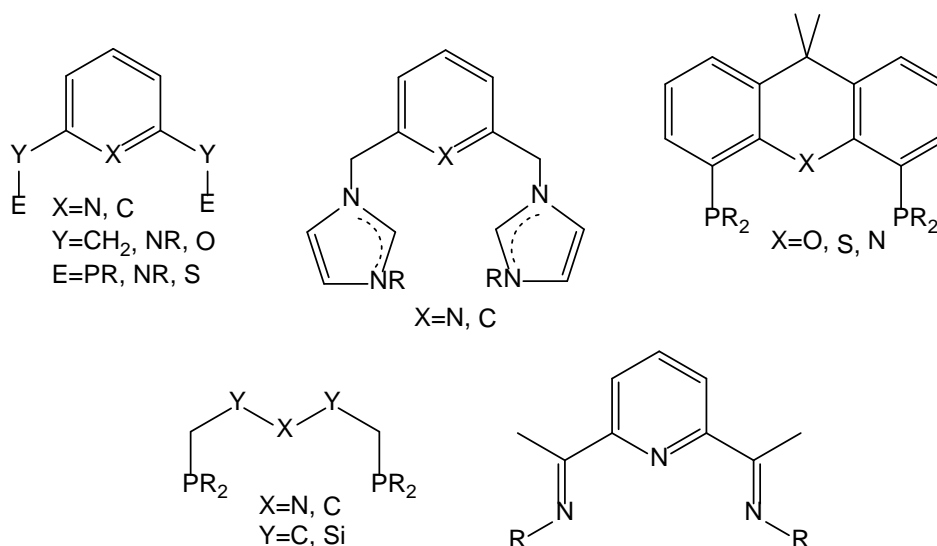
Figure 5: Selected examples of pincer ligands frequently used in literature

The ligands in this work feature a pyridine backbone with NR (R = H, Me, Et) as spacers in the two *ortho* position and phosphines as donor groups.

2.2 Iron pincer complexes: synthesis, properties and applications

2.2.1 Iron pincer complexes in catalysis

In recent years well defined Iron pincer complexes gained a lot of interest for various catalytic reactions to replace precious metals like ruthenium, iridium and rhodium. Iron is interesting not only by its low cost, but also its low toxicity. A rising number of new ligands and applications show the broad scope for pincer based iron complexes. A short overview of iron pincer complexes used for various catalytic applications is presented below.

A common ligand system is the NNN bis(imino)pyridine pincer scaffold. Brookhart *et al* used a 2,6-bis(imino)pyridyl iron(II) complex to polymerize ethylene upon *in situ* activation with MAO.[42] These ligands are prepared by a Schiff-base condensation reaction of 2 equivs of aniline with 2,6 diacetylpyridine (Figure 6**)**. Thse complexes are robust and extremely active for polymerization of ethylene to linear high density polyethylene (HDPE). These were the first reported iron based catalysts for ethylene polymerization. The synthesis of the precatalysts is straightforward and is carried out by mixing the ligand with iron dihalide (X = Cl, Br) in THF.
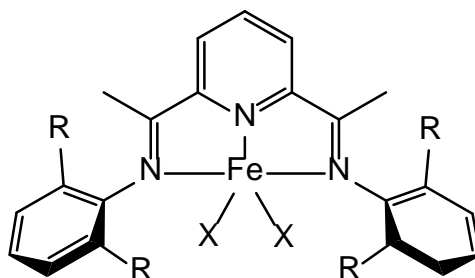
Figure 6: Fe(II) complexes based on a 2,6-bis(imino)pyridyl (PDI) ligand

Chirik *et al.* used the same ligand system for complexes **1** and **2** depicted in Figure 7. In 2004 Chirik and co-workers described the catalytic hydrogenation and hydrosilylation of olefins and alkynes by an iron(0) bis(dinitrogen) complex.[43] In solution this compound loses one equiv of N_2 to form a four coordinated complex. Complex **1** formed the catalytic active species and was active with very low catalyst loadings (0.3 mol%) at ambient temperatures. With complex **1** non-activated alkenes could be hydrogenated with TOF's up to 1814h^{-1}. This catalyst was also active for geminal, internal, tri-substituted olefins and diolefins. Furthermore, the hydrosilylation of olefins was examined under mild conditions using $PhSiH_3$.

The same complex was used for hydrosilylation of aldehydes and ketons.[44] The catalyst reduced *p*-tolualdehyde and acetophenone with Ph_2SiH_2 quantitatively in less than 1h at 23°C with 1 mol% and subsequent hydrolysis to the corresponding alcohol. Further studies with dialkyliron compounds showed that complex **2** is an efficient precatalyst for the hydrosilylation of aldehydes and ketons, tolerating functional groups and active at 23°C.

Complex **1** is synthesized by reducing the dihalide precursor under N_2 atmosphere with Na/Hg or by adding 2 eq $NaBEt_3H$. The dialkylated compound **2** was prepared by adding the ligand to $[Fe(py)_2(CH_2SiMe_3)_2]$.
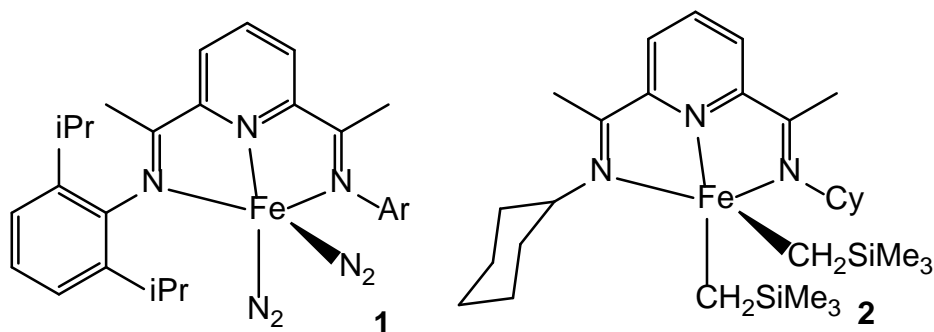

Figure 7: Chirik's 2,6-bis(imino)pyridyl Fe(0) and Fe(II) catalysts

In a subsequent publication complex **1** was used for the hydrogenation of functional olefins bearing unprotected amines, esters and ethers to demonstrate the tolerance of several functional groups.[45] In contrast, conjugated α,β-unsaturated ketones induce decomposition of the complex.

In 2010 Chirik's group described the synthesis of new, dimeric aryl-substituted bis-(imino)pyridine iron dinitrogen complexes by reduction of the corresponding iron dihalide with sodium naphthalenide.[46] When using sodium amalgam often catalytically inactive iron bis-chelate complexes were isolated. The catalytic performance of the new compounds was evaluated in the hydrogenation of ethyl-3-methyl-2-enonate with 5 mol% loading at 4 atm H_2 at 23°C. Compound **3** (see Figure 8) was the most effective, a complex bearing a bulky ligand with 2,6-disubstituted aryl groups.
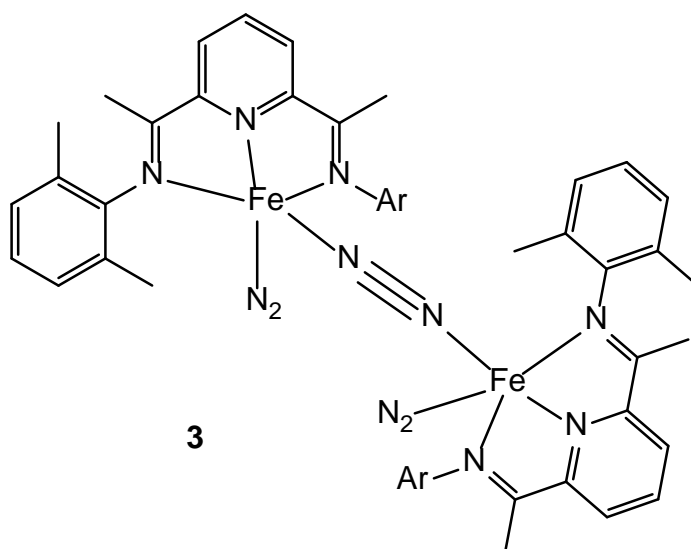

Figure 8: Chirik's Fe(PDI) N_2-bridged dimer

Using the same catalyst **3** Chirik *et al.* showed the selective *anti*-Markovnikov alkene hydrosilylation of 1-octene with tertiary silanes at 23°C and catalyst loading as low as 500 ppm.[47] Because of the absence of competing olefin isomerization during the hydrosilylation further studies were performed. In the hydrosilylation of styrene complex **3** was able to furnish the *anti*-Markovnikov product exclusively after 30 min with 200 ppm catalyst loading. The tolerance of functional groups was shown by hydrosilylation of amino substituted olefins and polyethers. In addition the catalysts were tested in silicon cross-linking and immediate cross-linking was observed after the addition of the catalyst.

Further complex **1** and **3** were active in the catalytic intermolecular [2π+2π] cycloaddition of ethylene and butadiene to form vinylcyclobutane.[48] Interestingly the iron keeps its oxidation

state (II) during the catalytic cycle which was proven by preparing structures of likely intermediates formed. These were synthesized by stoichiometrical reactions.

Very recently Chirik *et al.* showed the iron catalyzed hydrogenation of hindered unfunctionalized alkenes using iron dinitrogen complexes bearing aryl substituted bis(imono)pyridine and bis(arylimidazol-2-ylidene)pyridine ligands.[49] Complex **4a** was able to hydrogenate 2,3-dimethyl-1*H*-indene (conversion 68 % after 48h and 3:1 *cis : trans* ratio) with a catalyst loading of 5 mol% and 4 atm H_2 at 23°C. Further he discovered that more electron-rich iron dinitrogen complexes are effective for the catalytic hydrogenation of unfunctionalized alkenes. The catalyst **4a** is depicted in Figure 9.
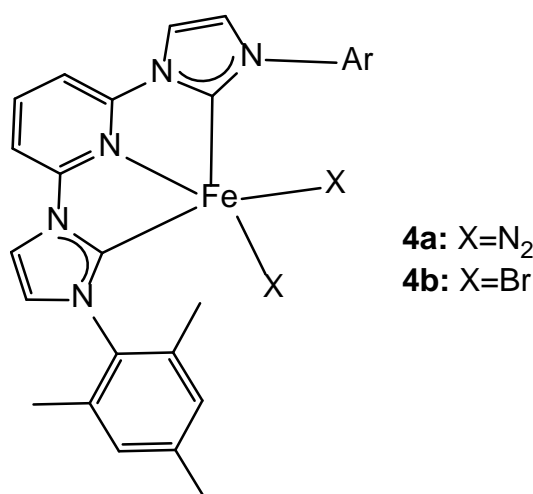

4a: $X=N_2$
4b: X=Br

Figure 9: Iron NHC complexes used in catalysis

NHC (NHC = N-heterolytic carbene) iron complexes were also used for the coupling of primary and secondary alkyl halides with Grignard reagents.[50] Using 5 mol% **4b** the reaction of 4-tolylmagnesium bromide with alkyl halides bearing β-hydrogen afforded the product.

Chirik's group also reported the hydrosilylation of carbonyl compounds with iron dialkyl complexes **5a-d** bearing pybox and bisoxazoline ligands (see Figure 11) at 23°C and 0.3 mol% catalyst loadings.[51] Various functional groups were tolerated, but the reductions are sensitive to steric effects. The first moderate enantioselectivities with *ee*'s up to 49% could be increased to 93% for catalyst **5a** by treatment with $B(C_6F_5)_3$ for the substrate 2,4,6-trimethylacetophenone although conversion was poor.

At first glance, the bis(imino)pyridine iron dinitrogen complexes were assigned as Fe(0) species. However, based on detailed Mössbauer, IR and NMR studies as well as DFT calculations, these complexes were better described as Fe(II) where the metal has transferred two electrons on to the ligand.[52,53]
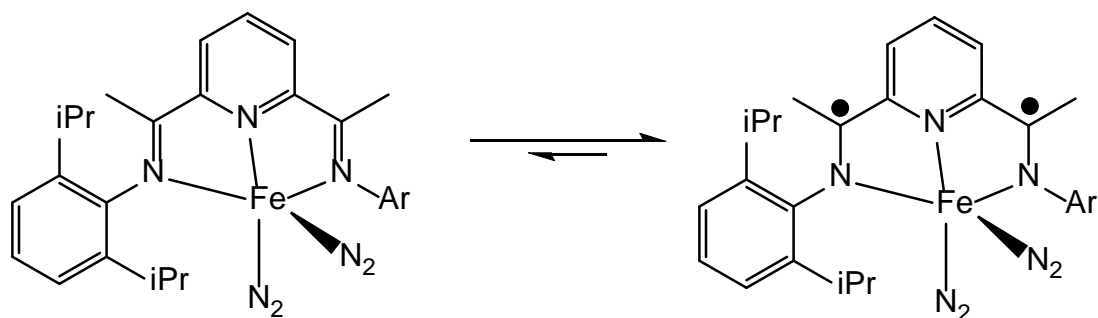
Figure 10: The electronic non-innocence of PDI ligands

In 2010 Nishiyama *et al.* described the chiral pincer complex **6** (Figure 11) bearing a phebox ligand, synthesized by oxidative addition of $Fe_2(CO)_9$ to the 2-bromo-substituted ligand.[54] This compound was able to catalyze the enatioselective hydrosilylation of ketones with an *ee* up to 66% at 50°C using $(EtO)_2MeSiH$.

His group also described the application of complex **7** (see Figure 11) for the asymmetric hydrosilylation of ketones using Zn as an additive and $(EtO)_2MeSiH$ to isolate predominantly the alcohol in S-configuration.[55] In the same publication he used the same BOPA ligand in combination with $Fe(OAc)_2$ to isolate the R-isomer.

$L_1=CH_2SiMe_3$

5a: $R_1=iPr$
5b: $R_1=Bn$
5c: $R_1=tBu$
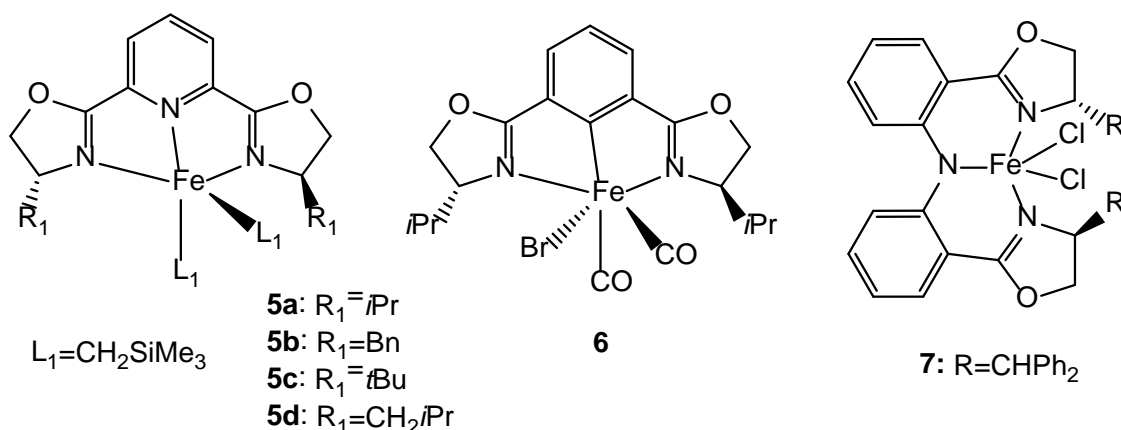**5d**: $R_1=CH_2iPr$

6

7: R=CHPh$_2$

Figure 11: Iron BOX (biy oxazoline) complexes used in catalysis

A different approach to chiral hydrosilylation of ketones was done by Gade in 2008 using a highly modular class of pincer ligands.[56] The complex could reduce acetophenone in 91% yield at 65°C and an ee of 78%. The complex is depicted in Figure 12 Compared to lower temperature the *ee* dropped, but the yield increased. Also bulky substrates like adamantylmethylketone and *t*-butylmethylketone were reduced, but in lower yields and lower *ee*'s.
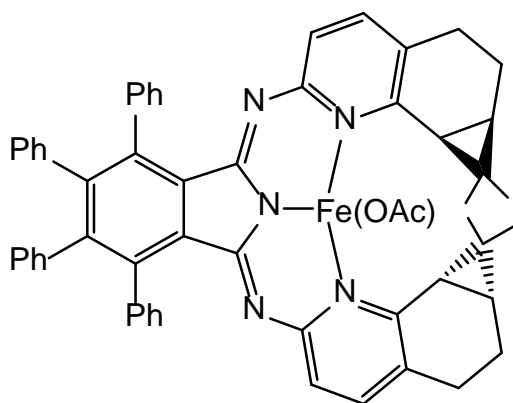
Figure 12: A chiral bis(pyridylimino)isoindoles complex for the asymmetric hydrosilylation of ketones

Nakazawa *et. al.* prepared iron complexes with terpyridine derivatives for the catalytic hydrosilylation of alkenes.[57] Using **8** (Figure 13) his group could selectively single/double hydrosilylate 1-octane using PhSiH$_3$ depending on the catalyst loading at 100°C. With more than 0.3 mol% the double alkylated hydrosilane was selectively isolated, with less than 0.05 mol% only the mono alkylated product was formed.
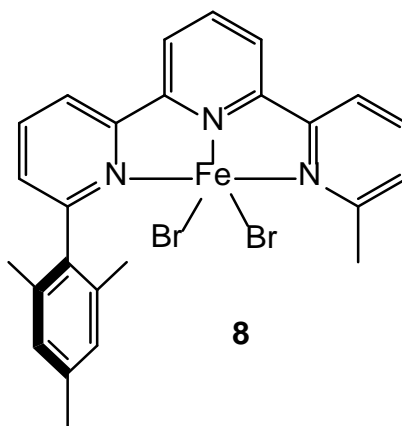

8

Figure 13: A terpy-based complex used for hydrosilylation

Very recently Milstein *et al*. introduced a new efficient iron pincer catalyst for hydrogenation of ketones.[58] His group used the hydride complex **9** (Figure 14) to reduce ketones under mild conditions (26-28°C, 4.1 atm H$_2$) with TONs up to 1880 in the presence of 0.1 mol% KO*t*Bu. Multinuclear NMR experiments suggest that the reaction proceeds through a dearomatized intermediate.

Lately Milstein's group published another complex **10** (Figure 14), a complex bearing a tetrahydridoborate ligand, which is able to catalyze the base-free hydrogenation of ketones to their corresponding alcohols at 40°C and 4.1 atm. H$_2$ pressure with TONs up to 1980.[59] This is

the highest turnover number reported to date for iron-catalyzed hydrogenation. Further the reaction mechanism was examined using DFT calculations.

Using **11** (see Figure 14) his group could show the catalytic hydrogenation of carbon dioxide under low pressure (total pressure of 10 bar in a 2:1 ratio of H_2:CO_2) and high turnover numbers (up to 532) with NaOH as base. Investigating the mechanism, complex **11** in pentane was exposed to CO_2 and the formate salt could be isolated. This reaction suggests a direct attack on the *trans*-hydride. This complex is also active in the catalytic decomposition of formic acid to hydrogen and carbon dioxide.[60] The mechanism is predicted as a novel, non-classical intramolecular β-H elimination supported by DFT calculations.
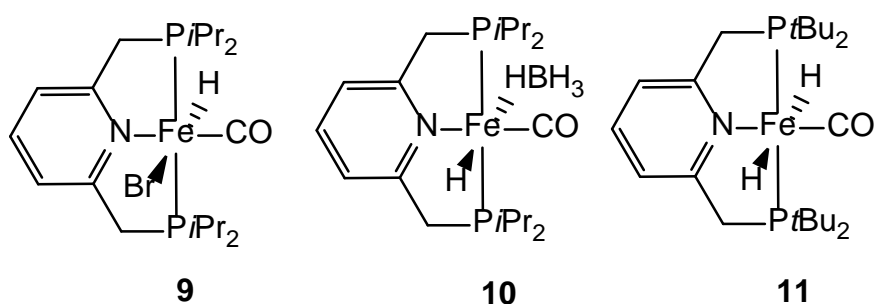

Figure 14: PNP-based iron hydride catalysts developed by Milstein

Milstein also developed catalyst **12** (see Figure 15) with a novel acridine based PNP ligand for the E-selective semi-hydrogenation of alkynes.[61] After optimizing the conditions, diphenylacetylene was hydrogenated with a catalyst loading of 0.6 mol % and 4 bar H_2 pressure at 90°C using THF as a solvent without adding a base to give the stilbene in 99% yield. Interestingly carbonyl, nitrile and chloro substituents were kept intact.
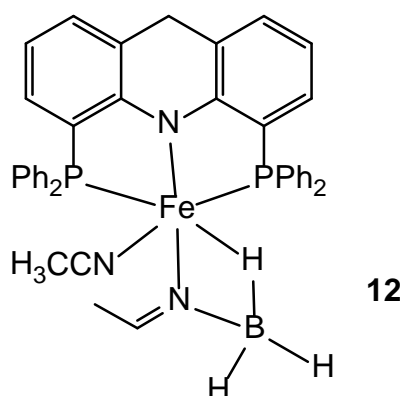

Figure 15: E-selective hydrogenation catalyst used for alkynes

Recently Beller published the PNP iron complexes **13** and **14** (Figure 16) for the selective hydrogen production from methanol.[62] The compounds were synthesized form the *trans*-

[Fe(PNP)(CO)Br$_2$] precursor; treating it with NaBH$_4$ in EtOH afforded **13** and the reaction with NaBHEt$_3$ in THF gave **14** in moderate yields. The catalysis was studied using compound **13** and a TOF up to 734 h^{-1} and a TON of nearly 10000, in the presence of a base, was reached. He postulated that the ligand is non-innocent and suggests an outer-sphere mechanism where the active species is an amide complex.

Figure 16: Iron PNP complexes used by Beller

In a subsequent publication Beller used complex **13** for the mild and selective hydrogenation of aromatic and aliphatic (di)nitriles to amides.[63] The catalysis was performed in *i*PrOH with 30 bar H$_2$ at temperatures between 70 and 180°C for 3h without adding a base to give mostly good to excellent yields with high chemoselectivity, even in the presence of reducible functional groups like ester, amido and α,β unsaturated double bonds. Further a two-step mechanism is proposed. At first an imine is formed which is reduced to the amine in a second cycle. Both reactions are proposed to be catalyzed by the same in situ generated trans-dihydride [Fe(PNP)(CO)H$_2$] complex which is regenerated by H$_2$ from the amido complex.

Recently Morris group showed the catalytic asymmetric hydrogenation of ketones and imines by an unsymmetric iron PNP complex.[64] The complex was synthesized by a template strategy condensating phosphine-amines with phosphine-aldehydes, using a cyclic phosphonium salt, KO*t*Bu and 2-(diphenylphosphino)ethylamine, CO, FeBr$_2$ as the iron source and AgBF$_4$ to abstract a halide. The complex is depicted in Figure 17. The catalysts were used at 50°C and a H$_2$ pressure of 5 bar under basic conditions. A TOF up to 2000 h^{-1}, TON up to 5000 and an *ee* up to 85% was reached.
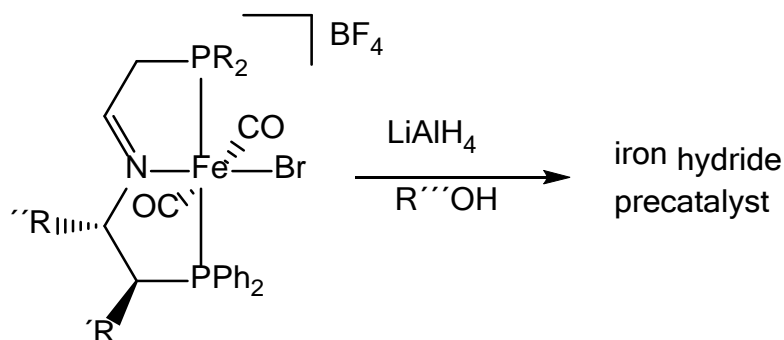
Figure 17: Morris hydrogenation pre-catalyst and activation

Guan's working group described the synthesis and catalytic activity of iron(II) hydride complexes bearing a POCOP pincer type ligand as well as mechanistic investigations of the catalytic cycle of the hydrosilylation of various aldehydes and ketones.[65] The complexes were synthesized by reacting the POCOP ligand with PMe_3 in THF. Complex **16** (see Figure 18) was the most effective one and tested and gave good to excellent yields with 1 mol% loading and $(EtO)_3SiH$ as silane; further he proposed two possible catalytic cycles. The lability of the PMe_3 ligand *trans* to the hydride was shown by reacting the complex with CO. The catalysis with complexes bearing a CO ligand didn't work as well as with complex **16** and the complex with two CO ligands only showed 6% conversion after 48h. Further it has to be noted that the hydride ligand does not participate directly in the reaction, but it is important because it exerts a strong *trans* effect that facilitates the ligand dissociation and creates a vacant coordination site.
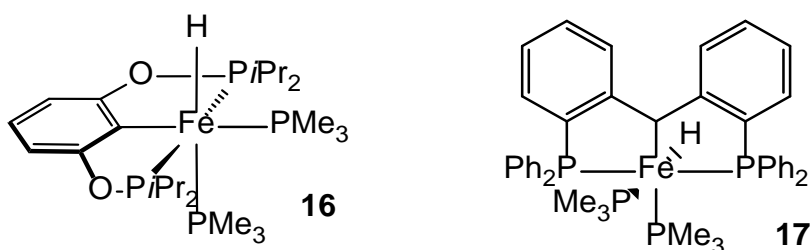

Figure 18: Iron PCP pincer complexes for hydrosilylation

Also complex **17** (see Figure 18) bearing a PCP type pincer ligand was described to catalyze the hydrosilylation of ketones and aldehydes using $(EtO)_3SiH$ as silane under mild conditions.[66] The catalyst was synthesized by mixing the ligand and $Fe(PMe_3)_4$ as an iron precursor. The catalysis was carried out at 50°C and a catalyst loading of 0.3 to 1 mol %.

Huang reported a series of phosphinite-iminopyridine iron catalysts for the chemoselective alkene hydrosilylation.[67] With bulky substituents on the phosphorus and 2,6 aryl positions (R = *t*Bu, R' = *i*Pr) the complexes (Figure 19) showed higher activity in the selective *anti-*

Markovnikov alkene hydrosilylation using primary silanes. Further the hydrosilylatoin of alkenes bearing various functional groups like amides, esters and ketones highlights the chemoselectivity of these complexes. For the catalysis 1 or 2 mol % complex and 2 or 4 mol % NaBHEt$_3$ were used.
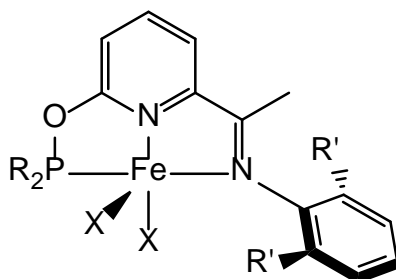

Figure 19: Huangs alkene hydrosilylation catalysts

The same group reported the first iron-catalyzed alkene hydroboration with pinacolborane using complex **18** (see Figure 20) bearing a PNN bipy based pincer ligand.[68] This compound could catalyze the alkene hydroboration with HBPin, with a catalyst loading, depending on the educt down to 0.25 mol% **18** and 0.75 mol% NaBHEt$_3$ at 25°C to give the *anti*-Markovnikov product in excellent yields for most of the products. The reaction was also successful with various functional groups.

Also Chirik reported a system for the catalytic alkene hydroboration using bis(imino)pyridine iron dinitrogen complexes showing high activity and selectivity.[69]
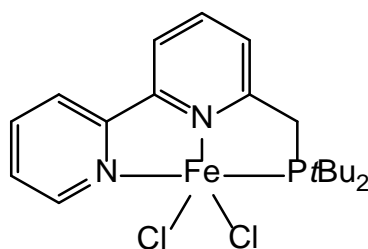

Figure 20: Hydroboration precatalyst **18**

Our working group reported that the complex *trans*-[Fe(PNP-*i*Pr)(CO)$_2$Cl]BF$_4$ (Figure 21) is active in the catalytic coupling of aromatic aldehydes with ethyl diazoacetate to give 3-hydroxy-acrylates instead of β-oxo esters.[29] The reaction turned out to be strongly dependent on the counterion.
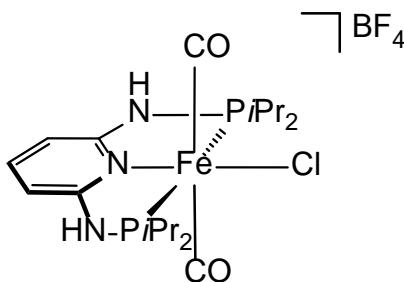
Figure 21: Precatalyst for the coupling of aromatic aldehydes with ethyl-diazoacetate

2.2.2 Low valent iron pincer complexes

In this chapter the chemistry, synthesis and characterization of iron pincer complexes in oxidation states Fe(I) and Fe(0) is discussed.

Approximately at the same time Chirik (PNP-*i*Pr) and Goldman (PNP-*t*Bu) published two very similar complexes, the only difference was in the phosphine size.[70,71] Both complexes are depicted in Figure 22. The compounds were synthesized by reducing the di-halide precursor under CO atmosphere. Chirik compared his new compound with the previously [Fe(PDI)(CO)$_2$] complex.[43] He concluded that the PNP system has a more reducing iron center than the bis(imino)pyridine ligands. In a different report the electronic structure was elucidated, showing that the bis(imino)pyridine system can be described as an low-spin Fe(II) compound with a singlet dianionic ligand.[52,72] However Goldman reported different findings. In his paper he studied the unusual structure of the [Fe(PNP^{CH2}-*t*Bu)(CO)$_2$] complex. He discovered unusual bend Fe-C-O angels and four different signals in the IR. According to the publication the complex has an unusual SQP structure in solid state and in solution the isomers are in equilibrium (SQP-TBP) Further it was not possible to measure NMR of the *bis*-carbonyl at room temperature, the spectrum only showed the free ligand. At -80°C it was possible to detect the compound. The findings were supported by DFT calculations.
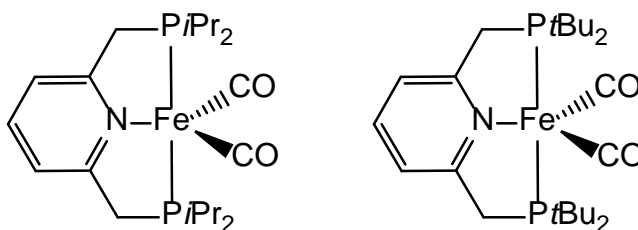

Figure 22: Fe(0) complexes reported by Chirik and Goldman

Milstein published new iron dicarbonyl complexes [Fe(PNN-R)(CO)$_2$] (R = Ph, *i*Pr, *t*Bu) based on bipyridine PNN pincer ligands.[73] The compounds (see Figure 23) were prepared by reducing the [Fe(PNN)X$_2$] (X = Cl, Br) complexes under CO atmosphere or directly by reacting the ligand with Fe(CO)$_5$. Further the electronic structure and bond distances are discussed and studied (bpy ligands can have different oxidation states) concluding that the complexes are best described as Fe(0) compounds.
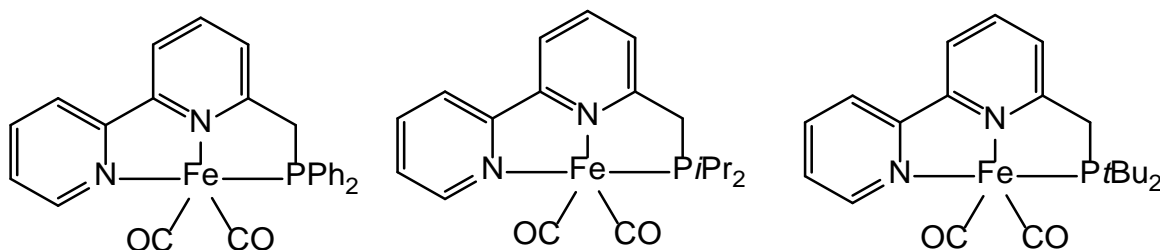

Figure 23: Milsteins PNN bis-carbonyl complexes

NHC based iron(0) pincer pyridine bis(imidazole-2-ylidene) dicarbonyl complexes were reported by Danopoulus and Saßmannshausen.[74] This complex (see Figure 24) was synthesized by bubbling CO through a solution of the [Fe(CNC)(N$_2$)$_2$] complex, replacing the dinitrogen ligands with carbon monoxide.
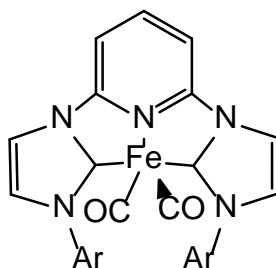

Figure 24: A Fe(0) CNC bis carbonyl complex

Comparison of CO Stretching Frequencies:

Table 1 shows the different wavenumbers exhibited by iron(0) bis-carbonyl pincer complexes depending on the donor strength of the co-ligand. It correlates with the electron density at the metal and the reducing power. Complexes with PNP ligands are stronger π bases to the coordinating CO. Further Table 1 depicts the different Fe-C-O bond angles, only Goldman's [Fe(PNP^{CH2}-*t*Bu)(CO)$_2$] complex has the interesting feature of nonlinear Fe-C-O angles of nearly 170°.

Table 1: CO stretching frequencies and Fe-C-O bond angles of different Fe(0) dicarbonyl complexes

	ν_{co} cm^{-1}	ν_{co} cm^{-1}	Fe-C-O (°)	Fe-C-O (°)
PNP^{CH2}-*i*Pr	1842	1794	174.84	174.84
PNP^{CH2}-*t*Bu	1870 (1846)	1819 (1797)	176.68	171.87
PNN-*t*Bu	1920	1860	178.25	174.06
PNN-*i*Pr	1913	1860	178.8	176.12
PNN-Ph	1925	1863	176.27	175.14
PDI^{iPr}	1974	1914	178.72	176.32
CNC NHC 1	1928	1865	178.89	177.36
CNC NHC 2	1925	1858		
^{tBu}PNN^{iP}r	1956	1902		

An interesting Fe(I) pincer complex was reported by Caulton, bearing an anionic PNP pincer ligand (Figure 25).[75] This compound was synthesized by reducing the [Fe(PNP)Cl] (PNP = (*t*Bu$_2$PCH$_2$SiMe$_2$)$_2$N) complex with sodium-naphtalide and subsequent conversion with CO. In the first reaction step the three coordinated [Fe(PNP)] complex was isolated. The isolated product was characterized by X-ray diffraction showing a square pyramidal structure with one CO *trans* to an empty site and one trans to the amide N. Further IR spectroscopy was performed with stretching frequencies of ν_{co} 1943 and 1870 cm^{-1}.
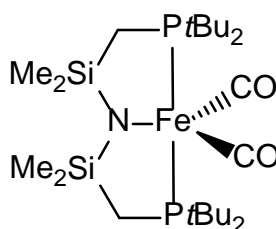

Figure 25: Caultons Fe(I) PNP *bis*-CO complex

3. Ligand synthesis

A lot of different pincer systems are known in literature, they differ in structure, properties and have different donor atoms and can be commercially available (Sigma Aldrich, Strem chemicals). Unfortunately some of these ligands are hard to synthesize or several reaction steps are necessary. In the last couple of years our group has developed and modified a modular system for the synthesis of PNP pincer ligands based on 2,6-diaminopyridine.[76] The synthesis is straightforward; mixing diaminopyridine with a chloro-phosphine in presence of a base affords the corresponding ligand in good to excellent yields. The synthesis and the various phosphines used in this work are shown in Scheme 1. The ligands were characterized by ^{1}H, ^{13}C{^{1}H} and ^{31}P{^{1}H} NMR. In the phosphorus NMR the ligands can be exactly characterized and distinguished by each other.

R = **1a:** Ph
1b: iPr
1c: Et
1d: Cy
1e: tBu
1f: Ad
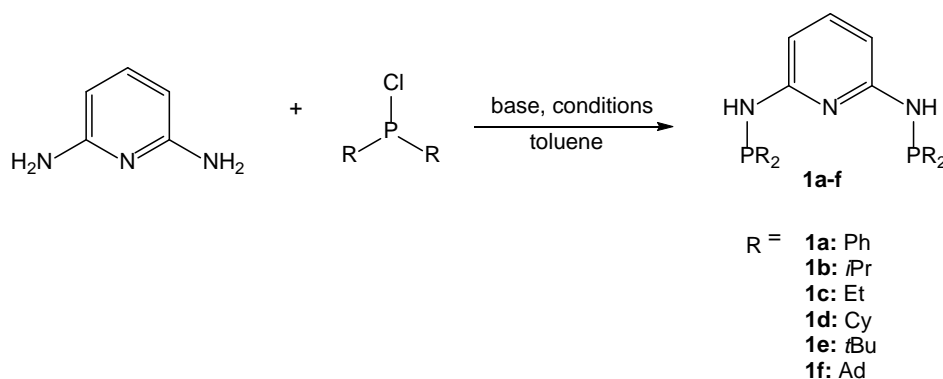
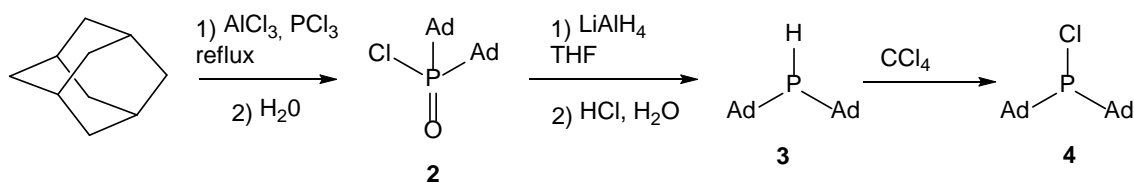**Scheme 1:** Synthesis of PNP-R ligands

Depending on the phosphine moiety different conditions have to be used. With phosphines bearing Ph, iPr, Et, and Cy substituents NEt$_3$ was used as a base. Heating the reaction mixture at 80°C overnight, removal of the ammonium salt by filtration, and evaporation of the solvent affords the PNP ligands in excellent yield. With the bulky substituents R = tBu and Ad different reaction conditions had to be developed. In order to obtain these ligands n-BuLi was used as a base in order to deprotonate the 2,6-diaminopyridine before adding the respective chlorophosphine at -78°C. After workup the yield of PNP-tBu is good, but the reaction conditions for the adamantyl chlorophsophine have yet to be improved. The ^{31}P{^{1}H] NMR shows resonances only for the mono phosphorylated 2,6-diaminopyridine, starting material and oxidized starting material. All the synthesized ligands are white to pale yellow solids. The phosphorus shift of the PNP-Ad ligand is at 67.8 ppm, the others are already known to literature or synthesized by coworkers (PNP-Cy and PNP-Et). The different ^{31}P{^{1}H} NMR shifts are summarized in Table 2.

Table 2: $^{31}P\{^1H\}$ NMR shifts of different PNP ligands

	Ligand	$^{31}P\{^1H\}$ NMR shifts [ppm]
1a	PNP-Ph	28.0
1b	PNP-*i*Pr	49.0
1c	PNP-Et	33.2
1d	PNP-Cy	41.3
1e	PNP-*t*Bu	60.2
1f	PNP-Ad	67.8

3.1 Synthesis of PAd$_2$Cl

Albeit all the chlorophosphines are commercially available it was decided to prepare some of them by ourselves because of the high price (sigma Aldrich: PAd$_2$Cl 1g/190 €). In the literature two synthetic pathways are described. At first we tried a Grignard reaction with 15 eq magnesium, 1 eq 1-bromo adamantane and 0.5 eq PCl$_3$.[77] This synthesis turned out to be inefficient and failed a couple of times without any reason. A second approach was done using a Friedl-Crafts type reaction.[78] In a first step AlCl$_3$, PCl$_3$ and admanatane were refluxed, followed by hydrolysis to obtain di-1-adamantylphosphonic chloride **2** in 90% yields. The reduction of **2** with LiAlH$_4$ afforded di-1-adamantylphosphine **3** in nearly quantitative yields. Refluxing the phosphine with carbon tetrachloride overnight **4** was obtained in quantitative yields. The last step was published using phosgene and DBU (1,8-Diazabicyclo[5.4.0]undec-7-ene), but because of phosgene being poisonous we decided to try a different route using CCl$_4$. After evaporating the excess of CCl$_4$ **4** crystallized as a white solid and was used without any further purification. All the intermediates and the final product were characterized by ^1H and $^{31}P\{^1H\}$ NMR. The shifts were in agreement with literature data. The reaction is shown in Scheme 1.

Scheme 2: Synthesis of the di-adamantyl phosphinechloride

3.2 Introducing ring substituted PNP ligands

In this work also modified pyridine rings as well as N-alkylated diaminopyridine (DAP) derivatives were used for ligand synthesis to tune electronic and steric properties or to increase the solubility. The different precursors are shown in Figure 26 and were synthesized according to literature.[79]
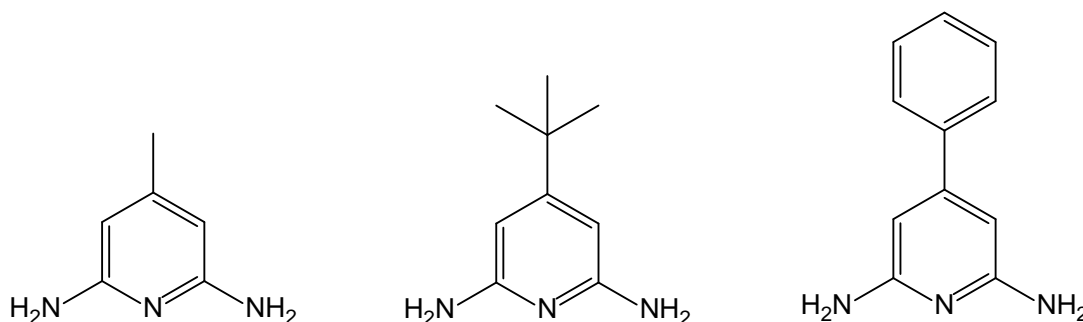

Figure 26: Different 2,6-diaminopyridine derivatives used in this work.

The following ligands were synthesized:

Table 3: Ring modified DAP based PNP ligands

	DAP-derivative	P-R$_2$	^{31}P{^{1}H} shifts [ppm]
1g	p-Me DAP	*i*Pr	55.7
1h	p-Me DAP	Ph	25.4
1i	p-*t*Bu DAP	*i*Pr	59.9
1j	p-Ph DAP	Ph	26.2

All the new ligands were synthesized based on our well established procedure, adding NEt$_3$ to a solution of the DAP derivative in toluene and adding the corresponding PR$_2$Cl upon heating at 80°C to afford the ligands in good yields. The ligands were characterized by ^{1}H, ^{31}P{^{1}H} and ^{13}C{^{1}H} NMR spectroscopy. From the *p*-Me-PNP-*i*Pr **1g**, while trying to crystalize a different compound, a single crystal was obtained and characterized by X-ray diffraction. The molecular structure is presented in Figure 27. The phosphorus NMR signals were similar to the non-substituent PNP ligands, so the ligands could be easily identified. The NMR shifts are summarized in Table 3.
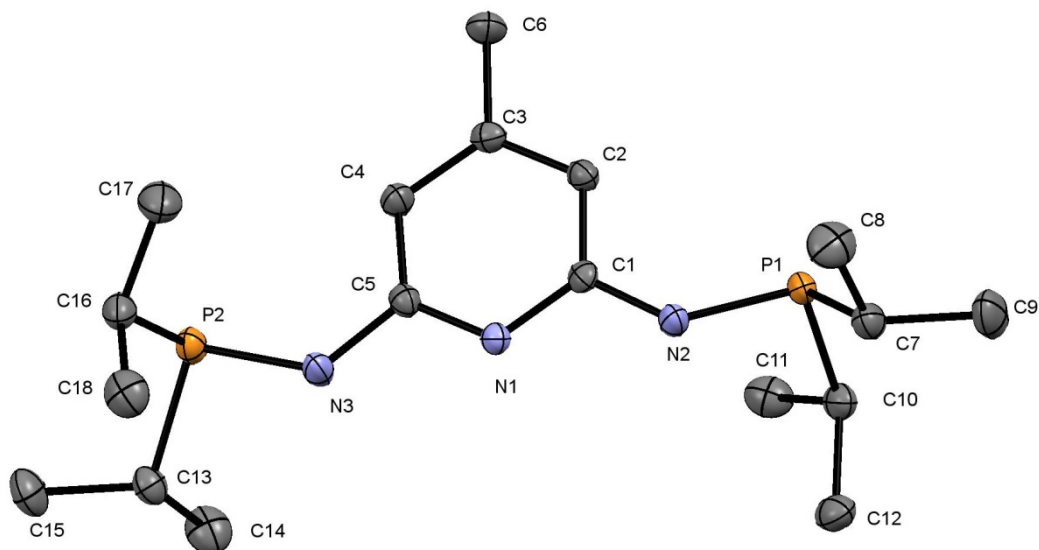
Figure 27: Molecular structure of the p-Me-PNP-*i*Pr **1g** ligand

In the ligand **1g**, the methylpyridine-2,6-diamine moiety is almost planar, with a maximum deviation of 0.0129 (9) Å for one of the amine N atoms. Whereas one of the P atoms is coplanar with this mean plane [deviation = 0.0158 (10) Å], the other P atom is considerably displaced out of the mean plane by 0.5882 (10) Å. In the crystal, no directional intermolecular interactions beyond van der Waals contacts could be identified.[80]

3.3. N-alkylated PNP ligands

Further modifications were performed to get rid of the N-H moiety. When using N-alkylated diamino-pyridine precursors in our established synthesis the desired product was not afforded, even using different bases like LDA showed no conversion.

In a first attempt the N-alkylated ligand was synthesized by protecting the phosphine moiety of the PNP ligand with BH_3 upon deprotonation with n-BuLi and methylation the amine bridge with MeI. In a last step the phosphine was deprotected with $NHEt_2$ under reflux to afford the PNP^{Me}-*i*Pr ligand **1k**. The reaction is shown in Scheme 3.[33]
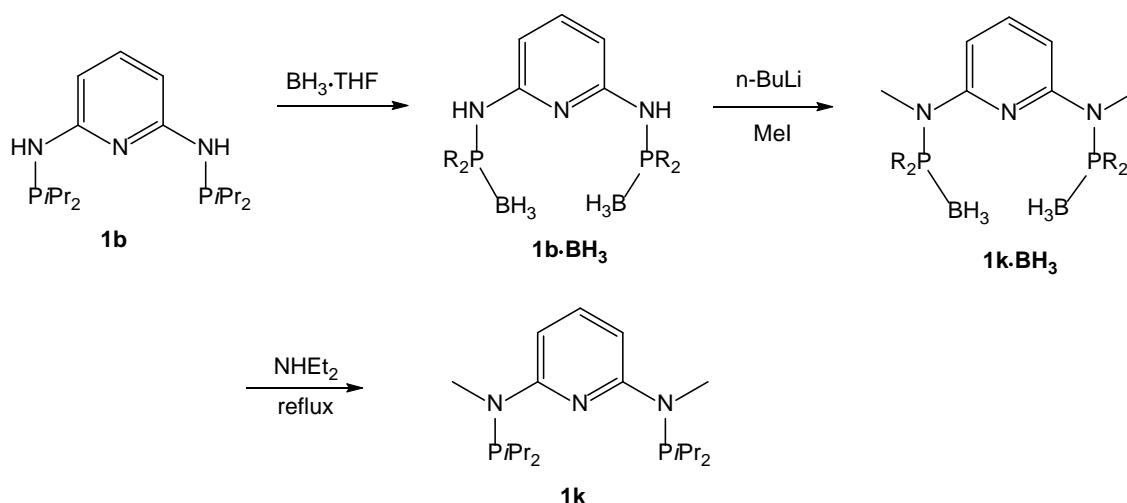
Scheme 3: First successful synthesis route to PNP^{Me}-iPr

Combined, this procedure has four steps and is not very convenient. So a second method was established to make this class of ligands available. Starting from the N-alkylated diamino-pyridine and treating it with 1 eq of n-BuLi and 1 eq PR$_2$Cl afforded the mono phosphorylated diamino-pyridine derivative. This compound can be deprotonated a second time with n-BuLi upon phosphorylation afforded the PNP^{alk}-R ligands. The reaction is shown in Scheme 4. It has to be noted that the reaction can be performed in one pot without workup of the mono-phosphorylated intermediate. Yields up to 90 % (PNP^{Et}-iPr) were achieved.

1k: R=iPr, R'=Me
1l: R=iPr, R'=Et
1m: R=Ph, R'=Me
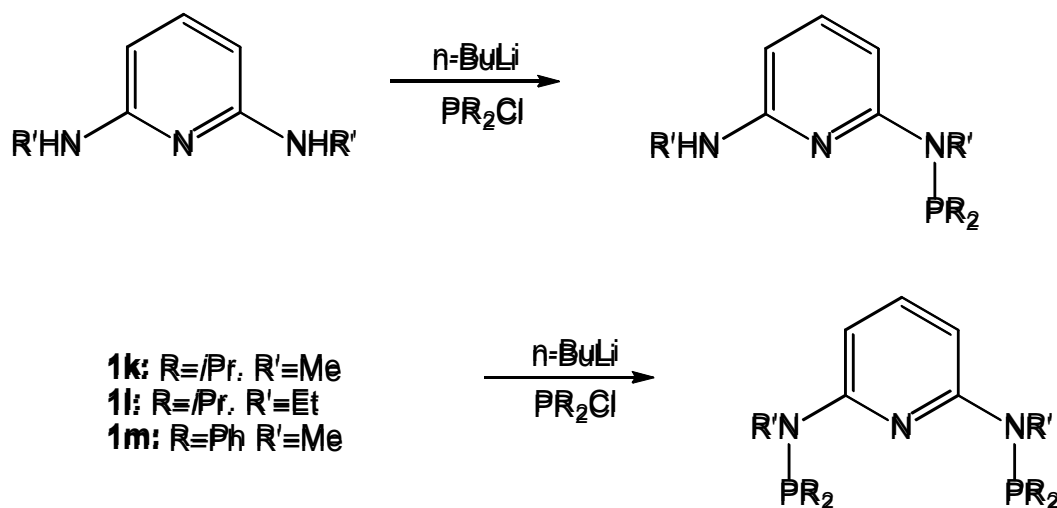
Scheme 4: Stepwise phosphorylation for the synthesis of N-alkylated PNP ligands

The new ligands were characterized using ^{1}H, ^{31}P{^{1}H} and ^{13}C{^{1}H} NMR. The phosphorus shifts can be used to distinguish between the products which differ from the N-H bridged PNP ligands. These values are summarized in Table 4.

Table 4: ^{31}P{^{1}H} NMR shifts of the N-alkylated PNP ligands

	Ligand	chemical shifts [ppm]
1k	**PNP^{Me}-*i*Pr**	88.5
1l	**PNP^{Et}-*i*Pr**	91.1
1m	**PNP^{Me}-Ph**	62.5

4. Iron complexes based on PNP-Ph ligands

4.1 Iron(II) complexes featuring κ^3- and κ^2-bound PNP ligands: the unusual κ^2 bonding mode of a PNP pincer ligand

A neutral ENE pincer ligand, where E is a donor, typically coordinates via a meridional κ^3-*E,N,E* coordination mode. Unsaturated 16e high spin square pyramidal iron ENE complexes of the type [Fe(κ^3-*E,N,E*-ENE)X$_2$] (X = Cl, Br) are an important class of compounds and obtained from Fe(II) halides with stoichometrical amounts of ligand[42,43,70,71,73,81,21]. In most cases bulky substituents such as *i*Pr and *t*Bu are introduced to prevent the formation of the bis chelated dicationic low spin complexes of the type [Fe(κ^3-*E,N,E*-ENE)$_2$]$^{2+}$. Some of these compounds are used as catalysts in polymerization reactions or as precursors for Fe(0) complexes which are useful catalysts for hydrogenation[71] and hydrosilylation[47] reaction.

Iron complexes bearing tridentate PNP pincer ligands based on a central pyridine donor with a CH$_2$ or NH bridge in ortho position are widely used in literature.[58,59,29,71,76,26,82,83,25] However most of these ligands feature bulky and electron donating phosphine moieties like *i*Pr or *t*Bu, less bulky and electron poor Ph are rare.[84,85]

Coordinativeley unsaturated 16 electron Fe(II) complexes of the type [Fe(PNP-R)Cl$_2$] were prepared with pyridine based PNP ligands PNP^{CH2}-*i*Pr, PNP^{CH2}-*t*Bu and PNP^{CH2}-Ph with CH$_2$ spacers between the phosphine donor and the pyridine ring by reacting FeCl$_2$ with the corresponding ligand. The bulkiness and donor strengths of these ligands decrease in the order PNP-*t*Bu > PNP-*i*Pr > PNP-Ph and apparently seems to have no influence on these reactions. Our working group has recently reported similar complexes but with the bulky PNP ligands N,N'-bis(di-*iso*-propylphosphino)-2,6-diaminopyridine (PNP-*i*Pr) and N,N'-bis(di-*tert*-butylphosphino)-2,6-diamino-pyridine (PNP-*t*Bu) where the central pyridine ring contains NHPR$_2$ (R = *i*Pr, *t*Bu) substituents in the two *ortho* positions. The reaction is shown in Scheme 5. In this course we were interested in the chemistry of the N,N'-bis(diphenylphosphino)-2,6-diaminopyridine PNP-Ph ligand, because reacting it with anhydrous FeCl$_2$ gives a new unknown green complex.
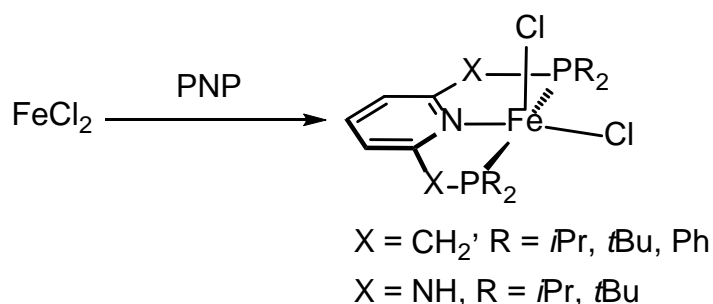
Scheme 5: Reaction of FeCl$_2$ with different PNP pincer ligands

In contrast to the previously mentioned work in Scheme 5, treating anhydrous FeCl$_2$ with PNP-Ph (**1a**) in THF for 4h the diamagnetic green octahedral and cationic complex **2** of the general formula [Fe(κ^3-*P,N,P*-PNP)(κ^2-*P,N*-PNP)Cl]$^+$ is afforded in essentially quantitative yields (Scheme 6). The formation of these complexes is independent of whether 1 or 2 equivs of ligand are used. When using 1 equiv of ligand remaining FeCl$_2$ further reacts to form the paramagnetic [FeCl$_3$(THF)]$^-$·counterion.
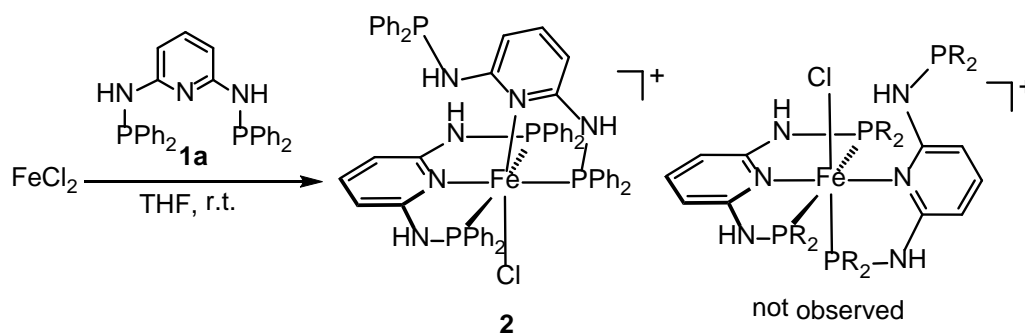
Scheme 6: Reaction of PNP-Ph with FeCl$_2$

The reaction of anhydrous FeCl$_2$ with the related ligand PNP^{CH2}-Ph yields the pentacoordinated complex [Fe(PNP^{CH2}-Ph)Cl$_2$] revealing striking differences between CH$_2$ and NH bridging groups in pyridine-based PNP pincer ligands (Scheme 5). The formation of **2** is very selective and only one isomer was observed where the pyridine moiety of the κ^2-*P,N* bound PNP ligand is *trans* to the halide ligand. There was no evidence for the formation of a second isomer **B** (Figure 28 and Figure 29) where the pyridine moiety of the κ^2-*P,N* bound PNP ligand is *cis* to the halide ligand. DFT calculations for the two possible isomers of **2** in agreement with the experiment indicate that the unobserved isomer is less stable by 6.9 kcal/mol. That stability difference is essentially due to steric effects.

That orbital belongs to what would be the t$_{2g}$ group of a perfect octahedral species and is essentially Fe–Cl π^* in character. Another indication for the stereochemical stress associated

with **B** involving in particular the Cl ligand is the Cl-Fe-X angle, X being the atom *trans* to N_{py} of the κ^3-*P,N,P* bound PNP ligand. That angle is 88° in **A** and becomes 104° in **B** showing that the Cl ligand is considerably bent towards the κ^3-*P,N,P* bound PNP ligand in the latter species. This geometrical constraint has clear consequences in the bonding of the two isomers. Thus, the κ^3-*P,N,P* bound PNP ligand binds strongly to the metal in **B** in order to compensate the weakening of the coordination of the κ^2-*P,N* bound PNP ligand due to the repulsion with the Cl⁻ ligand in that molecule. It is interesting to note that the intramolecular H-bond does not explain the stability difference because it is actually stronger in the case of **B** (Cl···H-N) as can be seen, for example, by the N-H bonds (covalent) in both cases. That bond is weaker in the case of **B** (d = 1.027 Å) than in **A** (d = 1.015 Å) which is also apparent from the respective Wiberg indices for the H-bond being 0.02 for N···HN in **A**, and 0.09 for Cl···HN in **B.**

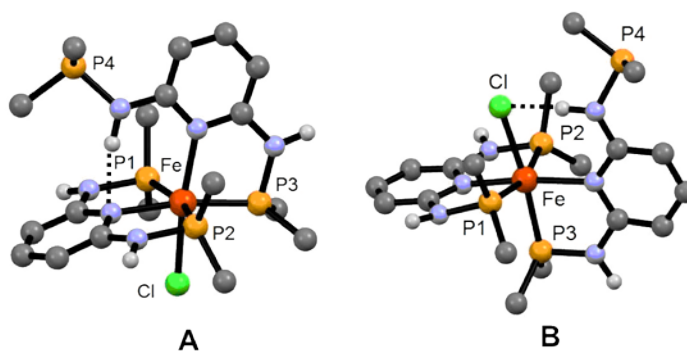**Figure 28:** Optimized B3LYP geometries of the two possible isomers **A** and **B** of [Fe(κ^3-*P,N,P*-PNP-Ph)(κ^2-*P,N*-PNP-Ph)Cl]⁺ (**2**). Most hydrogen atoms are omitted and only ipso carbon atoms of the Ph substituents are shown for clarity.
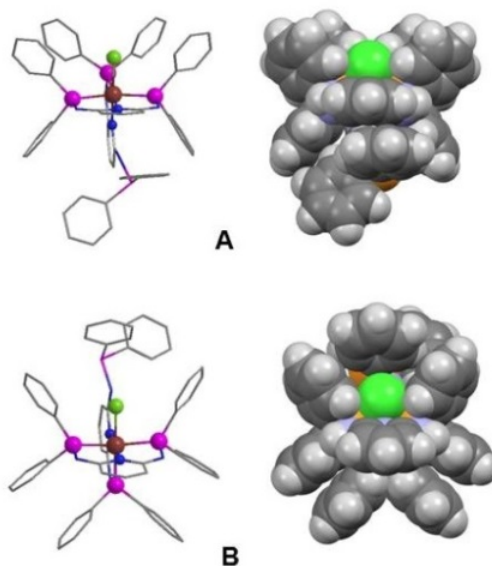
Figure 29: Space filling representation of optimized B3LYP geometries of the two possible isomers **A** and **B** of [Fe(κ^3-*P,N,P*-PNP-Ph)(κ^2-*P,N*-PNP-Ph)Cl]$^+$ (**2**) viewed along the Fe-N(py, κ^3-PNP) bond to illustrate steric crowding around the Cl$^-$ ligand (green).

Treating complex **2** with 1 equiv AgBF$_4$ or NaBF$_4$ after the reaction gives the corresponding **2BF$_4$** compound, which precipitates in THF, but is good soluble in CH$_2$Cl$_2$. Also the color is more intensive compared to **2Cl**.

Complex **2** was fully characterized by ^{1}H, ^{13}C{^{1}H} and ^{31}P{^{1}H} NMR spectroscopy. While the ^{1}H NMR spectra was not very informative due to the overlapping of the aromatic rings in the phenyl area as well as the ^{13}C{^{1}H] NMR, the ^{31}P{^{1}H} NMR spectrum revealed a characteristic A$_2$B pattern. The spectrum gives rise to multiplets centered at δ_A = 108.7 (κ^3-PNP) and δ_B = 100.9 (κ^2-PNP) with a coupling constant J_{PP} = 50 Hz, which can be assigned to the two phosphorus atoms of the κ^3-PNP-bound ligand, and one phosphorous atom of κ^2-PNP-bound ligand. In addition, the pendant PPh$_2$-NH-arm of the κ^2-bound PNP ligand gives rise to a singlet at 47.0 ppm. From A$_2$B spectra chemical shifts and coupling constants cannot be derived directly from the spectrum as in a first order NMR spectrum such as a A$_2$X spin system. Accordingly, all ^{31}P spectra had to be simulated in order to obtain chemical shifts and coupling constants. Additionally, also line broadening had to be considered. The experimental and simulated spectra are superimposed as shown in Figure 30. The singlet of the pendant PR$_2$ arm at 47 ppm is not shown. The simulated spectrum matches the recorded very well.
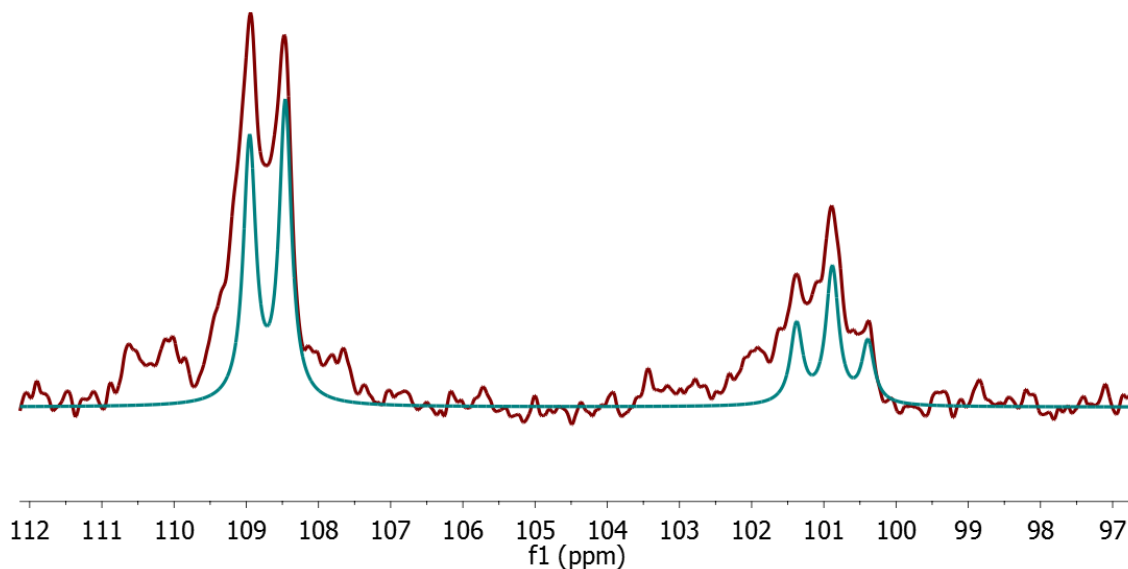
Figure 30: Superimposed ^{31}P NMR spectra of complex **2** red: measured, blue: simulated

Further characterization was performed by single crystal X-ray diffraction. Crystals suitable for crystallographic analysis were grown by slow diffusion of Et_2O into a saturated solution of **2BF₄** in THF. The molecular structure of **2** is shown in Figure 31 with selected bond distances given in the caption. The crystals are a solvate with two well-ordered THF solvent molecules hydrogen bonded to NH-groups. A third solvent molecule, not hydrogen bonded to NH, was badly disordered and is thought from its elongated shape to be an Et_2O molecule. Also affected by this solvent disorder is the BF_4 anion. The BF_4 anion is hydrogen bonded to one of the NH-groups of the Fe complex. This complex adopts a severely distorted octahedral geometry with the P1-Fe1-P2, N1-Fe1-P3, Cl1-Fe1-N1, P1-F1-N1, P3-F1-N4, N1-Fe1-N4 and N4-Fe1-Cl1 angles deviating from the ideal 180° or 90° being 170.02(6), 163.33(3), 81.43(6), 81.96(6), 84.06(6), 105.91(8) and 172.36(6)°, respectively.
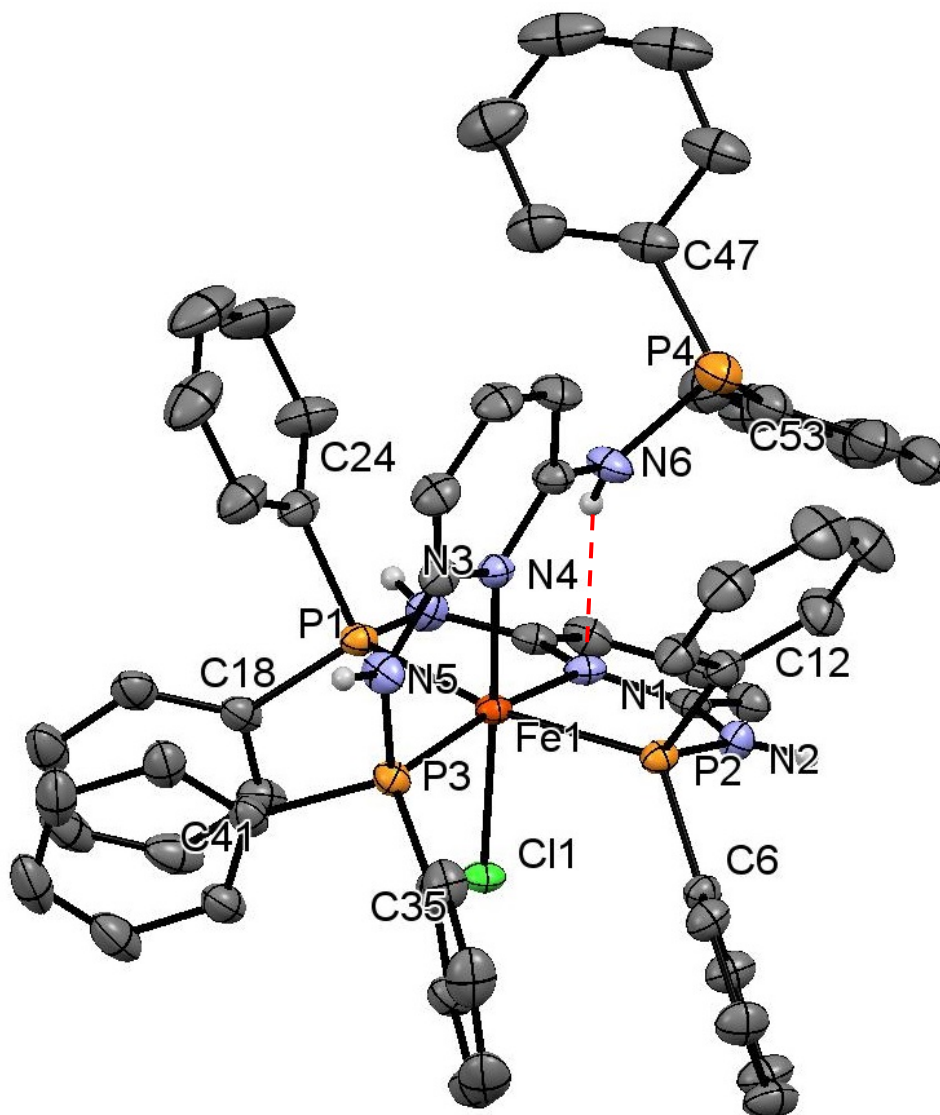
Figure 31: Molecular structure of complex **2** showing only N-bonded H-atoms and 40%-ellipsoids (solvent molecules and BF_4^- counterion are omitted for clarity). Selected bond distances and angles (Å, deg): Fe1-N1 2.064(2), Fe1-N4 2.084(2), Fe1-P3 2.1845(7), Fe1-P1 2.2439(7), Fe1-P2 2.2530(7), Fe1-Cl1 2.3330(7); P1-Fe1-P2 163.33(3), N1-Fe1-P3 170.02(6), N4-Fe1-Cl1 172.36(6), C34-N6-P4 120.3(3); hydrogen bond N6H···N1 2.184

Complex **2** is stable in THF for several days, but readily rearranges in CH_3CN or MeOH within a few minutes and CH_2Cl_2 within a few hours to give the known complex [Fe(κ^3-*P,N,P*-PNP-Ph)$_2$]$^{2+}$, both ligands are coordinated in a κ^3 fashion. In the presence of halide scavengers like $AgBF_4$ (or other silver salt) this reaction proceeds immediately, the color changes from green to red. The formation of [Fe(κ^3-*P,N,P*-PNP)$_2$]$^{2+}$ requires halide dissociation which is strongly dependent on the solvent followed by a 90^0 rotation about the P-Fe-P axis of the κ^2-*P,N*-bound

ligand. The *bis*-PNP complex **3** was already prepared by an alternative method recently.[25] It has to be noted that an analogous complex [Fe(κ^3-*P,N,P*-PNP^{CH2}-Ph)]$_2^{2+}$ bearing CH$_2$-bridges between the pyridine ring and the PPh$_2$ moieties was reported.[86]
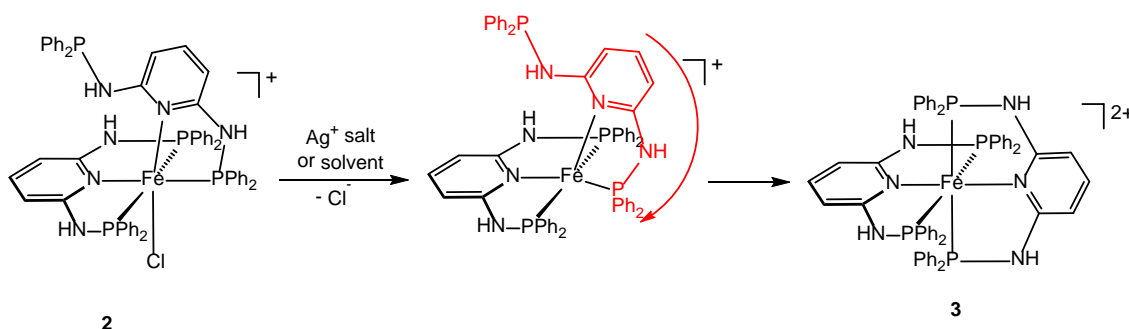
Scheme 7: Rearrangement to complex **3**

In addition to the spectroscopic data ESI-MS (electron spray ionisation) of complex **2Cl** was performed. Compound **2** was dissolved in MeOH, and the solution was injected into the MS in the positive ion mode. The most abundant signal observed at *m/z* 1045.4 corresponds to the positively charged complex **2$^+$** emphasizing the stability of this complex. Further abundant fragments are [Fe(κ^3-*P,N,P*-PNP-Ph)(κ^3-*P,N,P*-PNP-Ph)^{deprot}]$^+$ (**[M-Cl-H]$^+$**) where both ligands are coordinated in a κ^3 fashion and one ligand is deprotonated at *m/z* 1009.4, [Fe(κ^3-*P,N,P*-PNP-Ph)(κ^2-*P,N*-PN^{NH2}-Ph)Cl]$^+$ (**[M-PPh$_2$+H]$^+$**) where the pendant phosphine arm is cleaved off at *m/z* 861.3, [Fe(κ^3-*P,N,P*-PNP-Ph)Cl]$^+$ (**[M-PNP]$^+$**) where the κ^2 bond ligand is dissociated at *m/z* 568.2 and [Fe(κ^3-*P,N,P*-PNP-Ph)$_2$]$^{2+}$ (**[M-Cl]$^{2+}$**) at *m/z* 505.2. The fragmentation pattern is shown in Scheme 8. The bis-PNP complexes (deprotonated and doubled charged) are observed due to the isomerization of complex **2** to **3** in MeOH.
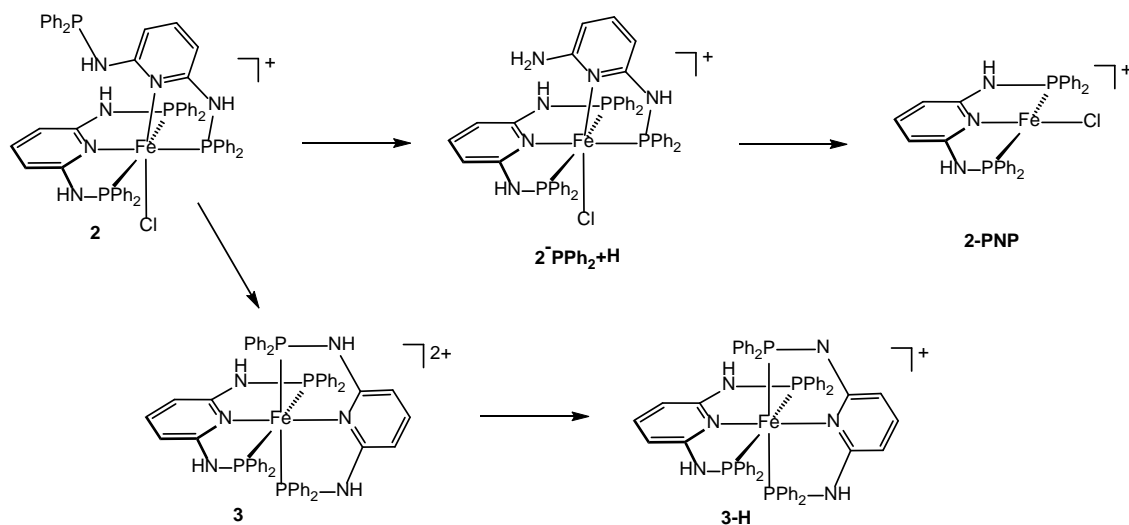
Scheme 8: ESI-MS fragmentation pattern of complexes **2** and **3**

The full scan of complex **2** is shown in Figure 32 with the isotope splitting pattern of **M⁺** displayed separately.
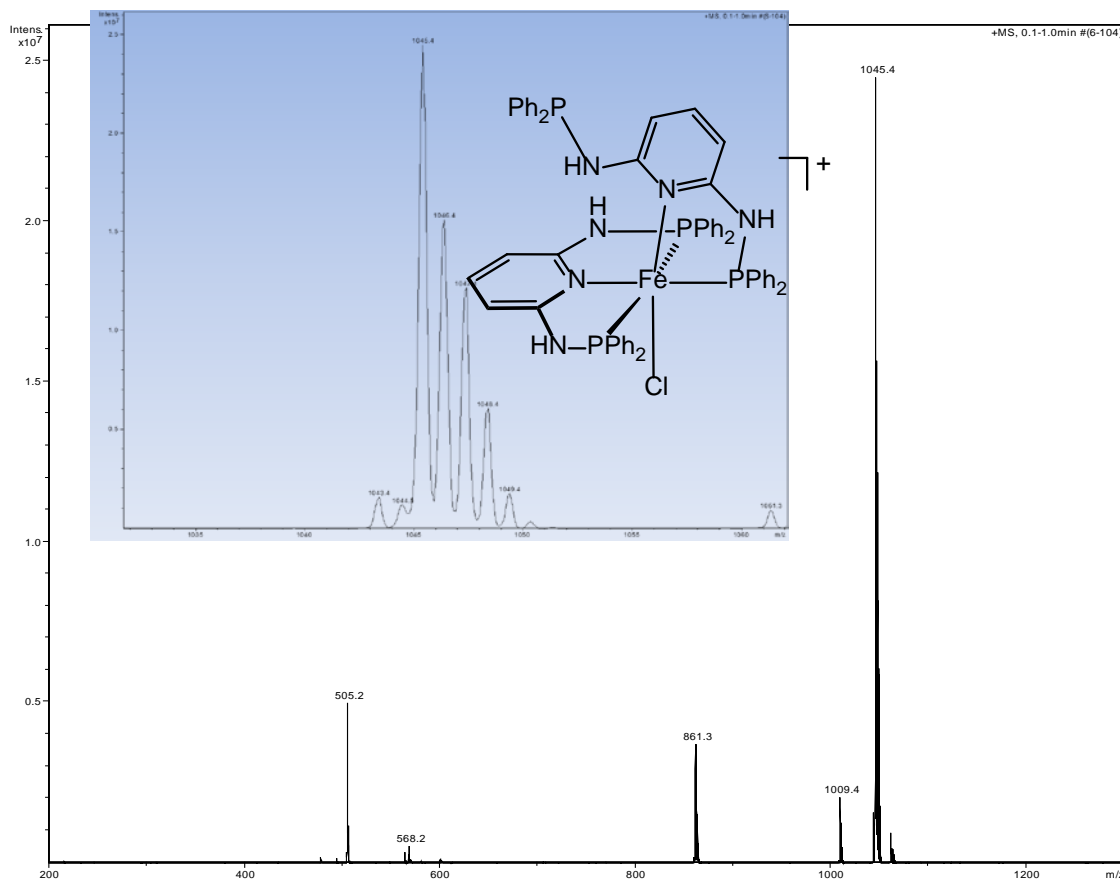

Figure 32: Positive-ion full scan ESI-MS of [Fe(κ^3-*P,N,P*-PNP-Ph)(κ^2-*P,N,P*-PNP-Ph)Cl]Cl (**2**) in MeOH. Inset shows the isotope pattern match for [Fe(κ^3-*P,N,P*-PNP-Ph)(κ^2-*P,N,P*-PNP-Ph)Cl]+ (**[M]⁺**)

To prevent the formation of the κ^3, κ^2 complex and coordination of a second ligand to synthesize the pentacoordinated coordinativeley unsaturated [Fe(PNP-Ph)Cl$_2$] compound the N-methylated ligand **1m** was introduced assuming that κ^2-*P,N*-coordination of **1m** is highly unlikely due to unfavorable steric interactions with the pyridine unit of the κ^3-*P,N,P*-bound ligand. Interestingly, reacting anhydrous FeCl$_2$ with 1 or 2 equiv. of **1m** proceeded differently than expected yielding the cationic complex [Fe(κ^3-*P,N,P*-PNP^{Me}-Ph)(κ^2-*P,N*-PN^{HMe})Cl]⁺ **4**. The reaction is shown in Scheme 9. AgBF$_4$ was added for better solubility and crystallization properties, after the reaction didn't afforded the desired product. This reaction is accompanied by P-N bond cleavage thereby forming the new κ^2-*P,N*-bound N-diphenylphosphino-N,N'-methyl-2,6-diaminopyridine ligand. This reaction may be facilitated

by traces of water. The fate of the "PPh$_2$"-moiety is unclear and was not further investigated. It is not uncommon that aminophosphines bearing phenyl substituents at the phosphorus site are prone to hydrolysis, forming for instance Ph$_2$POH[87].
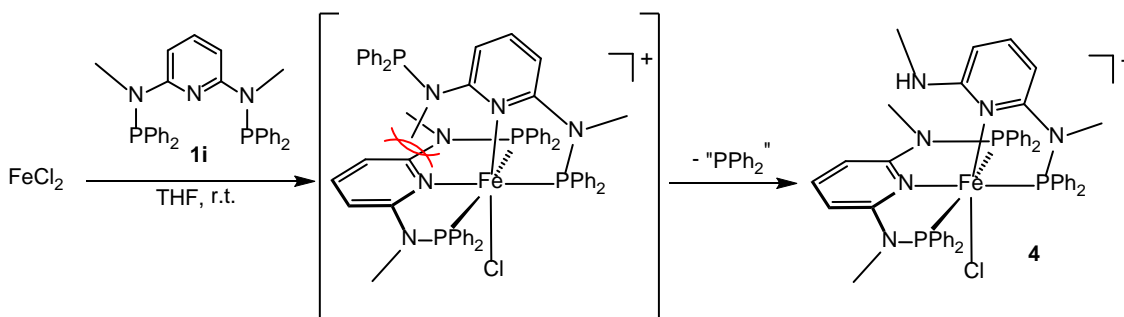
Scheme 9: Reaction of ligand **1i** with FeCl$_2$

Complex **4** was fully analyzed by ^{1}H, ^{13}C{^{1}H} and ^{31}P{^{1}H} NMR spectroscopy. While the ^{1}H NMR spectra was not very informative due to the overlapping of the aromatic rings in the phenyl area as well as the ^{13}C{^{1}H] NMR, the ^{31}P{^{1}H} NMR spectrum revealed a characteristic A$_2$B pattern. The spectrum gives rise to multiplets centered at 128.13 (κ^2 bond PN-NHMe) and 122.62 (κ^3 bond PNP) ppm. The recorded spectrum shows a coupling constant of J_{PP} = 30 Hz, however multiplet analysis revealed a coupling constant of about 45.5 Hz. The superimposed spectra are shown in Figure 33 where the blue is the simulated spectrum. Furthermore, the multiplet analysis of the recorded spectrum is shown with the chemical shifts and coupling constants.
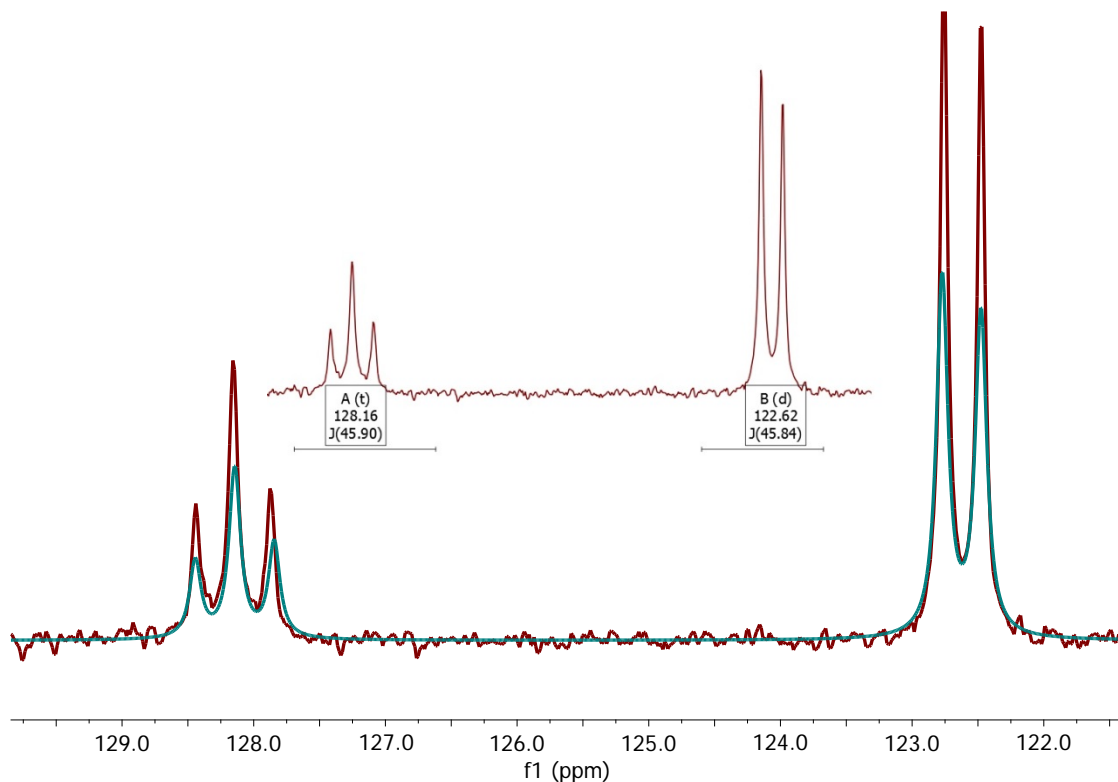
Figure 33: Superimposed ^{31}P{^{1}H} spectra of complex **4** red: measured, blue: simulated

Further single crystals suitable for X-ray diffraction could be grown and the molecular structure is depicted in Figure 34 with selected bond length and bond angels given in the caption. Like complex **2**, compound **4** isn't perfectly octahedral. It is severely with the Cl1-Fe1-N1, Cl1-Fe1-N4, P1-Fe1-P2, P1-Fe1-P3, P1-Fe1-N1, P2-Fe1-P3, P2-Fe1-N1, P3-Fe1-N1, P3-Fe1-N4 and N1-Fe1- N4 distorted angles deviating from the ideal 180° or 90° being 82.06(3), 173.32(3), 163.97(1), 97.93(1), 82.43(3), 97.94(1), 82.19(3), 171.60(3), 83.79(3) and 104.61(4) respectively. The hydrogen bond between N6H-N1 is shorter than in complex **2** with 1.977 Å.

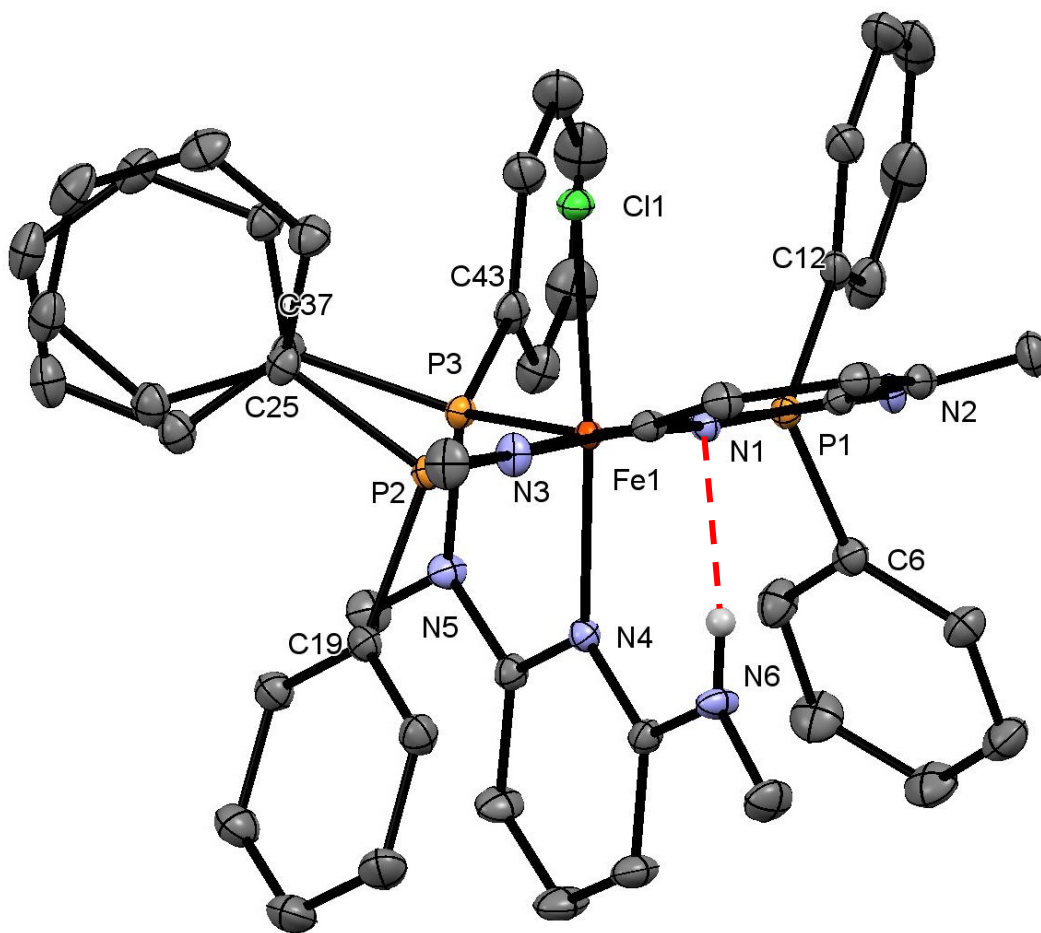**Figure 34:** Structural view of [Fe(κ^3-*P,N,P*-PNPMe-Ph)(κ^2-*P,N*-PN^{NHMe}-Ph)Cl]BF$_4$ (**4**) showing 50% thermal ellipsoids (H-atoms and BF$_4^-$ omitted for clarity). Selected bond lengths (Å) and bond angles (deg): Fe(1)-P(1) 2.2333(4), Fe(1)-P(2) 2.2410(4), Fe(1)-P(3) 2.1833(4), Fe(1)-N(1) 2.0472(9), Fe(1)-N(4) 2.0668(9), Fe(1)-Cl(1) 2.3323(3), P(1)-N(2) 1.7059(9), P(2)-N(3) 1.7055(9), P(3)-N(5) 1.6908(9), N(2)-C(1) 1.381(1), N(3)-C(5) 1.381(2), N(5)-C(32) 1.398(1), N(6)-C(36) 1.354(1), P(1)-Fe(1)-P(2) 163.97(1), N(1)-Fe(1)-P(3) 171.60(3), Cl(1)-Fe(1)-N(4) 173.32(3),; hydrogen bond N6H···N1 1.977

In a second attempt to obtain the pentacoordinated [Fe(PNP-Ph)Cl$_2$] species and to prevent the coordination of a second ligand, ligands with substituted rings were introduced. The ligand **1h** incorporates a methyl group in para position and the ligand **1j** a phenyl moiety (see Figure 35).
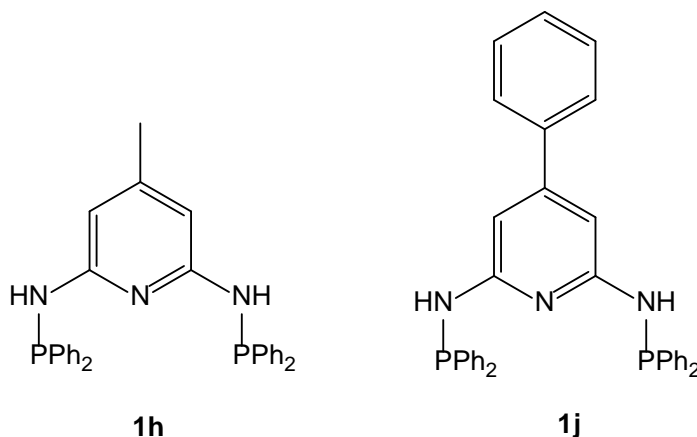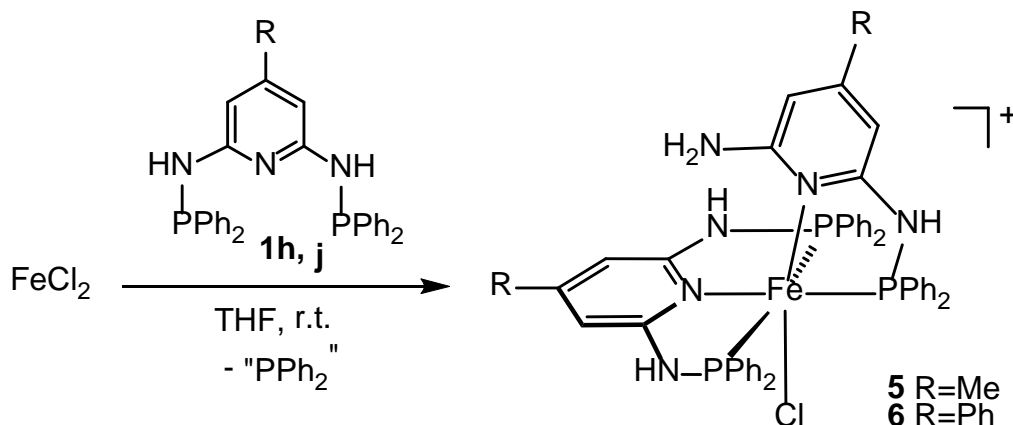
Figure 35: para substituted PNP-Ph ligands

The reaction with the ligand of **1h** and **1j** with anhydrous FeCl$_2$ didn't afford the desired product, the green κ^3, κ^2 complexes **5** and **6** were formed. As shown in the synthesis of **4**, a second ligand coordinates and the P-N bond is cleaved forming a new κ^2-*P,N* bound N-diphenylphosphino-N,N'-methyl-2,6-diamino-para-methyl-pyridine or N-diphenylphosphino-N,N'-methyl-2,6-diamino-parap-phenyl-pyridine ligand. Cationic complexes **5** and **6** with the formula [Fe(κ^3-*P,N,P*-PNP-pR-Ph)(κ^2-*P,N*-PN-pR^{NH2})Cl]$^+$ (R = Me or Ph) were afforded. The reaction is shown in Scheme 10.

Scheme 10: Reaction of FeCl$_2$ with ring-substituted PNP-Ph ligands

The complexes **5** and **6** were fully analyzed by ^{1}H, ^{13}C{^{1}H} and ^{31}P{^{1}H} NMR spectroscopy. The ^{31}P NMR showed a similar pattern as in complexes **2** and **4** and revealed that the pendant P-Ph$_2$ moiety was cleaved off during the coordination of the second ligand.

In this course for structural and reactivity comparisons we also prepared the related complex [Fe(κ^3-*P,N,P*-PNP-Ph)(κ^2-*P,N*-PN-Ph)Cl]BF$_4$ (**7**) by reacting anhydrous FeCl$_2$ with 1 equiv of **1a** and PN-Ph in the presence of 1 equiv of AgBF$_4$ according to Scheme 11. In this compound the

pyridine moiety of the PN-Ph lacks a substituent in the second *ortho* position. This complex was, like the other κ^3, κ^2 complexes, isolated as a green air-stable solid.
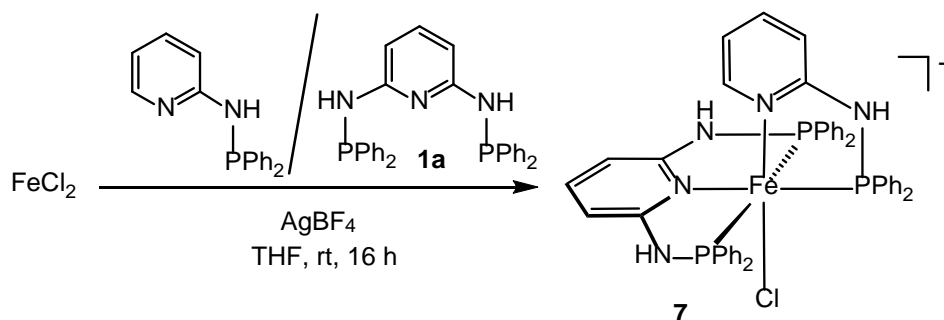
Scheme 11: Synthesis of complex **7** bearing a PNP-Ph and PN-Ph ligand

Complex **7** was fully analyzed by ^{1}H, ^{13}C{^{1}H} and ^{31}P{^{1}H} NMR spectroscopy. While the ^{1}H NMR spectra was not very informative due to the overlapping of the aromatic rings in the phenyl area as well as the ^{13}C{^{1}H] NMR, the ^{31}P{^{1}H} NMR spectrum revealed a characteristic A$_2$B pattern. The spectrum gives rise to multiplets centered at 112.5 (κ^2 bond PN-Ph) and 111.85 (κ^3 bond PNP) ppm with a coupling constant of J_{PP} = 50.5Hz. The recorded spectrum does not give insight about coupling constants because the chemical shifts of the two signals are nearly identical. The superimposed spectra are shown in Figure 36 where the blue is the simulated spectra.
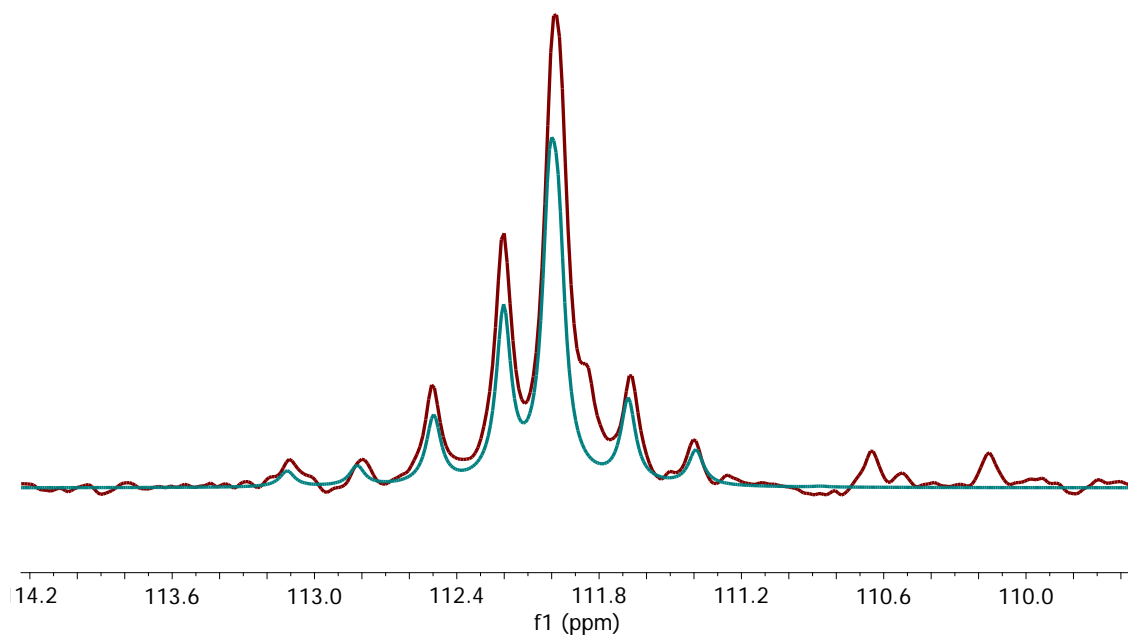
Figure 36: Simulated and experimental spectra of complex **7** red: measured, blue: simulated

Further crystals suitable for X-ray diffraction could be grown by Et$_2$O diffusion into a saturated solution of **7** in THF. The compound crystallized together with two molecules of THF. The structure is octahedral but barely distorted like complex **2** and **4**. The molecular structure of **7** is shown in Figure 37 with selected bond length and angels given in the caption.
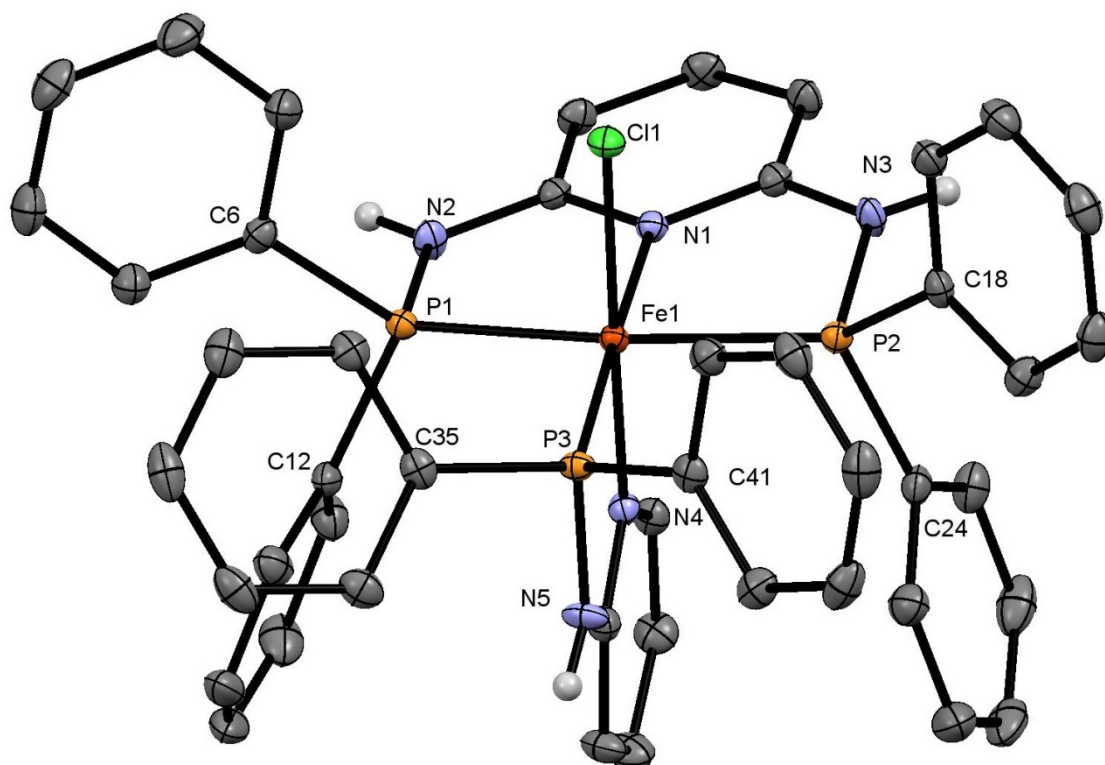
Figure 37: Molecular structure of [Fe(κ^3-*P,N,P*-PNP-Ph)(κ^2-*P,N*-PN-Ph)Cl]BF$_4$·2THF **7**, showing 50% thermal ellipsoids (H-atoms, solvents and BF$_4^-$ omitted for clarity). Selected bond lengths (Å) and bond angles (deg): Fe(1)-P(1) 2.2784(4), Fe(1)-P(2) 2.2533(4), Fe(1)-P(3) 2.1862(4), Fe(1)-N(1) 2.0172(9), Fe(1)-N(4) 1.9930(9), Fe(1)-Cl(1) 2.3331(4), P(1)-N(2) 1.696(1), P(2)-N(3) 1.690(1), P(3)-N(5) 1.686(1), N(2)-C(1) 1.370(2), N(3)-C(5) 1.377(2), N(5)-C(30) 1.380(2), P(1)-Fe(1)-P(2) 163.99(1), N(1)-Fe(1)-P(3) 178.08(3), Cl(1)-Fe(1)-N(4) 178.83(3)

4.2 Iron(II) PNP-Ph carbonyl complexes

As described in the previous chapter unusual κ^3, κ^2 PNP iron pincer complexes were synthesized and characterized by various techniques. Further we were interested in the reactivity of these new compounds especially towards CO to compare these carbonyl complexes bearing a CO ligand with the previously reported [Fe(PNP-*i*Pr)(CO)(Cl)$_2$] and [Fe(PNP-*i*Pr)(CO)$_2$Cl]$^+$ complexes.[29,26]

Treating complex **2** with CO in THF affords a red suspension within 1h due to the dissociation of the κ^2-*P,N*-bound PNP ligand. This reaction shows that the κ^2 coordinated ligand is only weakly bound and can easily be replaced. After workup the neutral complex [Fe(PNP-Ph)(CO)(Cl)$_2$] **8** is obtained in excellent yields. Washing the red solid with anhydrous Et$_2$O two times afforded pure **8**, by removing the excess **1a**. Apparently this compound is hardly soluble in any convenient solvent like THF or CH$_2$Cl$_2$, beside DMSO. When using the [Fe(κ^3-*P,N,P*-PNP)(κ^2-*P,N*-PNP)Cl]Cl **2Cl** salt as starting material the neutral complex **8** is the major product,

but when the BF_4 complex **2BF₄** is used, the cationic *trans*-CO complex **9** is obtained, which will be discussed later in this chapter.

[Fe(PNP-Ph)(CO)(Cl)₂] was characterized by by ^1H, $^{13}C\{^1H\}$ and $^{31}P\{^1H\}$ NMR as well as with IR spectroscopy. For NMR measurements it was necessary to add *d*6 DMSO to accomplish complete dissolution and achieve concentrations suitable for NMR spectroscopy. While the ^1H NMR spectra was not very informative due to the overlapping of the aromatic rings in the phenyl area, the $^{31}P\{^1H\}$ NMR spectrum shows two peaks at 88 and 85 ppm. The IR spectrum shows two bands at 1958 cm^{-1} and 2031 cm^{-1} that can be assigned to CO stretching frequencies. Performing NMR experiments with the crystals grown for X-ray diffraction showed that the desired product has its chemical shift at 88 ppm. In the $^{13}C\{^1H\}$ NMR the CO ligand exhibits a single low intensity triplet at 217 ppm with a coupling constant of J_{CP} = 29 Hz and the IR has the asymmetric CO stretching frequency ν_{CO} at 1958 cm^{-1}. The symmetric CO stretching band is IR inactive and thus not observed.

The second product could be identified as the cationic *trans*-CO complex **9**. Further complex **8** can be synthesized by immediate bubbling CO through a solution of 1 equiv of anhydrous FeCl₂ and 1 equiv of ligand **1a** in THF in nearly quantitative yields (90%). Complex **8** is an air and moisture stable red solid and can be stored under air for several weeks without any sign of decomposition.
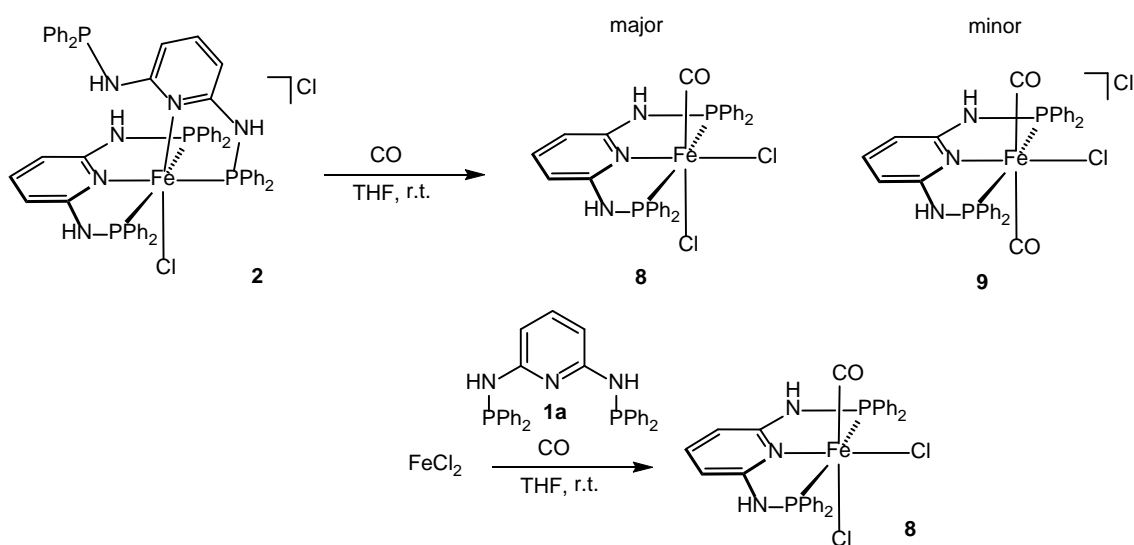
Scheme 12: Synthesis of **8**

Further single crystals suitable for X-ray diffraction were grown by slow diffusion of Et₂O in a saturated solution of **8** in DMSO. The molecule crystalized together with two molecules of DMSO and one molecule of Et₂O. Both DMSO molecules showed modest disorder, but interestingly the diethyl ether molecule showed no disorder. The molecular structure of **8** is shown in Figure 38 with selected bond length and bond angles given in the caption.
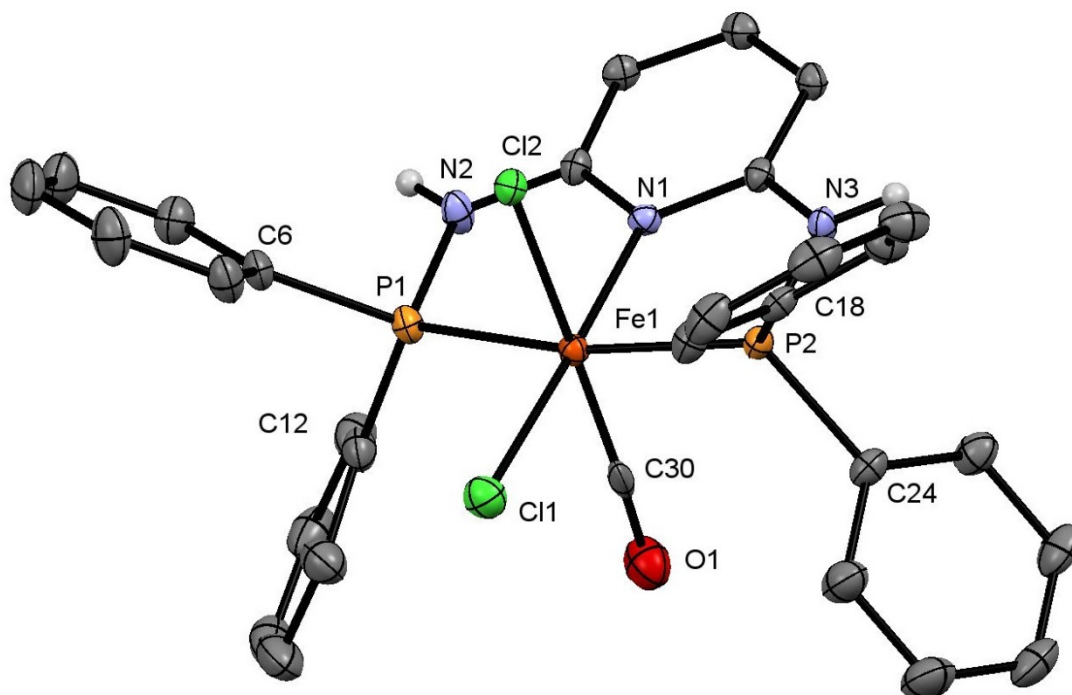
Figure 38: Molecular structure of **8**, showing 50% thermal ellipsoids (H-atoms, solvents and Cl⁻ omitted for clarity). Selected bond lengths (Å) and bond angles (deg): Fe1-P1 2.230; Fe1-P2 2.231; Fe1-N1 1.989; Fe1-Cl1 2.326; Fe1-Cl2 2.342; Fe1-C30 1.798; P1-N3 1.687; P2-N3 1.683; N2-C1 1.376; N3-C5 1.374; C30-O1 1.092; P1-Fe1-P2 166.77(2); Cl1-Fe1-Cl2 92.30(2); Cl1-Fe1-C30 85.58(7); Fe1-C30-O1 174.6(2); Cl1-Fe1-N1 178.04/5)

As previously reported, neutral carbonyl complexes bearing the PNP-*i*Pr ligand can displace the CO ligand when heating up the compound under reduced pressure to afford the yellow pentacoordinated unsaturated starting material [Fe(PNP-*i*Pr)Cl₂].[26] Hence we heated complex **8** to cleave off the labile CO ligand and we obtained a pale olive green compound. Compared to the [Fe(PNP-*i*Pr)(CO)(Cl)₂] compound only 110°C under reduced pressure were needed instead of 200°C to produce the presumably pentacoordinated [Fe(PNP-Ph)Cl₂] complex **10**; the CO ligand was removed faster. Flushing the flask containing **10** with gaseous CO, the

compound turns red again and according to IR complex **8** is regenerate. The proposed reaction is shown in Scheme 13.
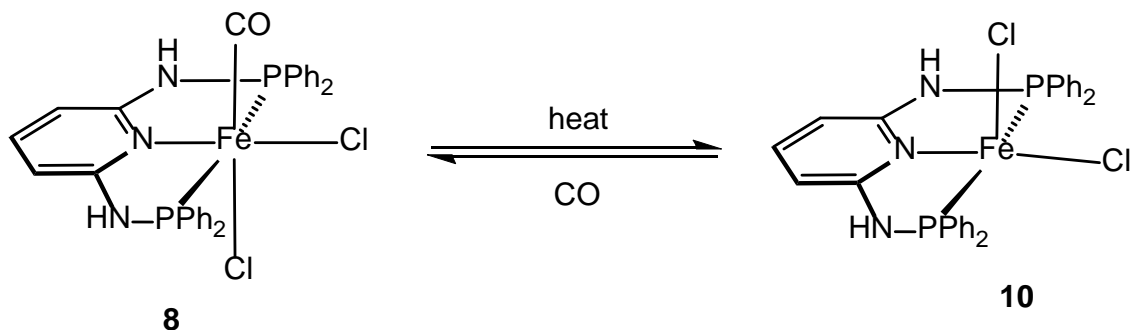
Scheme 13: CO displacement and recoordination of an iron(II) complex with the PNP-Ph ligand

Exposing compound **10** to air, it turns instantly brown upon decomposition (CO addition is impossible) showing that this complex is far more air sensitive than the closely related [Fe(PNP-iPr)Cl$_2$], which can be handled at air.

The same reaction was performed using UV-VIS (Figure 39) and IR (Figure 40) spectroscopy with a diffuse reflection chamber where we could observe decarbonylation of the starting material to afford **10**. Purging the chamber with pure CO gave the starting material **8**. No further characterization of **10** can be performed because dissolving the compound in any convenient solvent like THF or CH$_2$Cl$_2$ leads to the green [Fe(κ^3-P,N,P-PNP)(κ^2-P,N-PNP)Cl]$^+$ complex **2**. For UV-VIS the whole spectrum was recorded, for the time resolved IR only the CO stretching frequency was monitored.

The IR as well as the UV-Vis spectroscopy shows the reversibility of the CO addition for at least 4 cycles without any noticeable decomposition.
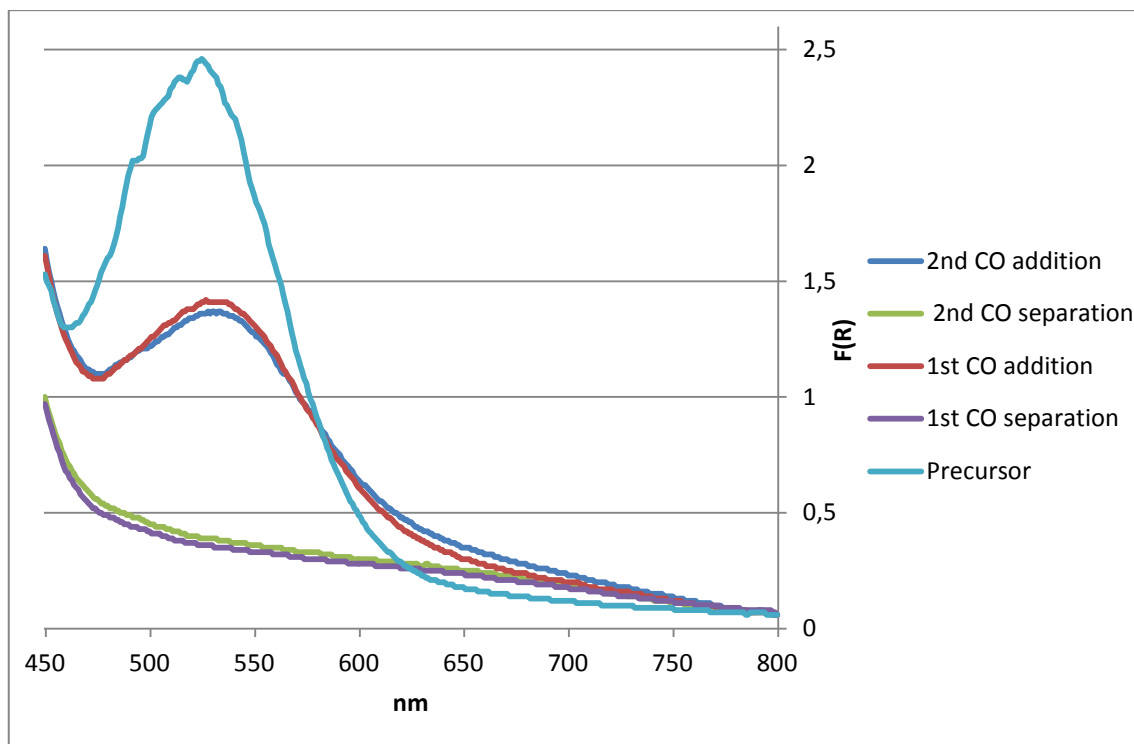
Figure 39: UV-Vis CO cleavage and recoordination on complex **8**

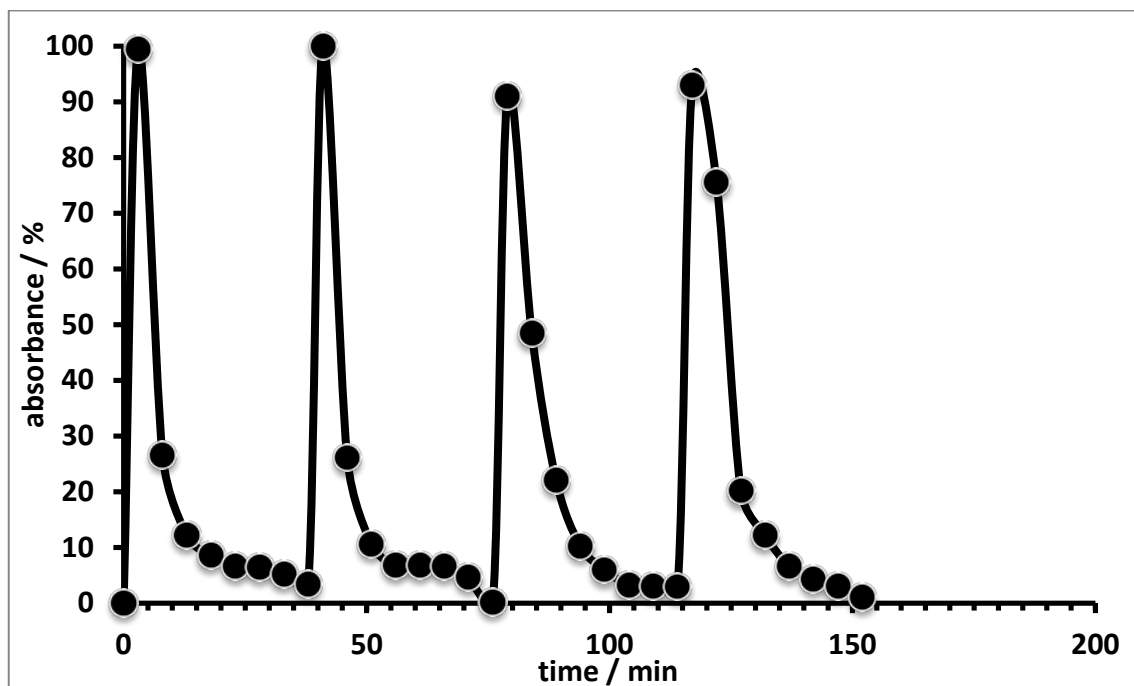**Figure 40:** IR of CO cleavage and recoordination on complex **8**

Compared to the [Fe(PNP-iPr)(CO)(Cl)$_2$] complex which forms the blue *trans* halide compound in solution, complex **8** bearing the PNP-Ph as a ligand only forms the red *cis*-Cl compound in

solution as well as in solid state.[26] Further this new system shows faster desorption at lower temperatures, the CO-addition rate seems to be the same.

As mentioned before also the cationic complex [Fe(PNP-Ph)(CO)$_2$Cl]$^+$ **9** was synthesized by two different approaches. Adding 1eq Ag$^+$ salt (AgBF$_4$ and AgSbF$_6$ were used) to the complex [Fe(PNP-Ph)(CO)(Cl)$_2$] **8** in THF while bubbling CO through the solution affords the red cationic *trans*-[Fe(PNP-Ph)(CO)$_2$Cl]$^+$ compound *trans*-**9** in 85% yield. Further this complex is formed as a side product during the synthesis of complex [Fe(PNP-Ph)(CO)(Cl)$_2$] **8** indicating that the counterion may play an important role.

Compound **9** was successfully synthesized by bubbling CO gas through a solution of [Fe(κ^3-*P,N,P*-PNP-Ph)(κ^2-*P,N,P*-PNP-Ph)$_2$Cl]BF$_4$ **2BF$_4$** forming **1a** as a side product, which can be removed by washing **9** with Et$_2$O. The solution turns immediately red when CO is introduced by cleaving off the κ^2 *P,N* bound PNP-Ph ligand. The reactions for the synthesis of **9** are shown in Scheme 14.
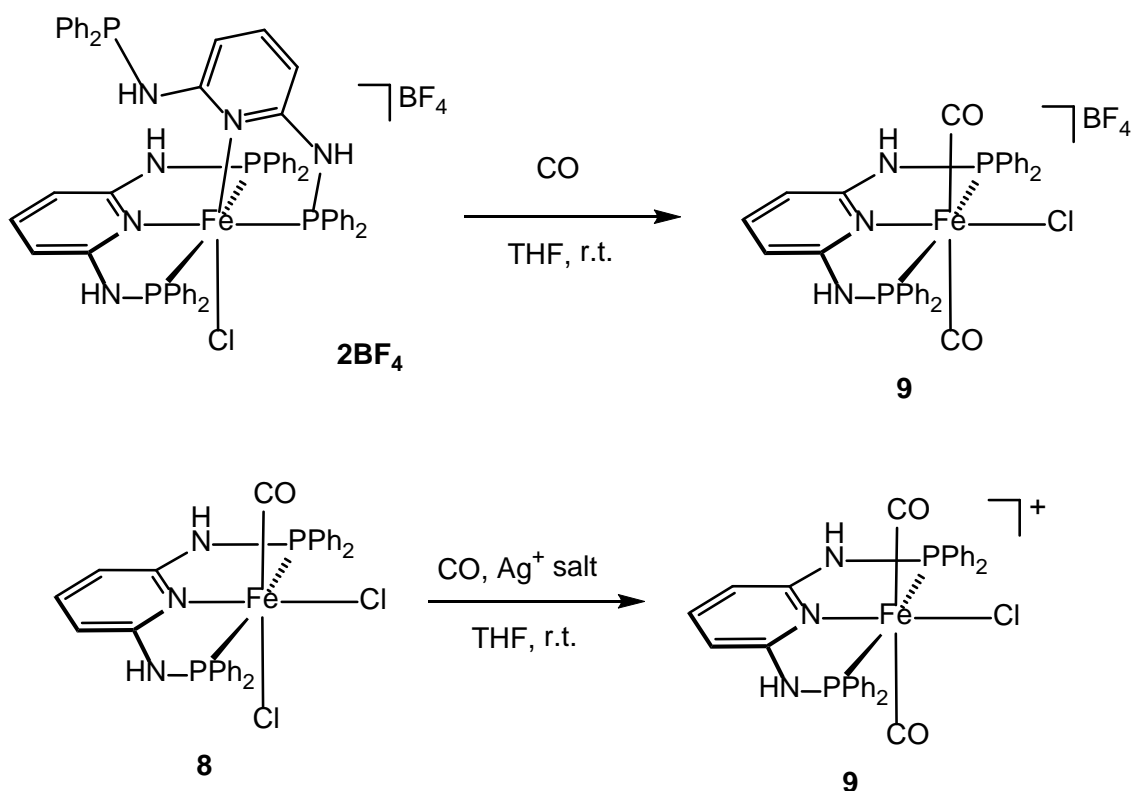
Scheme 14: Synthesis of complex **9**

Complex **9** was fully characterized by ^{1}H, ^{13}C{^{1}H} and ^{31}P{^{1}H} NMR as well as IR spectroscopy. Suitable crystals for X-ray diffraction were grown by slow diffusion of Et$_2$O to a saturated solution of **9** in THF. While the ^{1}H NMR spectra was not very informative due to the overlapping of the aromatic rings in the phenyl area, the ^{31}P{^{1}H] NMR exhibits a single peak at

85 ppm and the IR shows the asymmetric CO stretching frequency v_{CO} at 2031 cm^{-1} for the mutually *trans* CO ligands. The symmetric CO stretching band is IR inactive and thus not observed. For comparison, the related complex *trans*-[Fe(PNP-*i*Pr)(CO)$_2$Cl]$^+$ exhibits the CO stretch at 2015 cm^{-1} [29]. We had the same observation with the Fe(PNP-*i*Pr) carbonyl complexes where the cationic compounds had there v_{CO} band at higher wavenumbers. In the ^{13}C{^{1}H} NMR spectrum the two CO ligands exhibit a single low-intensity triplet resonance 207.2 ppm with a coupling constant J_{CP} of 25.8 Hz, thus, clearly revealing that the two CO ligands are *trans* to one another. Complex **9** is a thermally robust red solid that is air stable both in the solid state and in solution for several days.

Further single crystals suitable for X-ray diffraction were grown by slow diffusion of Et$_2$O in a saturated solution of **9SbF$_6$** in THF. The molecular structure of **9** is shown in Figure 41 with selected bon length and bond angles given in the caption.
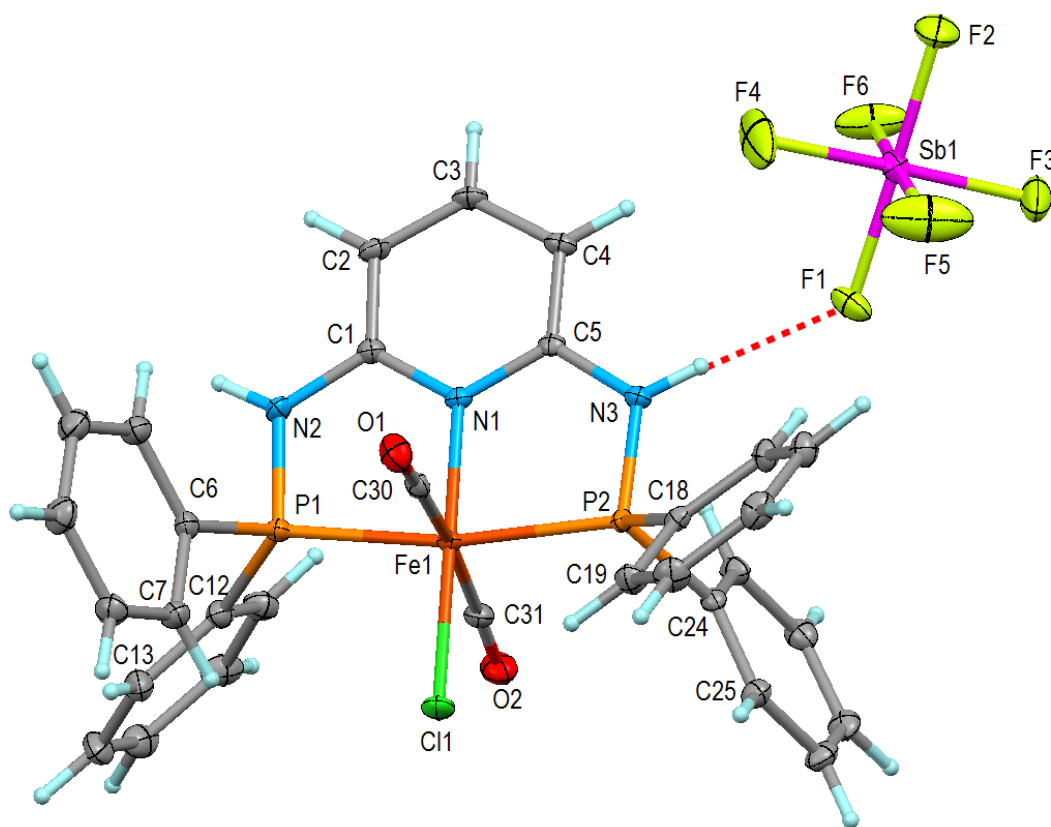
Figure 41: Molecular structure of **9**, showing 50% thermal ellipsoids, Fe(1)-C(30) 1.824(3); Fe(1)-C(31) 1.850(3); Fe(1)-N(1) 1.977(2); Fe(1)-P(2) 2.2190(7); Fe(1)-P(1) 2.2317(7); Fe(1)-Cl(1) 2.3029(7); C(30)-Fe(1)-C(31) 172.58(12); P(2)-Fe(1)-P(1) 168.33(3); O(1)-C(30)-Fe(1) 178.1(2); O(2)-C(31)-Fe(1) 173.6(2)

Further complex **4** was also studied in the reactivity towards CO to investigate the lability of the κ^2 *P,N* bound moiety As expected, bubbling CO through a solution of **4** affords the carbonyl compounds [Fe(PNP^{Me}-Ph)(CO)(Cl)$_2$] **11** and *trans*-[Fe(PNP^{Me}-Ph)(CO)$_2$Cl]$^+$ **12** depending on the

counterion as described in this chapter with complex **2**. Both compounds were washed with Et$_2$O for purification. They are red, air and moisture stabile compounds and can be stored under air without decomposition. Compound **12** can also be afforded by reacting **11** with AgBF$_4$ under CO atmosphere while **11** is afforded by reacting 1 equiv of FeCl$_2$ with 1 equiv of **1m** while bubbling CO through the solution in THF. The synthesis **11** and **12** are shown in Scheme 15.
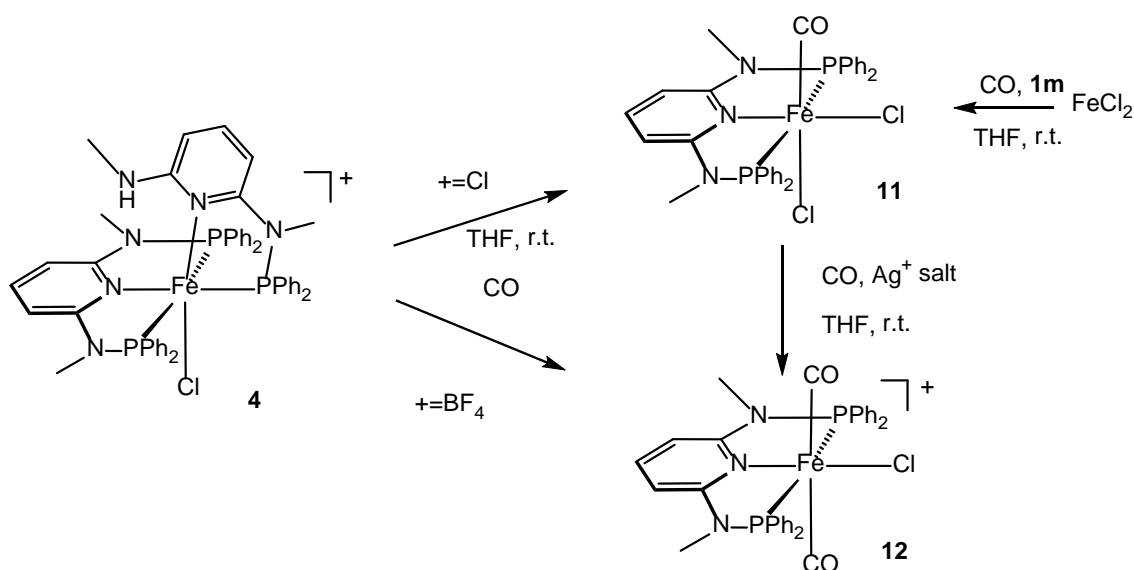
Scheme 15: Synthesis of **11** and **12**

Also complex **5** was tested in the reactivity towards CO and as it was expected the κ^2 *P,N* bond ligand was displaced. Both complexes [Fe(PNP-*p*Me-Ph)(CO)(Cl)$_2$] **13** and *trans*-[Fe(PNP-pMe-Ph)(CO)$_2$Cl]$^+$ **14** were afforded by bubbling CO through a solution of **5** in THF, depending on the counterion. Compound **14** can also be synthesized from **13** by reacting it with a silver salt under CO atmosphere. Both compounds were washed with Et$_2$O for purification. They are red, air and moisture stabile compounds and can be stored under air without decomposition. The synthesis is shown in Scheme 16.
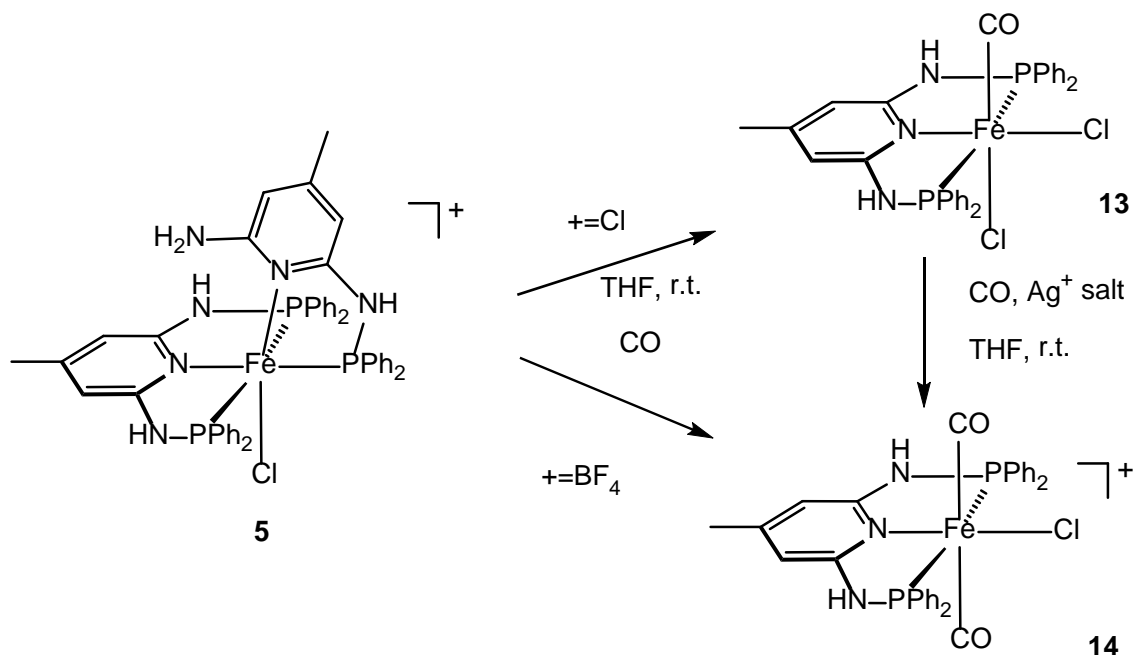
Scheme 16: Synthesis of complexes **13** and **14**

The complexes **11-14** were was fully characterized by ^{1}H, ^{13}C{^{1}H} and ^{31}P{^{1}H} NMR as well as IR spectroscopy. The complexes can easily be distinguished by ^{31}P{^{1}H} NMR and IR spectroscopy exhibiting a single signal and the asymmetric CO stretching frequency respectively. In the ^{13}C{^{1}H} NMR spectrum the CO ligands exhibit a single low-intensity triplet resonance with a given coupling constant. The cationic complexes exhibit a single signal in the IR as well as in the ^{13}C{^{1}H} NMR clearly revealing that the two CO ligands are *trans* to one another. The IR and the NMR data is summarized in Table 5.

Table 5: Spectroscopic data of PNP-Ph carbonyl complexes, *) NMR measurements not possible due to sample precipitation after 30 min

	ν_{CO} [cm^{-1}]	^{31}P{^{1}H} NMR [ppm]	^{13}C{^{1}H} NMR [ppm], *J* [Hz]
8	1985	88	216.92 J_{CP} = 29
9	2031	85	207.19 J_{CP} = 25.8
11	1961	115.1	216.39 J_{CP} = 28.9
12	2012	111.2	206.89 J_{CP} = 25.4
13	1974	87.5	*)
14	2038	85.8	207.65 J_{CP} = 25.8

In this survey the reactivity of the model complex **7** [Fe(PNP-Ph)(PN-Ph)Cl]BF$_4$ bearing two different ligands, towards CO was investigated because it shows similarities to the κ^3, κ^2 compounds; the phosphorus atom of the κ^2 coordinating ligand is *trans* to the pyridine of the second ligand and the chloro ligand is *trans* to the pyridine of the κ^3 coordinating ligand.

Interestingly no reaction took place, even at reflux and stirring **7** under CO atmosphere for several days. Due to the more steric demanding pendant phosphine arm and the free amine moiety respectively the pincer type ligand is more easily displaced than a bidentate ligand. The crystal structure shows that the pendant arm is very close to the second pyridine ring and forms an H-bond between the amine moiety and the pyridine N, hence more labile.

5. Heterolytic dihydrogen cleavage with an iron(II) PNP pincer complex vie metal-ligand cooperation

In organometallic chemistry, dihydrogen cleavage may occur *via* different methods. The most classic mechanism is the oxidative, the coordinated dihydrogen molecule is cleaved leaving two hydride ligands on the metal center. The reaction is shown in Scheme 17.
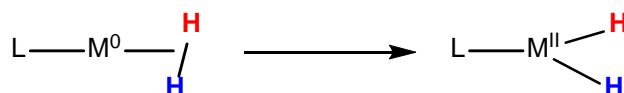
Scheme 17: Dihydrogen cleavage via the oxidative addition mechanism

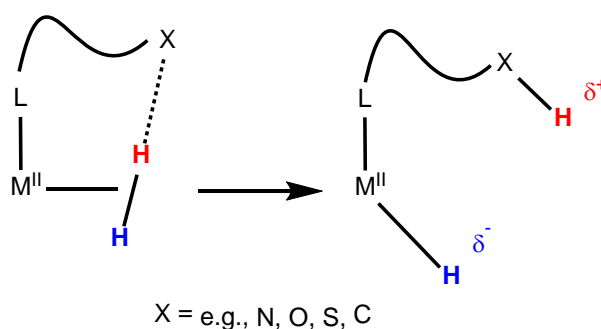An interesting way of bond activation by metal-ligand cooperation involves aromatization/dearomatization of the ligand in pincer type complexes.[35,88,89] In particular, pincer ligands in which a central pyridine-based backbone is connected with -CH_2PR_2 and/or CH_2NR_2 substituents were shown to exhibit this behavior.[89,90] This has resulted in the development of novel and unprecedented transition metal chemistry both under stoichiometric and catalytic[58,91,92] conditions involving, for instance, H-H, O-H, N-H, and C-H bond activation. Very recently, Milstein and coworkers also discovered highly efficient pyridine-based PNP pincer iron complexes that catalyze hydrogenation of ketones to alcohols, and hydrogenation of CO_2 to formate salts,[83] where this type of cooperation plays a key role in the heterolytic cleavage of H_2. In general, splitting of a highly acidic coordinated H_2 ligand in a fashion that a proton is accepted by an external or more efficiently by an internal Lewis base X (where X can be N, O, S, C, etc. donors) to leave a hydride ligand on the metal center was extensively studied in recent year (see Scheme 18).[93] The main difference to the oxidative addition is that the metal center keeps its oxidation state. Further Scheme 19 shows the bond activation by metal-ligand cooperation may involve aromatization/dearomatization of the ligand in pincer type complexes.

Scheme 18: Metal assisted H_2 cleavage

Scheme 19: Bond activation by metal-ligand cooperation may involve aromatization/dearomatization of the ligand in pincer type complexes

In the course of our investigations we observed that a reversible aromatization/dearomatization reaction, a prerequisite for heterolytic H-H activation, could be achieved in dicationic Fe(II) PNP complexes. In fact, treatment of the [Fe(PNP-BIPOL)(CH$_3$CN)$_3$]$^{2+}$ with an excess of NaHg (3%) resulted in an immediate evolution of H$_2$ gas affording the deprotonated and dearomatized monocationic complex [Fe(PNP-BIPOL)(CH$_3$CN)$_3$]$^+$ as shown in Scheme 20. This complex was also characterized by X-ray crystallography (see Figure 42). The deprotonation was reversible and addition of HBF$_4$ to a solution of [Fe(PNP-BIPOL)(CH$_3$CN)$_3$]$^+$ cleanly afforded the starting material where the pyridine ring regained full aromaticity.[25]

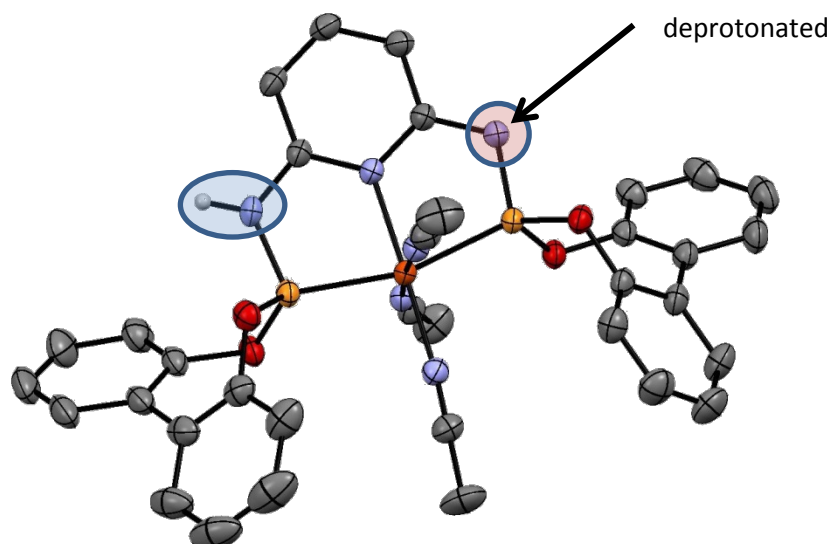**Scheme 20:** H$_2$ generation by treating an iron(II) pincer complex with Na/Hg

deprotonated

Figure 42: Molecular structure of a deprotonated Fe PNP pincer complex

In an attempt to obtain the Fe(0) complex [Fe(PNP-iPr)(CO)$_2$], the bis-carbonyl Fe(II) complex *trans*-[Fe(PNP-iPr)(CO)$_2$Cl]$^+$ **15** (as SbF$_6^-$ salt) was treated with Zn as reducing agent at room temperature in solvents such as THF, toluene, or dioxane. Surprisingly, instead of the expected Fe(0) complex the Fe(II) mono hydride *cis*-[Fe(PNP-iPr)(CO)$_2$H]$^+$ (**17**) was obtained in 40% isolated yield together with several intractable materials (see Scheme 21).
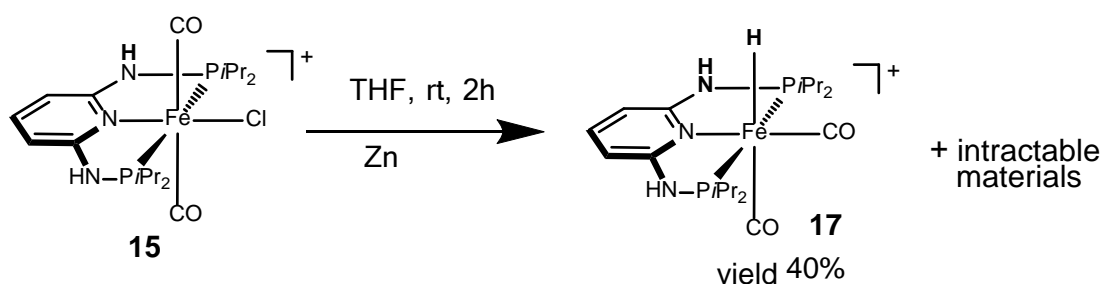
Scheme 21: Synthesis of an iron(II) hydride

The formation of this species was independent of whether deuterated or non-deuterated solvents were used, e.g. THF-d_8, toluene-d_8, or dioxane-d_8. If, on the other hand, **15** was reacted with Zn under a dihydrogen atmosphere (1 bar) **17** was afforded in 97% isolated yield. This clearly suggests that in the first case the hydride ligand solely originates from the acidic NH protons of the PNP ligand which are reduced to H$_2$ with concomitant formation of Zn^{2+} ions. The latter acts as a chloride scavenger.

IR and NMR monitoring of the reaction of **15** with Zn in THF-d_8 revealed that the formation of **16** proceeds *via* the *bis*-carbonyl intermediate *cis*-[Fe(PNP-iPr)(CO)$_2$Cl]$^+$ (**16**) as shown in Scheme 21. It has to be noted that the isomerization of **15** to **16** takes place only to some

extent and these species are apparently in equilibrium with one another. Accordingly, under this condition isolation of pure **16** was not possible. However quantitative isomerization of **15** (in the form of its BAr'_4^- (Ar' = 3,5-$C_6H_3(CF_3)_2$) salt) to **16** took place in CH_2Cl_2 as solvent if kept in the dark for several days. The BAr'_4 salt was used due to solubility reasons, BAr'_4 salts are very good soluble in every convenient solvent. If exposed to visible light complex **15** was reformed within 3 hours. While **15** exhibits a single ν_{CO} band at 2013 cm^{-1}, **16** displays the expected two signals of the symmetric and asymmetric CO stretching frequency at 2050 and 2001 cm^{-1}. In the $^{31}P\{^1H\}$ NMR **15** exhibits a singlet at 118.5 ppm, whereas the *cis*-CO complex **16** gives rise to a singlet at 134.2 ppm. Characteristic features in the $^{13}C\{^1H\}$ NMR spectrum of **16** are two low-field triplet resonances centered at 209.4 (J_{CP} = 17.4 Hz) and 208.4 ppm (J_{CP} = 22.7 Hz) assignable to the carbonyl carbon atoms *trans* and *cis* to the pyridine nitrogen, respectively. The starting material **15** displays only one triplet for the two CO carbon atoms centered at 211.6 ppm (J_{CP} = 24.4 Hz).

Complex **17** is a thermally robust pale yellow solid that is air stable in the solid state but slowly decomposes in solution. Characterization was accomplished by elemental analysis and by ^1H, $^{13}C\{^1H\}$, and $^{31}P\{^1H\}$ NMR, and IR spectroscopy. The ^1H NMR spectrum confirmed the presence of one hydride ligand, which appeared at -7.47 ppm (see Figure 43) as a well-resolved triplet with a $^2J_{HP}$ coupling constant of 47.7 Hz. The hydride section of the 1H NMR is displayed in Figure 43. In the $^{13}C\{^1H\}$ NMR spectrum the most noticeable resonances are the two low-field resonances of the carbonyl carbon atoms *trans* and *cis* to the pyridine nitrogen observed as two triplets centered at 212.2 (J_{CP} = 20.2 Hz) and 207.5 ppm (J_{CP} = 11.8 Hz), respectively. The $^{31}P\{^1H\}$ NMR spectrum of complex **17** gives rise to a singlet at 162.8 ppm. In the IR spectrum the two bands for the symmetric and asymmetric CO stretching frequencies are found at ν_{CO} 2027 and 1969 cm^{-1}.
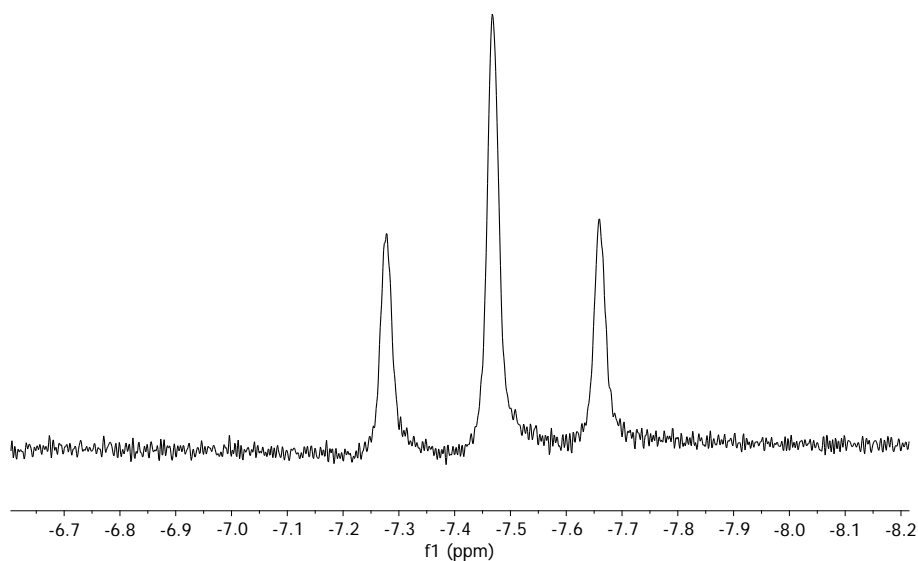
Figure 43: ^{1}H NMR of **17** showing the hydride region

In addition to the spectroscopic characterization, the solid state structure of **17** was determined by single-crystal X-ray diffraction. The molecular structural is shown in Figure 44 with selected bond distances and bond angels given in the caption. Complex **17** adopts a distorted octahedral geometry around the metal center with the hydride ligand being in *trans* position to a CO ligand. The PNP ligand is coordinated to the iron center in a typical tridentate meridional mode, with a P1-Fe1-P2 angle of 159.76(4)°. The Fe-C bonds of the CO ligand *trans* to the pyridine nitrogen of the PNP ligand is slightly shorter than the one *cis* to the PNP moiety due to the stronger *trans* influence of the hydride as compared to the pyridine ligand being 1.752(4) and 1.811(3) Å. The hydride and the N-H atoms could be unambiguously located in the difference Fourier maps. The Fe-H distance was restrained to 1.46(2) Å
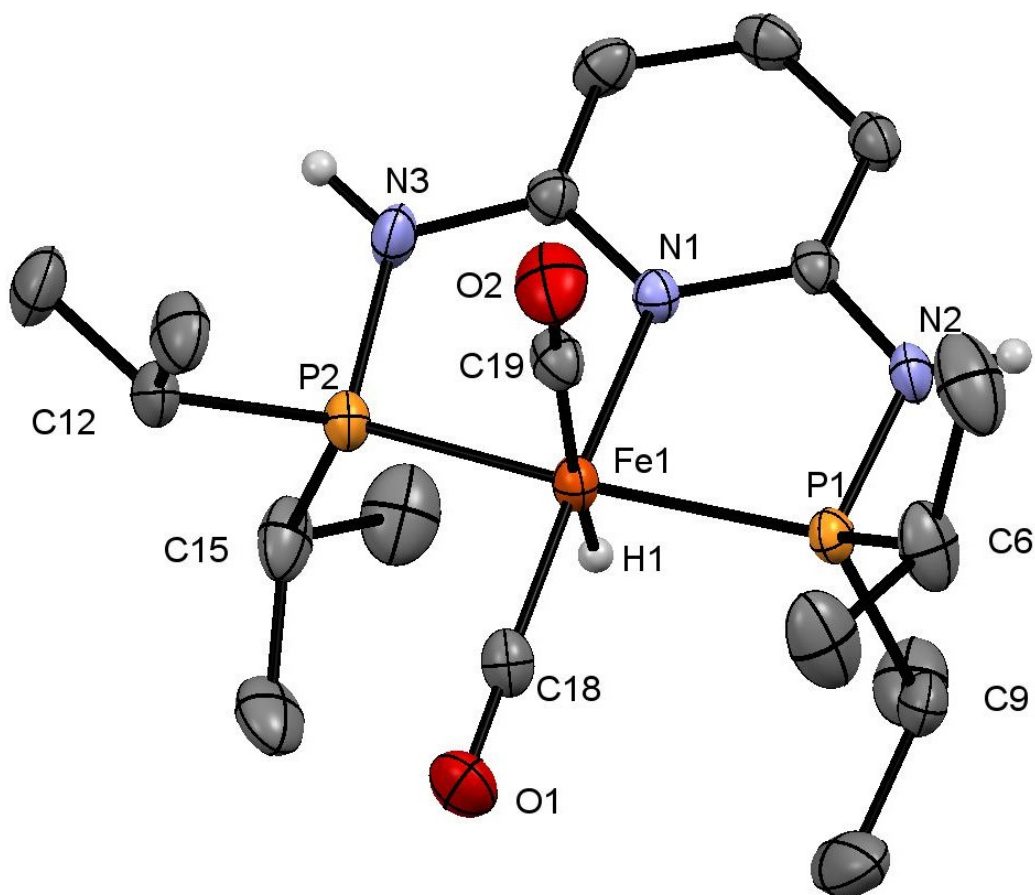
Figure 44: Molecular structure of **17**, showing 50% thermal ellipsoids (H-atoms, and counterion omitted for clarity). Selected bond lengths (Å) and bond angles (deg): Fe1-P1 2.198(2), Fe1-P2 2.112(2), Fe1-N1 2.007(3), Fe1-C18 1.752(4), Fe1-C19 1.811(3), Fe1-H1 1.45(2), P1-Fe1-P2 159.76(4), C18-Fe1-C19 97.6(2), N1-Fe1-C18 171.4(2), Fe1-C18-O1 177.1(3), Fe1-C19-O2 177.0(3)

A reasonable mechanism which accounts for the formation of *cis*-[Fe(PNP-*i*Pr)(CO)$_2$H]$^+$ (**17**) is proposed in Scheme 22. Upon partial isomerization of *trans*-[Fe(PNP-*i*Pr)(CO)$_2$Cl]$^+$ (**15**) to the thermodynamically more stable isomer *cis*-[Fe(PNP-*i*Pr)(CO)$_2$Cl]$^+$ (**16**), reduction of the acidic NH protons of the PNP-*i*Pr ligand by Zn results in the release of H$_2$ and concomitant formation of Zn^{2+} ions. The latter act as halide scavenger abstracting the chloride ligand and the coordinatively unsaturated cationic 16e complex [Fe(PNP^H-*i*Pr)(CO)$_2$]$^+$ (**A**) is formed. This step is also accompanied by dearomatization of the pyridine moiety. This species readily binds H$_2$ and yields [Fe(PNP^H-*i*Pr)(CO)$_2$(η^2-H$_2$)]$^+$ (**B**). Heterolytic cleavage of the coordinated and thus activated H$_2$ ligand finally results in the formation of the hydride complex **17**.
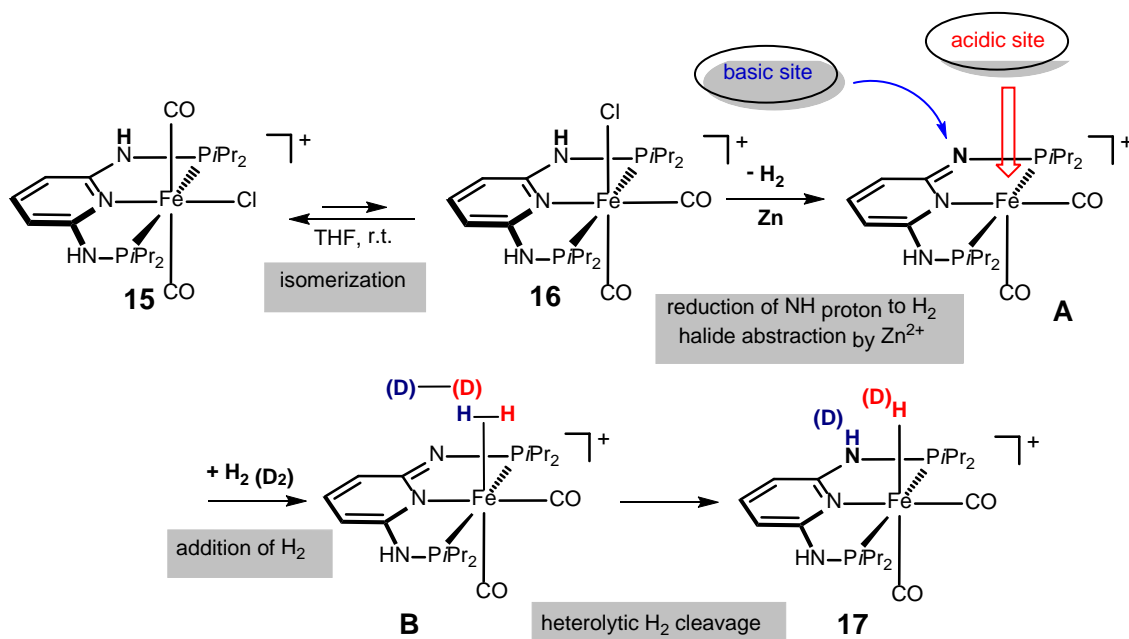
Scheme 22: Mechanism for the formation of cis-[Fe(PNP-*i*Pr)(CO)$_2$H]$^+$

In order to obtain further evidence in the proposed mechanism, several experiments including deuterium labeling studies were performed under the same reaction conditions. Broad deuteride and N-D signals were observed in the ^{2}H NMR spectrum when D$_2$ was used in place of H$_2$ due to the formation of the corresponding isotopologue of **17**, giving rise to deuterium resonances at 6.0 (N-D) and -7.5 ppm (Fe-D). The ^{2}H NMR is shown in Figure 45. The yield dropped to about 75% apparently due to a kinetic isotope effect (KIE), indicating that the H-H cleavage process is involved in the rate determining step. Increasing the reaction time from 2 to 4 h afforded 5 in 95%.
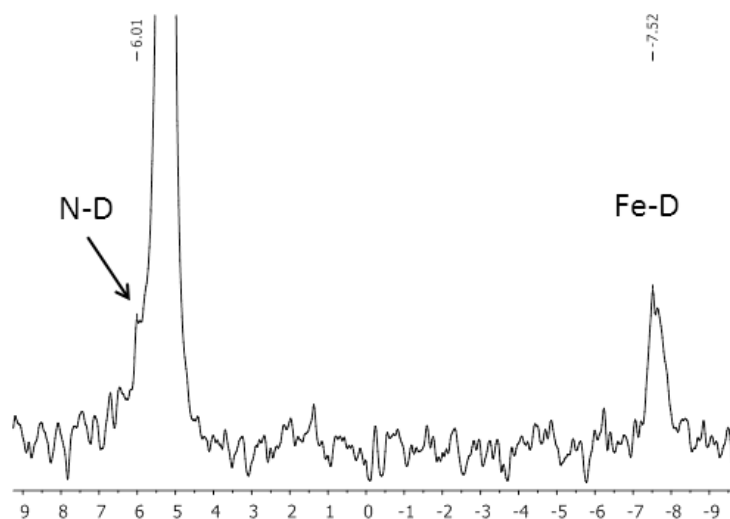
Figure 45: ^{2}H NMR of the isotopologue of **17**; Fe-D signal at -7.52 and N-D signal at 6.01 ppm

Further, the isotopologue **15-d2**, featuring N-D instead of N-H moieties, did not afford **17** under the same reaction conditions (see Scheme 23), pointing to a large KIE for the N-D bond cleavage under reductive conditions. Finally, as anticipated, also the N-methylated complex *trans*-[Fe(PNP^{Me}-*i*Pr)(CO)$_2$Cl]$^+$ **18** did not react with Zn in the absence or presence of H$_2$ (Scheme 23). Accordingly, all these experiments strongly favor our mechanistic proposal of an involvement of the acidic N–H protons of the PNP ligand and the iron center: i.e., metal–ligand cooperation.
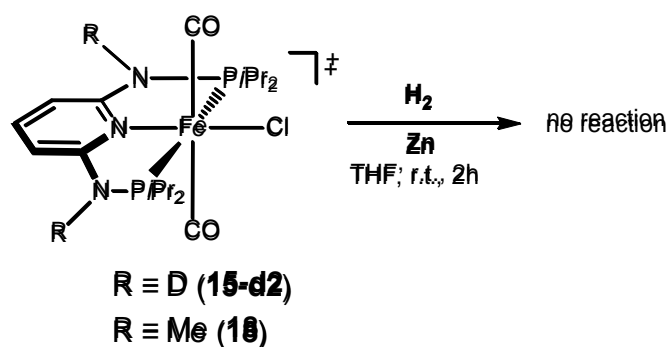
Scheme 23: Reaction with N-methylated and N-D ligands

The addition of H$_2$ to intermediate [Fe(PNP^H-*i*Pr)(CO)$_2$] (**A**) was also investigated by means of DFT calculations. The energy profile obtained is presented in Figure 46. Starting with the separated reactants there is formation of a van der Waals pair between the two reacting molecules, H$_2$ and [Fe(PNP^H-*i*Pr)(CO)$_2$]$^+$ (**A**), with a rather long Fe-C(CO) distance (5.67 Å), and the corresponding small stabilization of the system (3.9 kcal mol^{-1}). From here, [Fe(PNP^H-

iPr)(CO)$_2$(H$_2$)]$^+$ (**B**) is formed in a single step going over a negligible energy barrier (0.7 kcal mol$^-$^{1}). In the corresponding transition state, **TS$_{AB}$**, coordination of the dihydrogen molecule is only incipient with rather long Fe-H distances (2.83 and 3.18 Å) and an H-H bond length (0.74 Å) equal to the one existing in free H$_2$. In the final step of the mechanism, from **B** to **17**, occurs the splitting of the H-H bond with formation of the Fe-H hydride and protonation of the neighbor imine N-atom. In the transition state **TS$_{B4}$** the cleavage of the H-H bond is well advanced as shown by a distance of 0.92 Å, and there is a considerable distortion in the geometry of the PNP ligand in order to approach the imine N-atom to the incoming proton. Thus, in **TS$_{B4}$**, the pyridine ring is rotated with respect to the plane of the PNP ligand by an angle of 21° (taken as the angle between the mean plane defined by the six atoms of the pyridine ring and the one defined by the Fe-P-N-P frame.) bringing the incoming proton and the N-atom to a distance of only 1.55 Å. The last step is the rate limiting one of this path, with a calculated barrier of 22.8 kcal mol^{-1}, denoting a viable reaction.

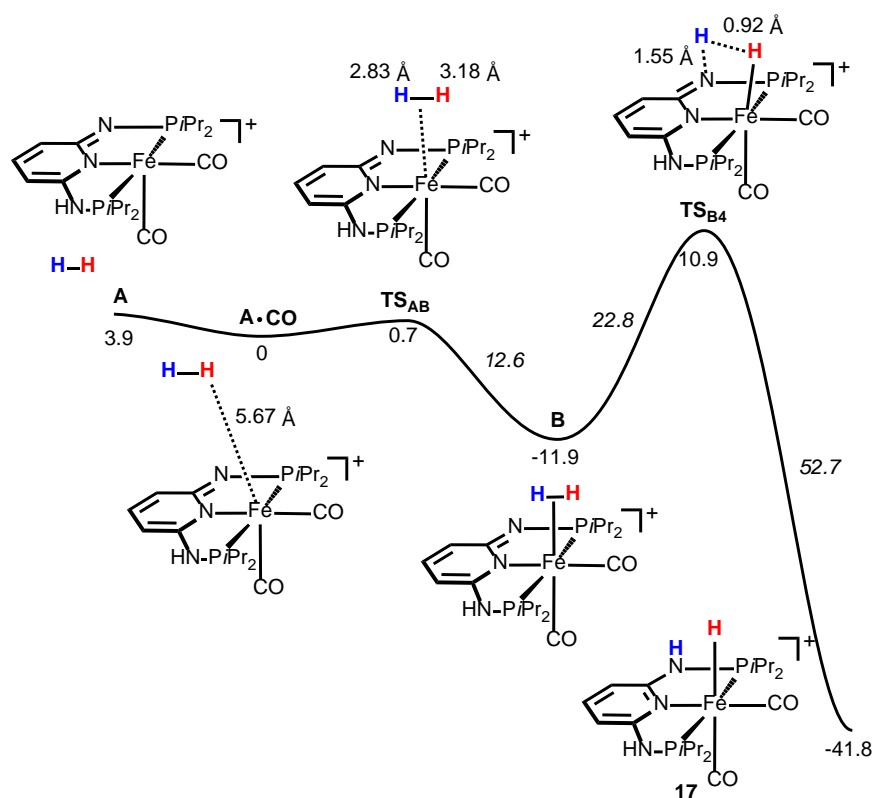**Figure 46:** Free energy profile for the intramolecular heterolytic dihydrogen cleavage and formation of octahedral cis-[Fe(PNP-iPr)(CO)$_2$H]$^+$ (**17**). Numbers in italics correspond to barriers and the relevant distances (Å) are indicated

6. Synthesis and reactivity of low valent iron PNP pincer complexes

6.1 Synthesis of iron(0) complexes from iron(II) compounds by reduction

In this work we also were interested in the synthesis of new Fe(0) compounds. We succeeded in synthesizing them by reducing the [Fe(PNP)(CO)Cl$_2$] complexes with strong reducing agents like Na/Hg or KC$_8$.

At first the synthesis of the Fe(0) complex [Fe(PNP-iPr)(CO)$_2$] (**21a**) was achieved by stirring [Fe(PNP-iPr)Cl$_2$] (**19a**) in THF with an excess of Na/Hg or KC$_8$ in the presence of carbon monoxide. While bubbling CO through the reaction mixture, the color changes immediately from blue, which is the intermediate **20a** to red. For the synthesis KC$_8$ turned out to be more convenient due to easier workup, and toxic Hg is avoided. After removing the remaining graphite by filtrating the solution over celite, this compound was obtained in 95% isolated yield as an air-sensitve but thermally stable orange solid. The identity of this complex was unequivocally established by ^{1}H, ^{13}C{^{1}H} and ^{31}P{^{1}H} NMR, IR spectroscopy, and elemental analysis. The synthesis of **21a** is depicted in Scheme 24.
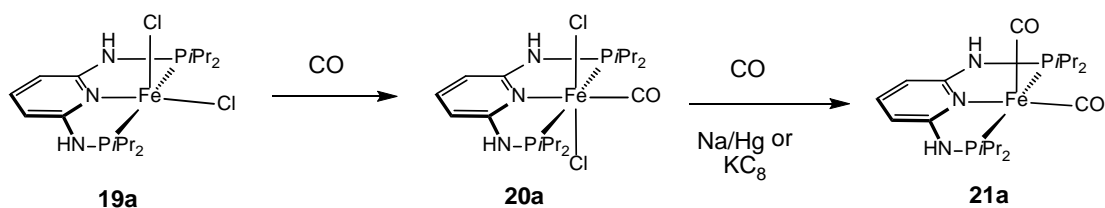
Scheme 24: Synthesis of **21a**

In the IR spectrum of **21a** in THF two intense carbonyl bands were observed for ν_{CO} at 1866 and 1816 cm^{-1}. For comparison, in the related Fe(0) complexes [Fe(PNP^{CH2}-iPr)(CO)$_2$] (PNP^{CH2}-iPr = bis(di-iso-propylphosphinomethyl)pyridine)[70] these bands were found at 1842 and 1794 cm^{-1}. The shift of the CO bands to somewhat higher frequencies is consistent with a less reducing Fe(0) centre in **21a** as compared to [Fe(PNP^{CH2}-iPr)(CO)$_2$], which is apparently the stronger π base to the coordinated CO. In the ^{13}C{^{1}H} NMR spectrum at -80°C the CO ligand gives rise to a low-field resonance triplet centered at 219.5 ppm with a coupling constant J_{CP} of 27.8 Hz. It has to be noted that at room temperature NMR measurements were impossible, because only signals for the free ligand were observed. In the ^{31}P{^{1}H} NMR spectrum gives rise to a singlet at 173.8 ppm.

Single crystals of **21a** were grown by cooling a saturated solution of CH$_2$Cl$_2$ and the molecular structure was determined by X-ray crystallography. The structural view is depicted in Figure 47

with selected bond distances and angles given in the caption. The overall geometry about the iron center is best described as distorted trigonal bipyramidal. For comparison, the related complexes [Fe(PNP^{CH2}-*i*Pr)(CO)$_2$] (PNP^{CH2}-*i*Pr = bis(di-*iso*-propylphosphino)pyridine) and [Fe(PhP[CH$_2$CH$_2$CH$_2$P(O*i*Pr)$_2$]$_2$)(CO)$_2$] adopt an almost perfect trigonal bipyramidal geometry[94], while the bulkier complex [Fe(PNP^{CH2}-*t*Bu)(CO)$_2$] (PNP^{CH2}-*t*Bu = bis(di-*tert*-butylphosphino)pyridine)[71] has an unusual square pyramidal structure. The two carbonyl ligands and the pyridine nitrogen define the equatorial plane with bond angles of 113.88(9), 127.45(7), and 118.67(7)° for C18-Fe1-C19, N1-Fe1-C18, N1-Fe1-C19, respectively. A significant distortion is observed in the axial phosphine ligands where the P1-Fe1-P2 bond angle of 163.01(3)° is contracted toward the pyridine ring. Moreover, one of the two Fe-C-O angles deviates significantly from linearity with Fe1-C19-O2 and Fe1-C18-O1 being 169.24(16)° and 175.47(15)°, respectively. The corresponding angles Fe2-C37-O3 and Fe2-C38-O4 of the crystallographically independent second complex are slightly larger being 172.72(15) and 176.29(18)°, respectively. A similar bending of the Fe-C-O angles was also observed in [Fe(PNP^{CH2}-*t*Bu)(CO)$_2$]. The Fe-C bond distances in **21a** are 1.719(2) and 1.737(2) Å for Fe1-C18 and Fe1-C19, respectively, which are similar to those in [Fe(PNP^{CH2}-*i*Pr)(CO)$_2$] (1.7325(9) Å) and [Fe(PNP^{CH2}-*t*Bu)(CO)$_2$] (1.7310(12) and 1.7708(12)Å).
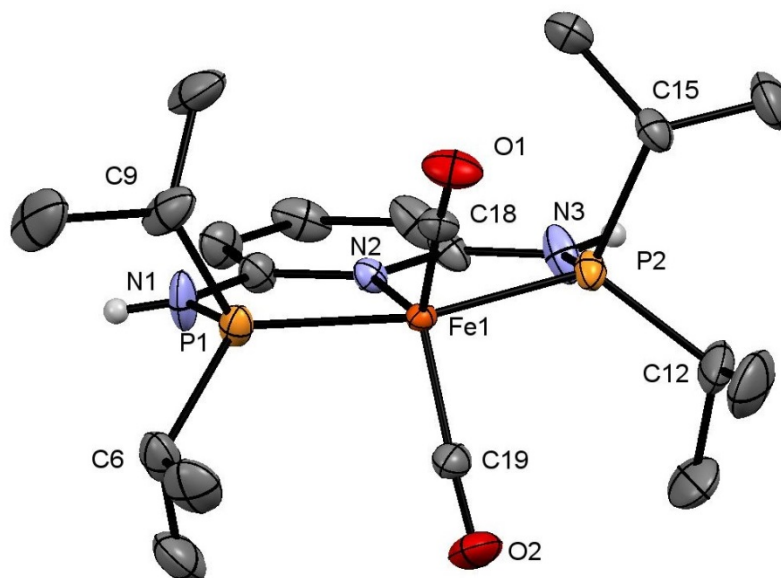
Figure 47: Structural view of [Fe(PNP-*i*Pr)(CO)$_2$]·CH$_2$Cl$_2$ (**21a·CH$_2$Cl$_2$**) showing 50% thermal ellipsoids (CH$_2$Cl$_2$ omitted for clarity). Only one of the two crystallographically independent complexes is shown, Selected bond lengths (Å) and bond angles (deg): P1-Fe1-P2 162.95(2); P1-Fe1-N2 82.80(4); P2-Fe1-N2 82.39(4); N2-Fe1-C18 127.27(7); N2-Fe1-C19 118.56(7); C18-Fe1-C19 114.17(8); Fe1-C18-O1 175.0(2); Fe1-C19-O2 169.0(2); Fe1-N2 2.034(3); Fe1-C18 1.719(2); Fe1-C19 1.737(2); Fe1-P1 2.189(2); Fe1-P2 2.188(3)

The calculated structure of **21a** is in excellent agreement with the crystallographically determined one and selected bond distances and angles are provided in Table 6. These gas phase calculations also reproduce very well the Fe-C-O angles and thus the bending seems to be not the results of crystal packing effects.[71]

Table 6: Selected experimental and calculated bond lengths and angles of [Fe(PNP-*i*Pr)(CO)$_2$] (**21a**) and [Fe(PNP^{CH2}-*i*Pr)(CO)$_2$];[a] crystallographically independent complexes, [b] taken from ref [70].

	Fe(PNP-*i*Pr)(CO)$_2$		Fe(PNP^{CH2}-*i*Pr)(CO)$_2$
	X-ray [a]	calcd	X-ray [b]
	Bond Lengths (Å)		
Fe1-N1/Fe2-N4	2.034(3)	2.032(3)	2.084	2.0684(8)
Fe1-C18/Fe2-C37	1.719(2)	1.745(3)	1.758	1.7325(9)
Fe1-C19/Fe2-C38	1.737(2)	1.755(3)	1.745	1.7325(9)
Fe1-P1/Fe2-P3	2.189(3)	2.172(3)	2.220	2.1941(2)
Fe1-P2/Fe2-P4	2.188(3)	2.178(3)	2.220	2.1941(2)

	Bond Angles (deg)		
Fe1-C18-O1/Fe2-C37-O3	175.47(15)	176.29(18)	175.4	174.84(11)
Fe1-C19-O2/ Fe2-C38-O4	169.24(16)	172.72(15)	173.9	174.84(11)
C18-Fe1-C19/C37-Fe2-C38	113.88(9)	116.31(10)	117.0	119.91(7)
C18-Fe1-N1/C37-Fe2-N4	127.45(7)	129.48(8)	131.2	120.04(3)
C19-Fe1-N1/C38-Fe2-N4	118.67(7)	114.21(8)	111.7	120.04(3)
C18-Fe1-P1/C37-Fe2-P3	91.00(6)	92.34(6)	92.6	91.83(3)
C19-Fe1-P1/C38-Fe2-P3	97.09(6)	95.65(6)	95.6	91.83(3)
P1-Fe1-P2/P3-Fe2-P4	163.01(3)	162.57(3)	164.2	165.990(12)

The frontier orbitals of **21a** are the expected ones for a trigonal bipyramidal d^8 complex (TBP),[95] with the five metal d orbitals split into the 2+2+1 set that would correspond to orbitals e'', e' and a$_1$' in a symmetric complex (Figure 48). Thus, the first two orbitals (HOMO-4 and HOMO-2) are perpendicular to the equatorial plane (the N$_{py}$–C$_{CO}$–C$_{CO}$ plane) and correspond to the e'' set of a perfect TBP complex; the following pair (HOMO and HOMO-1) is located on the equatorial plane and correspond to e' in a perfect TBP geometry; finally, the less stable one (LUMO+3) corresponds to the z^2 orbital aligned with the axial ligands, the two P-atoms, and it is the equivalent to a$_1$' in a totally symmetric TBP molecule.
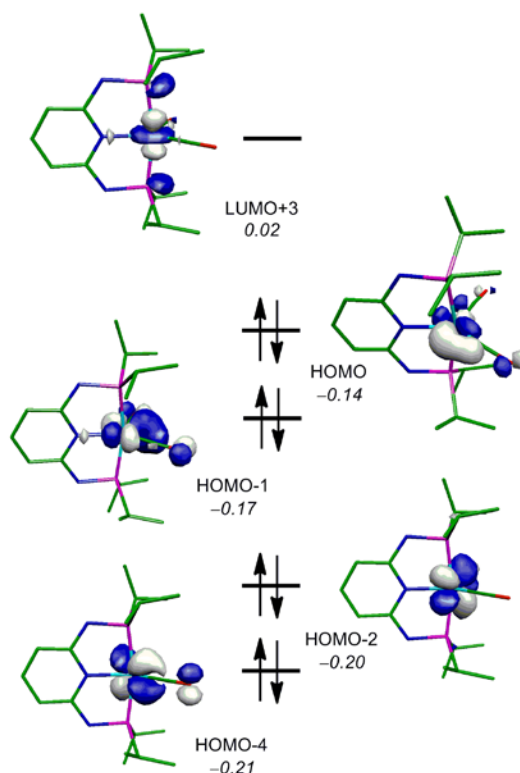
Figure 48: Frontier orbitals (d-splitting) of [Fe(PNP-iPr)(CO)$_2$] (**21a**). H-atoms are omitted for clarity and the energy values (atomic units) are presented in italics

The complex [Fe(PNP-tBu)X$_2$] (X = Cl, Br) **19b** was also tested in the reactivity towards carbon monoxide. Complex **19a** reacts with CO in solution as well as in solid state to afford the mono CO complex. The complex **19b** however does not react with CO, even stirring the complex under CO atmosphere over the weekend gave no conversion, and the IR does not show any frequency for CO. The PNP-tBu ligand, being very bulky, blocks the CO coordination. We tried to abstract a halide using a silver salt to obtain a cationic [Fe(PNP)(CO)$_2$X]$^+$ complex, but only insoluble material was isolated. Also the reaction with NaBH$_4$ did not afford any desired product (see Scheme 25).
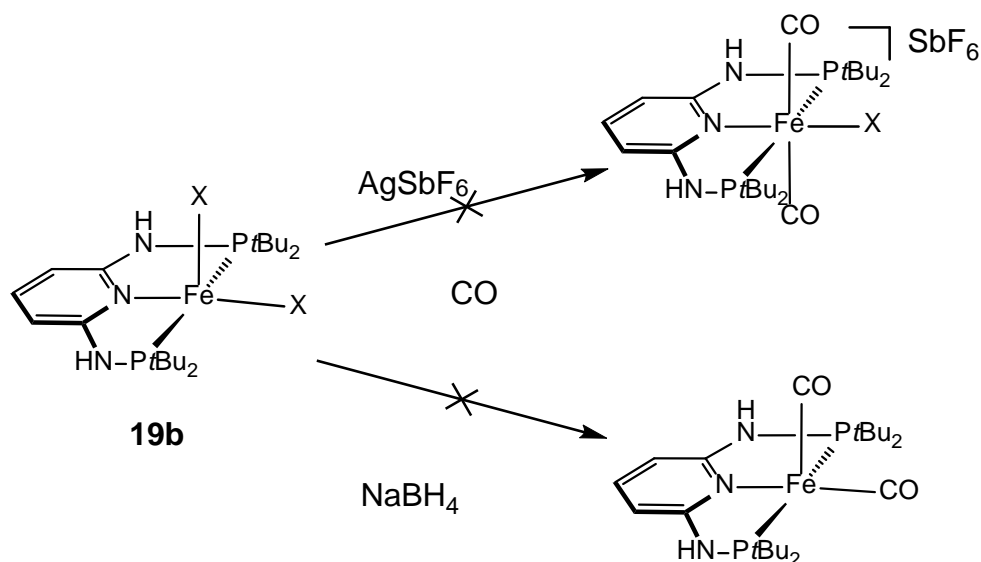
Scheme 25: Attempted reaction of **19b** with CO in the presence of AgSbF$_6$ and NaBH$_4$

The synthesis of the Fe(0) complex [Fe(PNP-*t*Bu)(CO)$_2$] (**21b**) was achieved by stirring [Fe(PNP-*t*Bu)Cl$_2$] (**19b**) in THF with an excess of Na/Hg or KC$_8$ in the presence of carbon monoxide. While bubbling CO through the reaction mixture, the color changes immediately from yellow, to red. For the synthesis KC$_8$ turned out to be more convenient due to easier workup, and toxic Hg is avoided. After removing the remaining graphite by filtrating the solution over celite, this compound was obtained in 80% isolated yield as a very air-sensitve red solid, it even decomposes in a glove box with argon atmpospher when storred in an open vial. The characterization was done by IR spectroscopy and X-ray diffraction, NMR could not be recorded because the compounds are NMR silent (at room temperature); the ^{1}H and ^{31}P{^{1}H} NMR only showed peaks for the free ligand. The [Fe(PNP-*t*Bu)(CO)$_2$] **21b** complex shows two bands in the IR in THF with ν_{CO} is 1865 and 1814 cm^{-1}. The synthesis of **21b** is shown in Scheme 26.
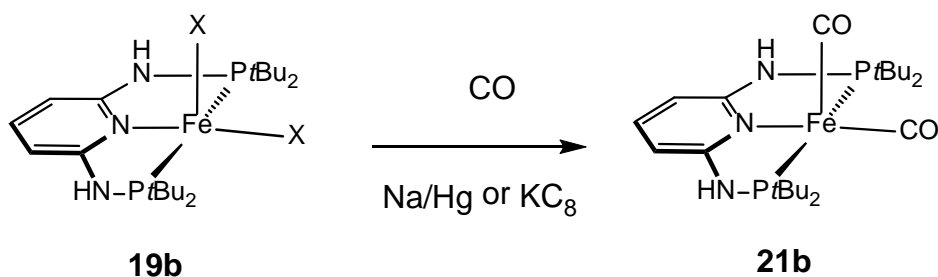
Scheme 26: Synthesis of **21b**

Single crystals of **21b** were grown by cooling a saturated solution in acetone and the molecular structure was determined by X-ray crystallography. The structural view is depicted in Figure 49

with selected bond distances and angles given in the caption. The overall geometry about the iron center is best described as an unusual square pyramidal structure, like the closely related complex [Fe(PNP^{CH2}-tBu)(CO)$_2$][71] of the two Fe-C-O angles deviates significantly from linearity with Fe1-C22-O1 and Fe1-C23-O2 being 167.2(1) and 172.1(1)°, respectively. The corresponding angles Fe2-C345-O3 and Fe2-C46-O4 of the crystallographically independent second complex are slightly larger being 174.6(1) and 168.1(1)°, respectively. A similar bending of the C-O ligand was also observed in [Fe(PNP^{CH2}-tBu)(CO)$_2$] with Fe-C-O angels of 176.68(1) and 171.87(1)°, respectively. The Fe-C bond distances in **21b** are 1.744 and 1.716 Å for Fe1-C22 and Fe1-C23, respectively, which are similar to those in [Fe(PNP^{CH2}-iPr)(CO)$_2$] (1.7325(9) Å) and [Fe(PNP^{CH2}-tBu)(CO)$_2$] (1.7310(12) and 1.7708(12)Å).
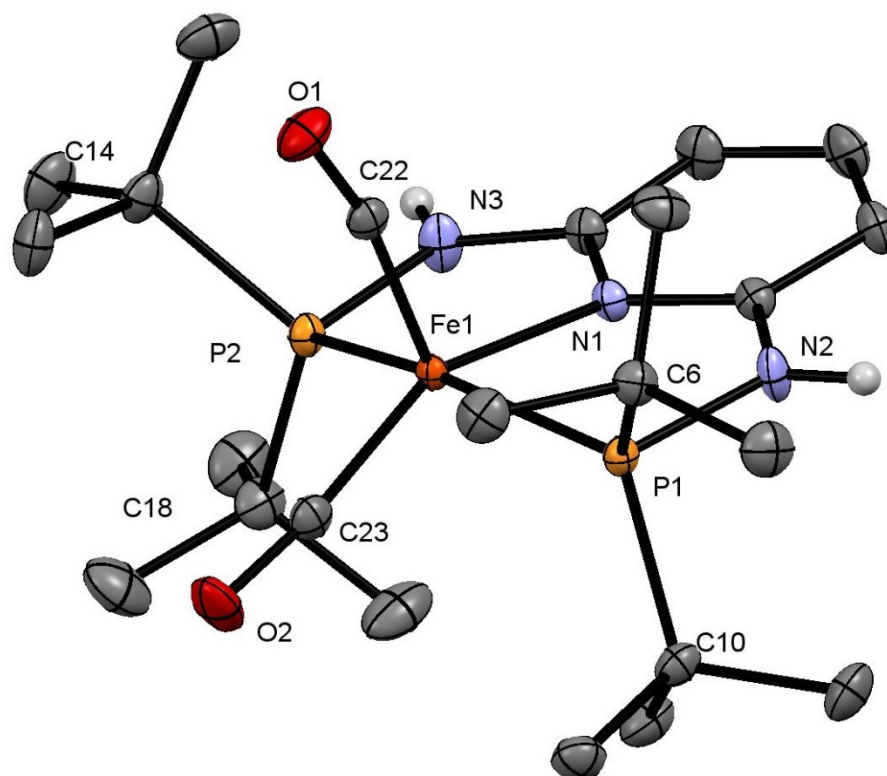
Figure 49: Molecular structure of [Fe(PNP-tBu)(CO)$_2$] **21b,** showing 50% thermal ellipsoids (CH$_2$Cl$_2$ and hydrogens omitted for clarity). Only one of the two crystallographically independent complexes is shown; selected bond lengths (Å) and bond angles (deg): P1-Fe1-P2 156.29(3); P1-Fe1-N1 81.94(3); P2-Fe1-N1 81.60(3); N1-Fe1-C22 108.44(5); N1-Fe1-C23 148.45(5); C22-Fe1-C23 103.09(6); Fe1-C22-O1 167.2(1); Fe1-C23-O2 172.1(1); C22-Fe1-P1 100.26(4); C23-Fe1-P1 93.66(4); Fe1-N1 2.037; Fe1-C22 1.744; Fe1-C23 1.716; Fe1-P1 2.224; Fe1-P2 2.221

The crystallographic data for the two independent molecules of **21b** and the data for the Fe(PNP^{CH2}-tBu)(CO)$_2$ are summarized in Table 7.

Table 7: Selected experimental and calculated bond lengths and angles of [Fe(PNP-*t*Bu)(CO)₂] (**21b**) and [Fe(PNP^CH2^-*t*Bu)(CO)₂]; ^a^crystallographically independent complexes, ^b^taken from Ref.[71]

	Fe(PNP-*t*Bu)(CO)₂		Fe(PNP^CH2^-*t*Bu)(CO)₂
	X-ray *ᵃ*	calcd	X-ray *ᵇ*
	Bond Lengths (Å)		
Fe1-N1/Fe2-N4	2.037	2.042	2.0503(9)
Fe1-C22/Fe2-C45	1.744	1.732	1.7310(12)
Fe1-C23/Fe2-C46	1.716	1.739	1.7708(12)
Fe1-P1/Fe2-P3	2.224	2.213	2.2322(3)
Fe1-P2/Fe2-P4	2.221	2.221	2.2066(4)

|	**Bond Angles (deg)**		
Fe1-C22-O1/Fe2-C45-O3	167.2(1)	174.6(1)	176.68(1)
Fe1-C23-O2/ Fe2-C46-O4	172.1(1)	168.1(1)	171.87(1)
C22-Fe1-C23/C45-Fe2-C46	103.09(6)	106.87(6)	105.78(5)
C22-Fe1-N1/C45-Fe2-N4	108.44(5)	140.69(5)	152.52(5)
C23-Fe1-N1/C46-Fe2-N4	148.45(5)	112.42(5)	101.57(4)
P1-Fe1-N1/P3-Fe2-N4	81.94(3)	81.52(3)	84.04(3)
P2-Fe1-N1/P4-Fe2-N4	81.60(3)	81.96(3)	81.55(3)
C22-Fe1-P1/C45-Fe2-P3	100.26(4)	91.93(4)	92.21(4)
C23-Fe1-P1/C46-Fe2-P3	93.66(4)	98.84(4)	103.35(4)
P1-Fe1-P2/P3-Fe2-P4	156.29(1)	158.53(1)	152.917(13)

In this course the following Fe(II) dihalide precursors were also reduced using KC₈: [Fe(PNP-pMe-*i*Pr)Cl₂] (**19c**), [Fe(PNP^Me^-*i*Pr)Cl₂] (**19d**) and [Fe(PNP^Et^-*i*Pr)Cl₂] (**19e**) to get the Fe(0) complexes [Fe(PNP-pMe-*i*Pr)(CO)₂] (**21c**), [Fe(PNP^Me^-*i*Pr)(CO)₂] (**21d**) and [Fe(PNP^Et^-*i*Pr)(CO)₂] (**21e**). The iron precursor was added to KC₈ and the reaction mixture was stirred in THF under CO atmosphere for 2h and worked up as described above. The synthesis of these new compounds is depicted in Scheme 27. Interestingly the N-alkylated compounds are less sensitive towards oxidation then **21a** and **21b**, even an ATR at air was recorded for **21d** and **21e** without decomposition of the complex.

Further the complexes [Fe(PNP-R)(CO)(Cl)₂] bearing small phosphine moieties with R = Me (**20f**) and R = Et (**20g**) were reduced with KC₈ in CO atmosphere to afford the complexes [Fe(PNP-Me)(CO)₂] (**21f**) and [Fe(PNP-Et)(CO)₂] (**21g**) respectively. It was necessary to start from the mono-CO compounds, because the dihalide precursors are synthetically not available due to κ³, κ² complexation as in the case of the PNP-Ph ligand. Further the complexes with the newly synthesized PNP-Ad and PNP-Cy ligands were reduced to the corresponding Fe(0)

species **21h** and **21j**. The synthesis is shown in Scheme 28. Like complex **21b** the compound [Fe(PNP-Ad)Cl$_2$] **19i** does not react with CO in solution or in solid state to obtain the mono-CO complex, due to steric reasons. Only when treated with a strong reducing agent the Fe(0) species [Fe(PNP-Ad)(CO)$_2$] (**21i**) is afforded. Further the PNP^{Ph}-Et ligand, bearing and N-Ph moiety, was introduced. The corresponding complex [Fe(PNP^{Ph}-Et)Cl$_2$] **19j** was reduced with KC$_8$ to afford complex [Fe(PNP^{Ph}-Et)(CO)$_2$] **21j** (see Scheme 27).
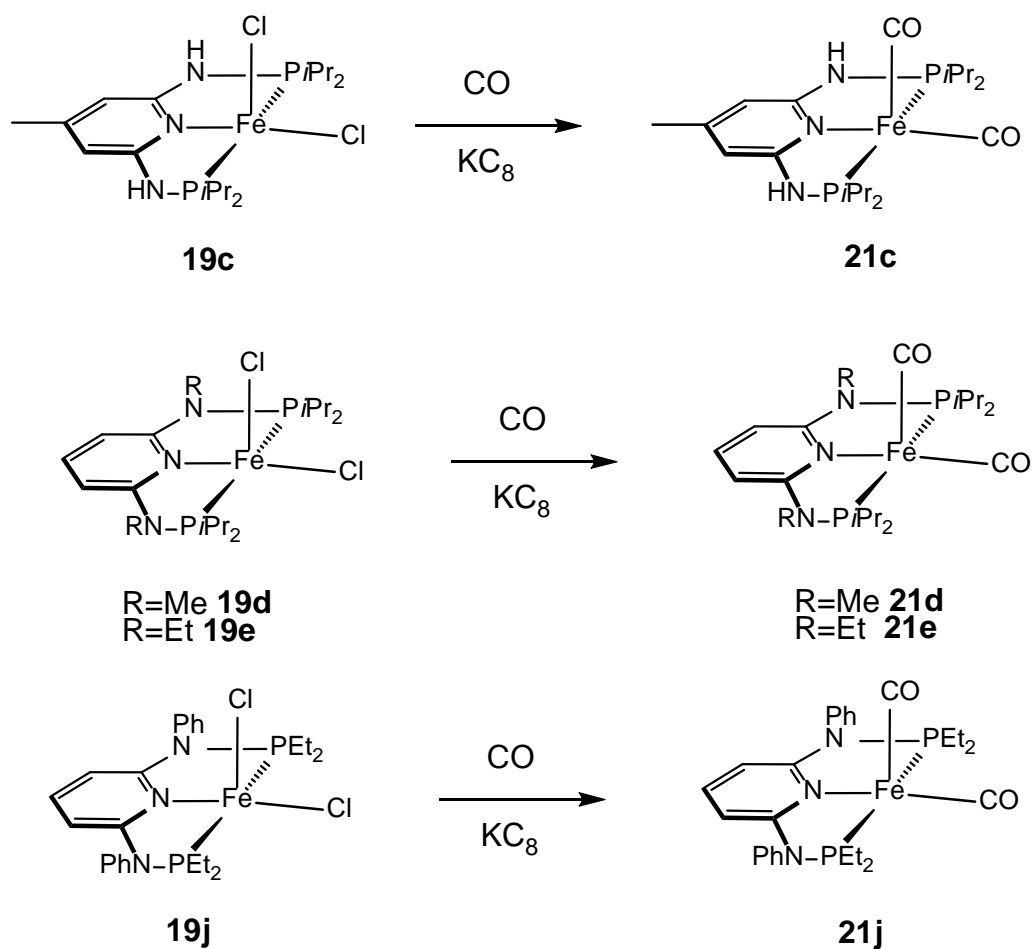
Scheme 27: Synthesis of Fe(0) with modified PNP-*i*Pr ligands and the PNP^{Ph}-Et ligand
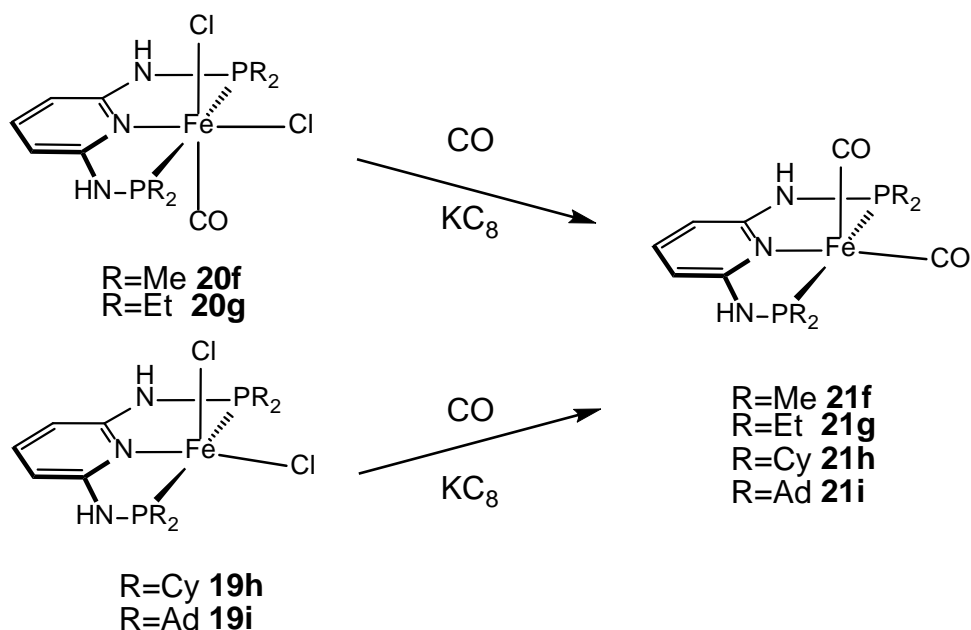
Scheme 28: Synthesis of Fe(0) complexes with PNP ligands bearing sterically non demanding phosphine moieties and the newly synthesized ligands PNP-Cy and PNP-Ad

Only the complexes with NR (R = Me, Et) could be characterized by NMR at room temperature, while for the other compounds no NMR signals could be detected. In the $^{31}P\{^1H\}$ NMR only the signal of the free ligand was observed due to partial decomposition. For the N-alkylated complexes the $^{31}P\{^1H\}$ NMR spectrum shows a single resonance at 181.7 ppm for **21d** and 183.7 ppm for **21e**. In the $^{13}C\{^1H\}$ NMR spectrum the CO ligand gives rise to a low-field resonance triplet centered at 219.6 ppm with a coupling constant J_{CP} of 28.0 Hz for **21d** and at 219.9 ppm with a coupling constant J_{CP} of 27.5 Hz for complex **21e**.

All complexes could be identified as Fe(0) dicarbonyl compounds by IR spectroscopy. They exhibit two strong bands for the symmetric and asymmetric CO stretch at similar frequencies. The complexes **21d** and **21e** with N-alkylated ligands were characterized by IR-spectroscopy both in THF solution and in the solid state (ATR). The solid state spectrum gives rise to slightly lower wavenumbers (**21d**: 1869, 1819 and 1856, 1802; **21e**: 1869, 1818 and 1858, 1801 cm^{-1}) like in Milstein's PNN dicarbonyl complexes.[73] In Figure 50 the IR spectra for compound **21e** in THF solution and as ATR are compared, showing the different wavenumbers for solid state and solution. Furthermore, the stretching bands are broader in the solid state than in solution. The IR spectra for **21d** show the same pattern.
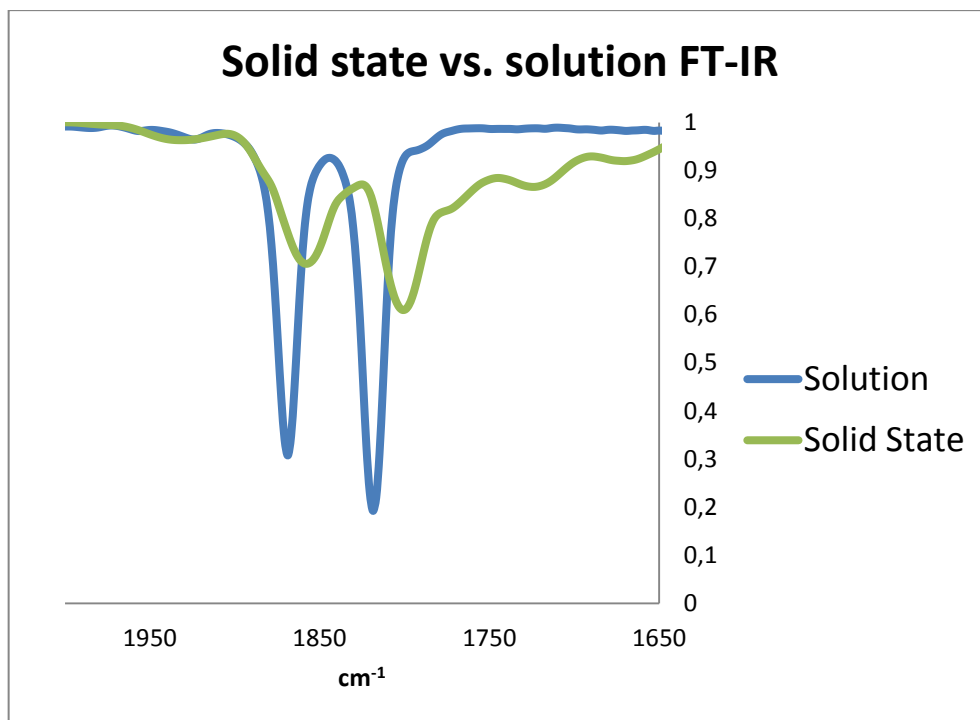
Figure 50: Carbonyl stretching frequencies of **21e**, blue: THF solution, green: ATR

Interestingly Complex **21h** [Fe(PNP-Cy)(CO)$_2$] shows two intensive IR bands (see Figure 51) similar to the ν_{CO} frequencies reported by Chirik for the [Fe(PNP^{CH2}-*i*Pr)(CO)$_2$] compound[70] at 1834 cm^{-1} and 1782 cm^{-1}. A second set of bands is visible at 1862 cm^{-1} and 1813 cm^{-1} similar to the signals for the other Fe(0) complexes. Goldman reported a similar pattern for the [Fe(PNP^{CH2}-*t*Bu)(CO)$_2$] complex.[71]
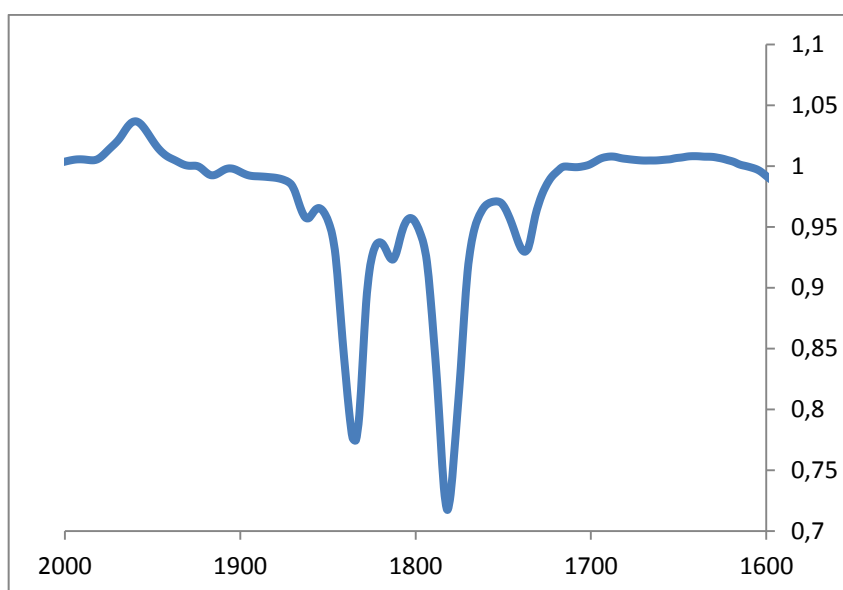
Figure 51: Solution IR of **21h**

From the complex **21e** bearing the N-Et bridge single crystals could be grown and X-ray diffraction was performed. The molecular structure is depicted in Figure 52 with selected bond length and bond angles given in the caption. The asymmetric unit of the crystal under investigation contains four different complexes ($Z' = 4$). The complexes are nearly symmetric by mirroring at a plane perpendicular to the pyridine ring. The Fe-CO (1.693(5){1.835(5) Å), Fe-N (1.972(4){2.089(4) Å) and Fe-P (2.1704(12){2.1980(18) Å) distances are in good agreement with fivefold Fe(0) coordination.

The complexes are pairwise related by pseudo-symmetry. The complexes not related by pseudo-symmetry differ distinctly by the N-Fe-CO angles, which vary by ≈ 7° (Table 8), thus demonstrating a certain flexibility of the coordination and the influence of packing effects. The OC-Fe-CO angles, on the other hand, are virtually identical in all four complexes (115.2(2){117.1(2)°).

Table 8: Selected interatomic distances and angles in the crystal structure of **21e**

Atoms	d [Å]	Atoms	d [Å]
Fe1-P1	2.1943(19)	Fe1'-P1'	2.1830(18)
Fe1-P2	2.1980(18)	Fe1'-P2'	2.1911(17)
Fe1-N1	2.051(3)	Fe1'-N1'	2.047(3)
Fe1-C22	1.801(5)	Fe1'-C22'	1.835(5)
Fe1-C23	1.693(5)	Fe1'-C23'	1.706(5)
Fe2-P3	2.1765(15)	Fe2'-P3'	2.1704(12)
Fe2-P4	2.1782(14)	Fe2'-P4'	2.1729(13)
Fe2-N4	2.089(4)	Fe2'-N4'	1.972(4)
Fe2-C45	1.786(6)	Fe2'-C45'	1.748(6)
Fe2-C46	1.721(6)	Fe2'-C46'	1.742(6)
Atoms	**angel [°]**	**Atoms**	**angel [°]**
N1-Fe1-C22	105.27(18)	N1'-Fe1'-C22'	106.56(18)
N1-Fe1-C23	139.51(19)	N1'-Fe1'-C23'	136.34(19)
C22-Fe1-C23	115.2(2)	C22'-Fe1'-C23'	117.1(2)
P1-Fe1-P2	161.10(8)	P1'-Fe1'-P2'	160.56(7)
Fe1-C22-O1	166.4(5)	Fe1'-C22'-O1'	171.9(4)
Fe1-C23-O2	174.7(6)	Fe1'-C23'-O2'	176.(4)
N4-Fe2-C45	112.6(2)	N4'-Fe2'-C45'	112.5(3)
N4-Fe2-C46	130.4(2)	N4'-Fe2'-C46'	130.9(3)
C45-Fe2-C46	117.0(3)	C45'-Fe2'-C46'	116.6(3)
P3-Fe2-P4	164.18(6)	P3'-Fe2'-P4'	164.40(6)
Fe2-C45-O3	171.4(4)	Fe2'-C45'-O3'	173.0(4)
Fe2-C46-O4	173.0(4)	Fe2'-C46'-O4'	177.4(4)

As expected, the Fe(0) atoms in the complexes feature a slightly distorted trigonal bipyramidal coordination with the P atoms located at the apices. Notably, the P-Fe-P angle differs from the ideal value of 180° (160.56(7)-164.40(6)°) due to the rigid geometry of the PNP-ligand. A very similar coordination with a P-Fe-P angle of 166° was described for an analogue of **21e**, whereby CH_2 methylene groups were substituted for the N-Et fragments[70]. Due to steric interactions, the corresponding *t*Bu analog, on the other hand, features highly distorted coordination which is more aptly described as tetragonal pyramidal[71].

Generally, if the coordinating P atoms are not connected in complexes featuring a first coordination sphere analogous to **21e**, more linear P-Fe-P angles are observed as for example in the [Fe(CO)$_2$(PEt)$_2$NCEt] (179°)[96], [Fe(CO)$_2$(NO)(PPh$_3$)$_2$]$^+$ (177°)[97] and [Fe(CO)$_2$(N$_2$Ph)(PPh$_3$)$_2$]$^+$ (176°) complexes[98].

The *i*Pr groups in **21e** generally feature the same orientation in all four complexes. The CH groups are exo oriented. In the Fe2 and Fe2' complexes, one *i*Pr group is disordered with occupational ratios 0.610:0.390(8) (Fe2) and 0.728:0.272(8) (Fe2'), whereby the proton of the secondary C atom and a methyl group change place.
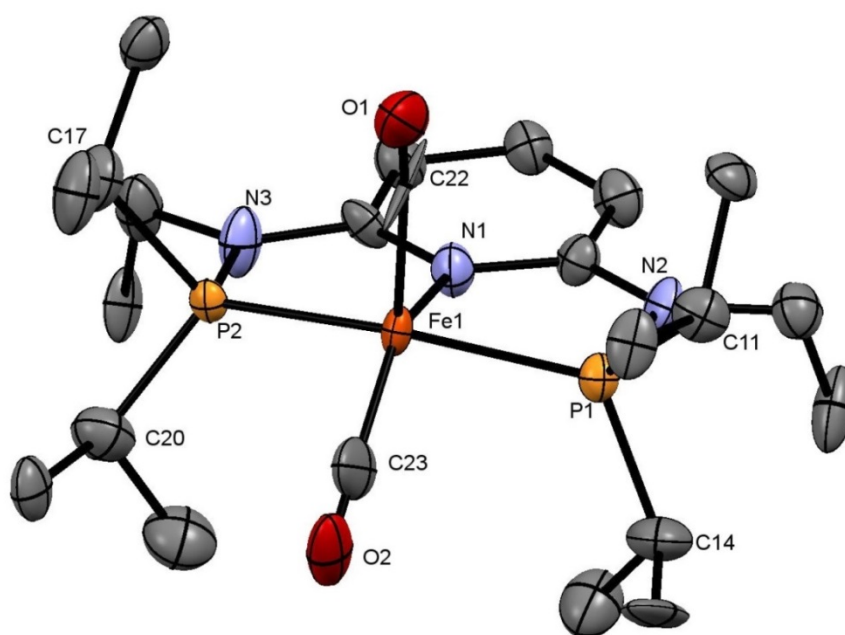
Figure 52: Molecular structure of [Fe(PNP^{Et}-*i*Pr)(CO)$_2$] **21e**, showing 50% thermal ellipsoids (hydrogens omitted for clarity). Only one of the four crystallographically independent complexes is shown; selected bond lengths (Å) and bond angles (deg): Fe1-P1 2.1943(19), Fe1-P2 2.1980(18), Fe1-N1 2.051(3), Fe1-C22 1.801(5), Fe1-C23 1.693(5), N1-Fe1-C22 105.27(18), N1-Fe1-C23 139.51(19), C22-Fe1-C23 115.2(2), P1-Fe1-P2 161.10(8), Fe1-C22-O1 166.4(5), Fe1-C23-O2 174.7(6)

The IR frequencies for the CO bands and X-ray data for the Fe-C-O bond angles (all measured crystals have Fe-C-O bond angles < 180°) are summarized in Table 9.

Table 9: Selected IR and X-ray data for some Fe(0) complexes

	ν_{CO} cm^{-1}	ν_{CO} cm^{-1}	Fe-C-O(°)	Fe-C-O(°)
PNP-*i*Pr	1872	1822	169.0(2)	175.0(2)
PNP-Et	1872	1821		
PNP-*t*Bu	1865	1814	167.2(1)	172.1(1)
PNP-Cy	1834 (1862)	1782 (1813)		
PNP^{Me}-*i*Pr	1869	1819		
PNP^{Me}-*i*Pr -ATR	1856	1802		
PNP^{Et}-*i*Pr	1869	1818	171.9(4)	176.7(4)
PNP^{Et}-*i*Pr-ATR	1858	1801		

Since Fe(0) complexes are known to undergo facile protonation at the metal center to afford Fe(II) hydride complexes, protonation of our new Fe(0) complexes should constitute an alternative synthetic route to obtain complex Fe(II) hydride compounds. As already expected, addition of HBF$_4$ to a CH$_2$Cl$_2$ solution of **21a** and **21b** resulted in an immediate color change from red to pale yellow consistent with protonation at the iron center to generate *cis*-[Fe(PNP-*i*Pr)(CO)$_2$H]$^+$ (**17a**) and *cis*-[Fe(PNP-*t*Bu)(CO)$_2$H]$^+$ (**17b**) in quantitative yield as established by NMR spectroscopy.

Compared to other Fe(0) dicarbonyl pincer complexes reported in literature[67,73,74] most of the reported compounds show CO frequencies shifted to higher wavenumbers suggesting that PNP ligands are more strongly electron donating. This observation is in keeping with the complexes reported by Chirik and Goldman bearing similar ligands.[70,71] The IR and X-Ray data for all these complexes are summarized in Table 10. The complex bearing the PNP^{CH2}-*i*Pr ligand could be analyzed with NMR at room temperature, while the compound with the PNP^{CH2}-*t*Bu ligand revealed NMR signals at -80°C.

Comparing the ν_{CO} frequencies we observed similar spectra as Goldman. However he observed a second set of bands in the IR which are similar to those of the [Fe(PNP^{CH2}-*i*Pr)(CO)$_2$] complex and complex **21h**. With respect to geometry, our complexes are comparable to Goldman's compounds. He reported similar geometries. Some of the Fe-C-O angles deviate significantly from 180° and the bulky complex **21b** adopts an SQP structure in solid state.

Table 10: Selected IR and X-Ray data for Fe(0) dicarbonyl pincer complexes

Fe(0)	ν_{CO} cm^{-1}	ν_{CO} cm^{-1}	Fe-C-O (°)	Fe-C-O (°)
PNP^{CH2}-*i*Pr	1842	1794	174.84	174.84
PNP^{CH2}-*t*Bu	1870 (1846)	1819 (1797)	176.68	171.87
PNN-*t*Bu	1920	1860	178.25	174.06
PNN-*i*Pr	1913	1860	178.8	176.12
PNN-Ph	1925	1863	176.27	175.14
PDI^{iPr}	1974	1914	178.72	176.32
CNC NHC 1	1928	1865	178.89	177.36
CNC NHC 2	1925	1858		
^{tBu}PNN^{iP}r	1956	1902		

Comparing the solid state structures (Figure 53) complex **21b** adopts a SQP conformation while **21a** is better described with a TBP structure. Complex **21e** has a distorted TBP conformation due to the sterically more demanding N-Et linker.
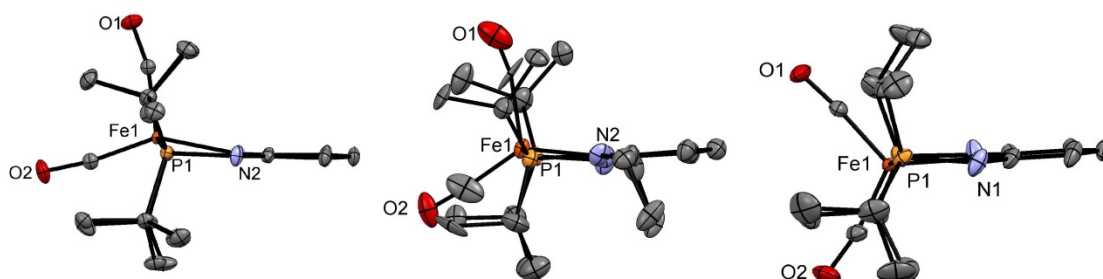
Figure 53: Side view of the solid state structures of **21b**, **21e** and **21a** (from left to right)

In order to explain the unexpected behavior of the bulky Fe(0) PNP complexes in solution, equilibria between SQP and TBP geometries were suggested by Goldman. However, we were unable to verify such a hypothesis. Based on DFT calculations, we could only find one minima fully in agreement with the structures determined by X-ray crystallography. Alternatively, we propose an equilibrium between complexes with singlet (S = 0) and triplet (S = 1) spin states. For complex **21a** the energy difference is 7.0 kcal/mol and for **21b**, being already in a SQP conformation, only 1.2 kcal/mol respectively. Calculations show that the SQP geometry is favored in high spin state and would explain why no signals are obtained in the NMR spectrum. The calculated free energies for complex **21a** and **21b** are depicted in Figure 54.
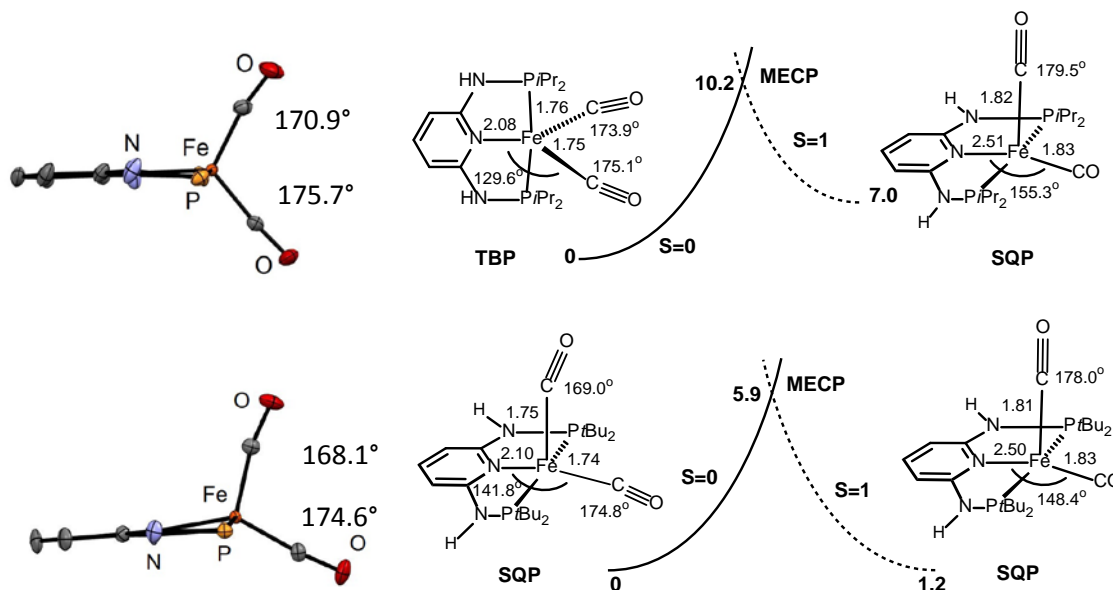
Figure 54: DFT/B3LYP (Fe sdd; C, H, N, O, P 6-31g**) of **21a** and **21b**

Goldman explained the nonlinearity of the Fe-C-O angles by the results and conclusions from Hoffmann's theoretical investigations of five-coordinated nitrosyl complexes.[71,99] While there are many examples of bent nitrosyl ligands, in the case of carbonyl ligands this is rarely observed. An explanation, based on calculations performed by Hoffmann,[99] was given by Goldman:

1. "The better the σ- or π-donating capability of the basal ligands, the more likely is the nitrosyl to be bend."

2. "In a compound of the type $ML_2DA(NO)$, D = π-donor trans to A = π-acceptor, if the NO group bends in the DMA plane, then it should bend toward the acceptor."

3. "A bent nitrosyl will move its nitrogen off the coordination axis in the direction of p-coordination."

4. "The nitrosyl is less likely to be bend in the equatorial position of a trigonal bipyramid than in the apical site of a square pyramid."

5. "Nitrosyl groups in axial positions in a trigonal bipyramid and basal sites in a square pyramid prefer to be linearly coordinated."

Performing Mössbauer spectroscopy and SQUID measurements of **21a** and **21e** to evaluate the electronic structure showed no evidence of any spin state change, indicating that only a change in the conformation takes place (see Figure 55) as Goldman described it in his publication.
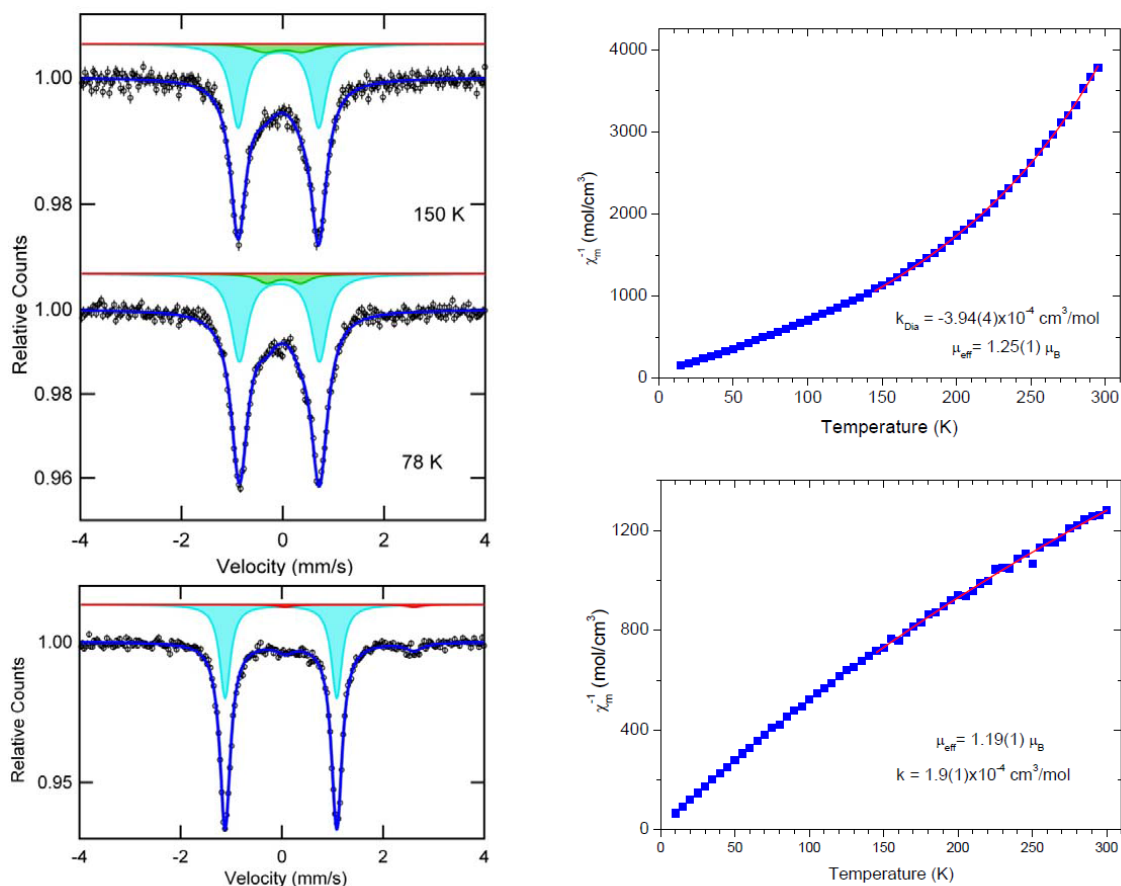
Figure 55: Mössbauer and SQUID spectra of **21a** (top) and **21e** (bottom)

The 78 K Mössbauer spectrum of **21a** is well-fit to a major species (ca. 87 %, blue) with isomer shift values are around or near zero. A spectrum at 150 K for **21a** was also recorded and the IS evolution is in the correct sense. The large majority of the Fe sites in complex **21e** in the Mössbauer spectrum at 78 K has an IS value close to zero and a QS larger than the one obtained for sample **21a**. A second Fe site with only 6% has IS and QS values that fit well with HS Fe(II). The Mössbauer data are summarized in Table 11.

Table 11: Mössbauer data of complexes **21a** and **21e**

	T(K)	Site	δ: IS (mms^{-1})	ΔE_q: QS (mms^{-1})	I(%)
21a	78	blue	-0.067(2)	1.579(4)	87.4
		green	0.02(2)	0.67(4)	12.6
	150	blue	-0.085(3)	1.591(6)	79.6
		green	0.01(2)	0.75(7)	20.4
21e	78	blue	-0.018(1)	2.207(2)	93.9
		red	1.34(1)	2.55(31)	6.1

Similar [57]Fe Mössbauer spectra were recently published by Milstein where similar findings were reported[73]. Complexes of the type [Fe(PNN-R)(CO)$_2$] were investigated for Mössbauer spectroscopy where R = tBu and Ph. Parameters of δ = 0.02 and 0.04 mms^{-1} and ΔE_q = 1.49 and 1.93 mms^{-1} were reported being in good agreement with our findings being δ = -0.67 mms^{-1} and ΔE_q = 1.58mms^{-1} for complex **21a** and δ = -0.02 mms^{-1} and ΔE_q = 2.21 mms^{-1} for **21e** respectivley. Further similar impurities were reported. The complex bearing the PNN-tBu ligand hat a second species with parameters δ = 1.30 mms^{-1} and ΔE_q = 2.67mms^{-1} and was described as an oxidized high-spin iron (I) or iron (II) impurity. These values are similar to the impurities of **21e** being δ = 1.34 mms^{-1} and ΔE_q = 2.55mms^{-1}. The second species with the PNN-Ph ligand had an impurity with values δ = 0.15 mms^{-1} and ΔE_q = 0.61mms^{-1} and was described as a high spin iron(III) compound. The impurity in complex **21a** has similar values with δ = 0.02 mms^{-1} and ΔE_q = 0.67 mms^{-1} which may be described as an iron (I) compound. Further Milstein acknowledges that the assignment of iron oxidation state in low-isomer shift iron species with pincer ligation is challenging without theoretical studies or additional experiments because iron(0), low-spin iron(I) and low-spin iron(II) can exhibit low isomer shifts. The major species of both complexes can be assigned to an iron(0) complex. The difference in the quadrupole splitting occurs due to structural variations as observed in Milstein's findings.

In order to examine the electrochemical behavior of **21a**, cyclic voltammograms were recorded. Measurements were carried out in a 0.1 M solution of Bu$_4$NPF$_6$ as the supporting electrolyte in THF at 25 °C. The Voltalab 40 system (Radiometer Analytical, France) was used for all cyclovoltammetry studies. Cyclovoltammograms were measured using a three electrode configuration. A glassy carbon electrode (GCE) was used as the working electrode, a silver wire as the reference electrode and a platinum disk as the auxiliary electrode. The redox potentials were referenced versus the Fc/Fc$^+$ couple. All measurements were done in a range from -1.0 V to 1.0 V with different scan rates (50, 100, 150, 200 mV/s). The number of cycles was 3 in each experiment.
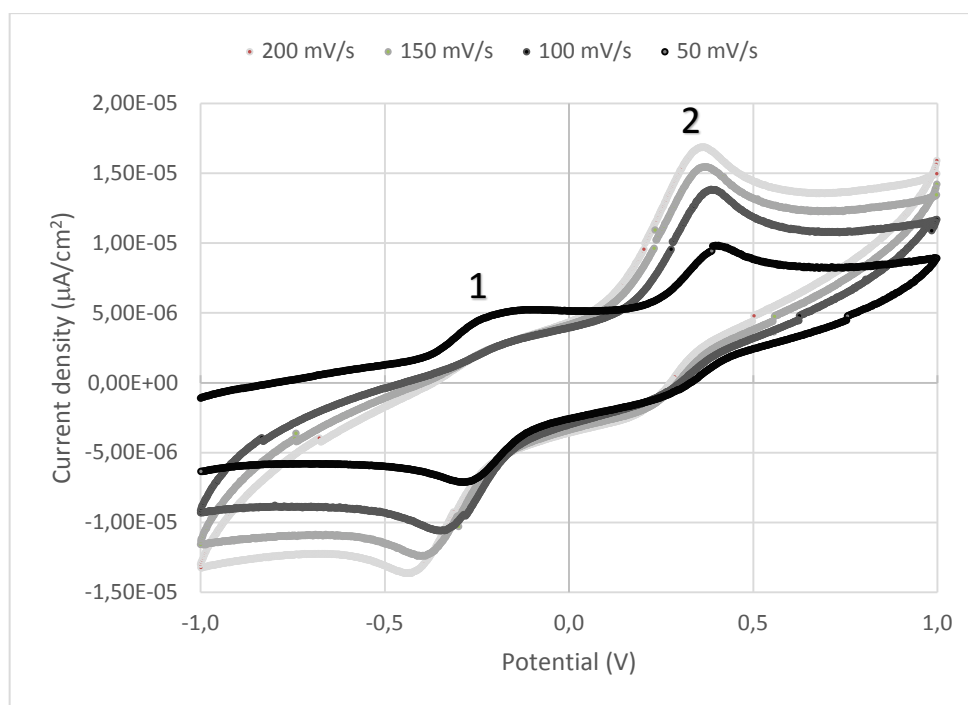
Figure 56: CV-measurements of **22a** at different scan rates (50, 100, 150, 200 mV/s)

As it is shown in Figure 56, the complex **22a** undergoes two redox processes in the investigated range, which were both found to be reversible one-electron transitions. In Table 12 the results of the CV-experiments are summarized.

Table 12: Redox potentials of **22a** (in V) measured with a scan rate of 100 mV/s *vs* $FeCp_2/FeCp_2^+$

	$E_{1/2}$	Oxidation	Reduction
1	-0.65 V	-0.55 V	-0.76 V
2	-0.10 V	-0.02 V	-0.18 V

One process was found to be at $E_{1/2}$ = -0.65 V (1), which corresponds to the Fe^0/Fe^+ redox couple. A second redox process was found at $E_{1/2}$ = -0.10 V (2). This process may be related to the Fe^+/Fe^{2+} couple.

Lower than -1.0 V the ligand and also the complex is electrochemically decomposed.

In addition ESI-MS (electrospray ionization mass spectrometry) of complexes **21a**, **21d**, **21e** and **21h** was performed. The compounds were dissolved in THF with NaCl, and the solution was injected into the MS in the positive ion mode. NaCl was added to facilitate the generation

of charged fragments because neutral compounds cannot be detected. Parts of the full scans are depicted in Figure 57 (complexes **21a** and **21d**) and Figure 59 (complexes **21e** and **21h**).

The most abundant signal for complex **21a** observed at *m/z* 425.2 refers to [Fe(PNP-*i*Pr)(CO)]$^+$ **[M-CO]$^+$** where a CO ligand is cleaved off. The second signal at *m/z* 454.2 has an unusual pattern for an single iron containing molecule, it turned out to be a mixture of [Fe(PNP-*i*Pr)(CO)$_2$]$^+$ **[M]$^+$** and [Fe(PNP-*i*Pr)(CO)$_2$H]$^+$ **[MH]$^+$** signals. Presumably the complex is oxidized during the ionisation and the **[M]$^+$** fragment is generated and an Fe(I) complex is formed. The species **[MH]$^+$** refers to a protonation reaction. Parts of the full scan for both signals M$^+$ and [M+H]$^+$ is depicted in Figure 58. Performing MS2 of *m/z* 454.3 shows the subsequent loss of CO if the protonated species. Isolation of the **[M]$^+$** signal was not successful, because of spontaneous formation of the **[MH]$^+$** fragment in MS2.

The most abundant signal for complex **21d** observed at *m/z* 481.3 refers to [Fe(PNP^{Me}-*i*Pr)(CO)$_2$]$^+$ **[M]$^+$** where the molecule is oxidized. Performing MS2 the signal at *m/z* 453.4 refers to [Fe(PNP^{Me}-*i*Pr)(CO)]$^+$ **[M-CO]$^+$** where one CO ligand is lost and in MS3 the signal at *m/z* 425.2 refers to [Fe(PNP^{Me}-*i*Pr)]$^+$ **[M-(CO)$_2$]$^+$** where both CO ligands are dissociated.
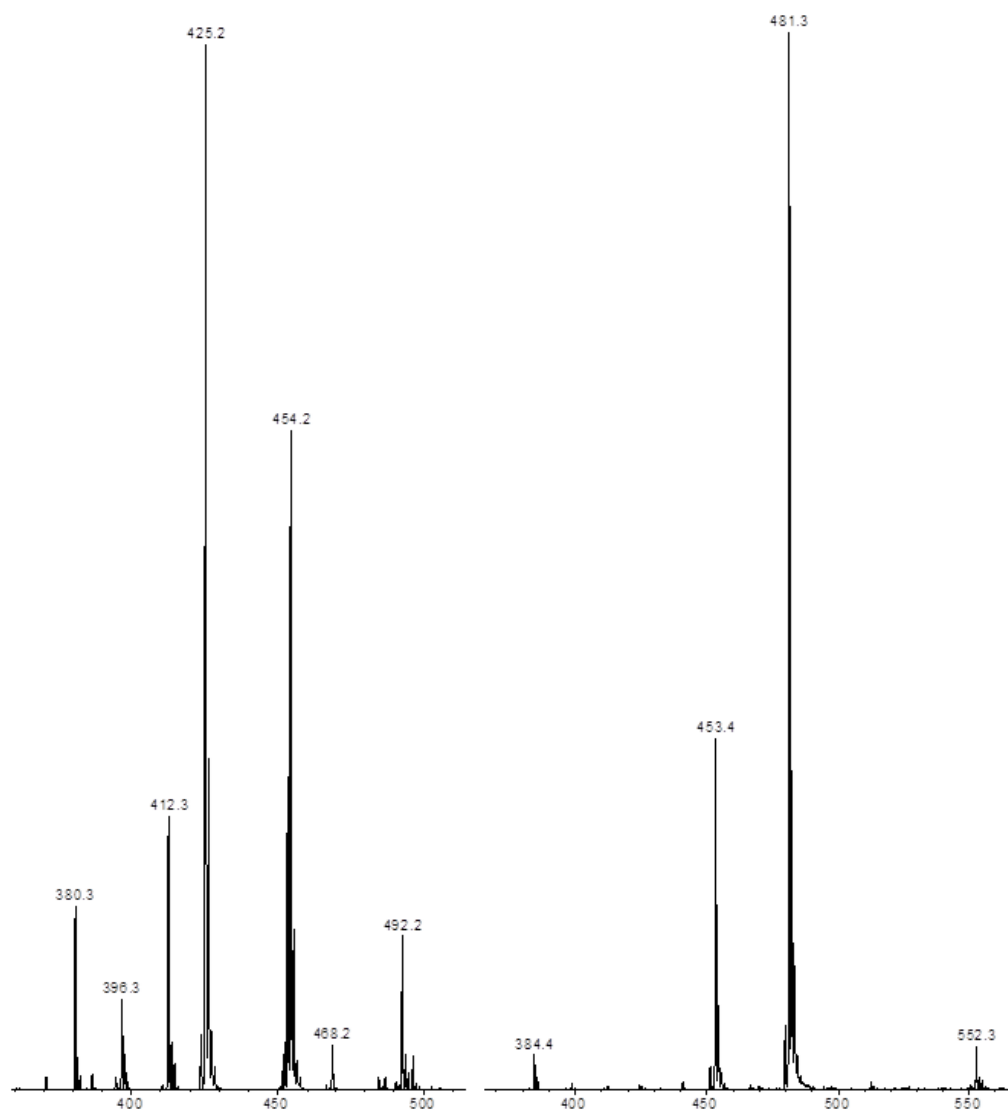
Figure 57: ESI-MS of complexes **21a** (left) and **21d** (right)
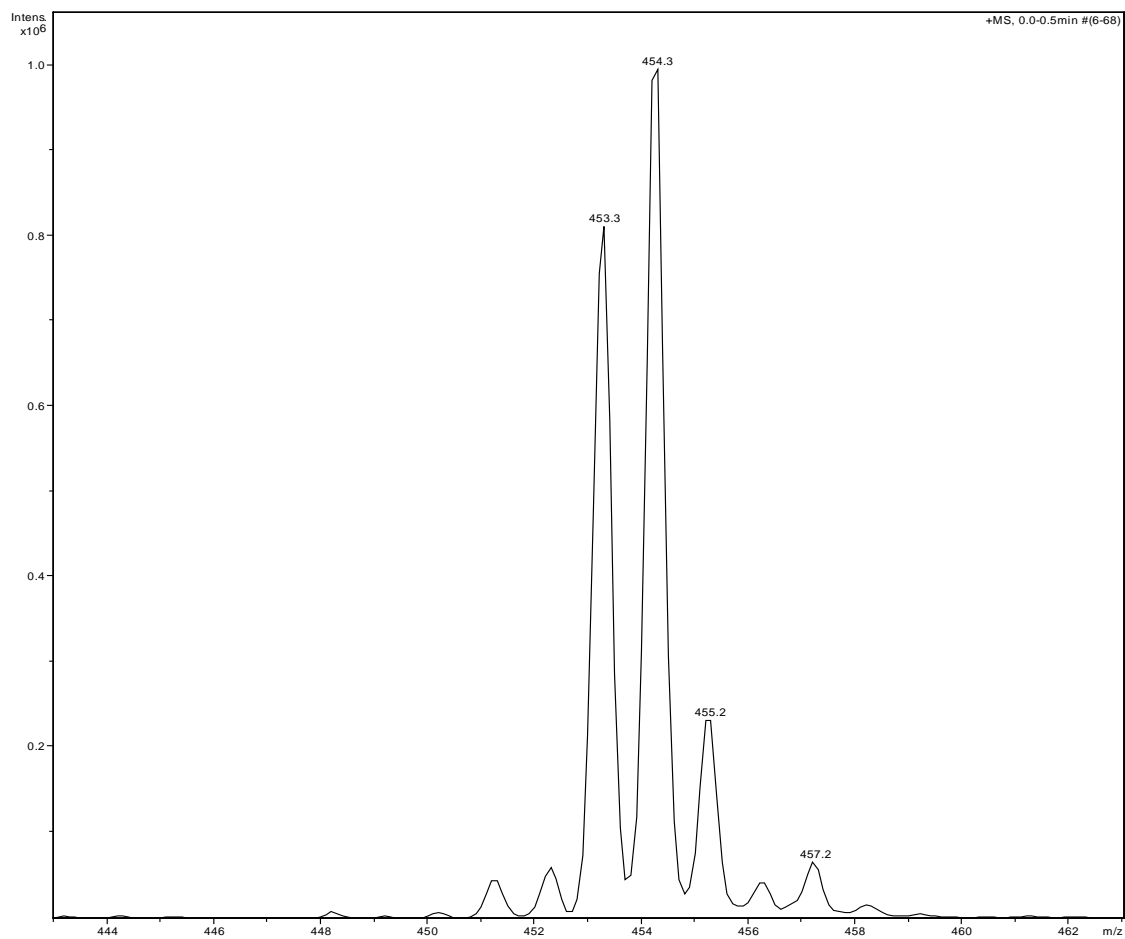
Figure 58: full scan od **21a [M]⁺/[M+H]⁺** *m/z* = 453/454, narrow range
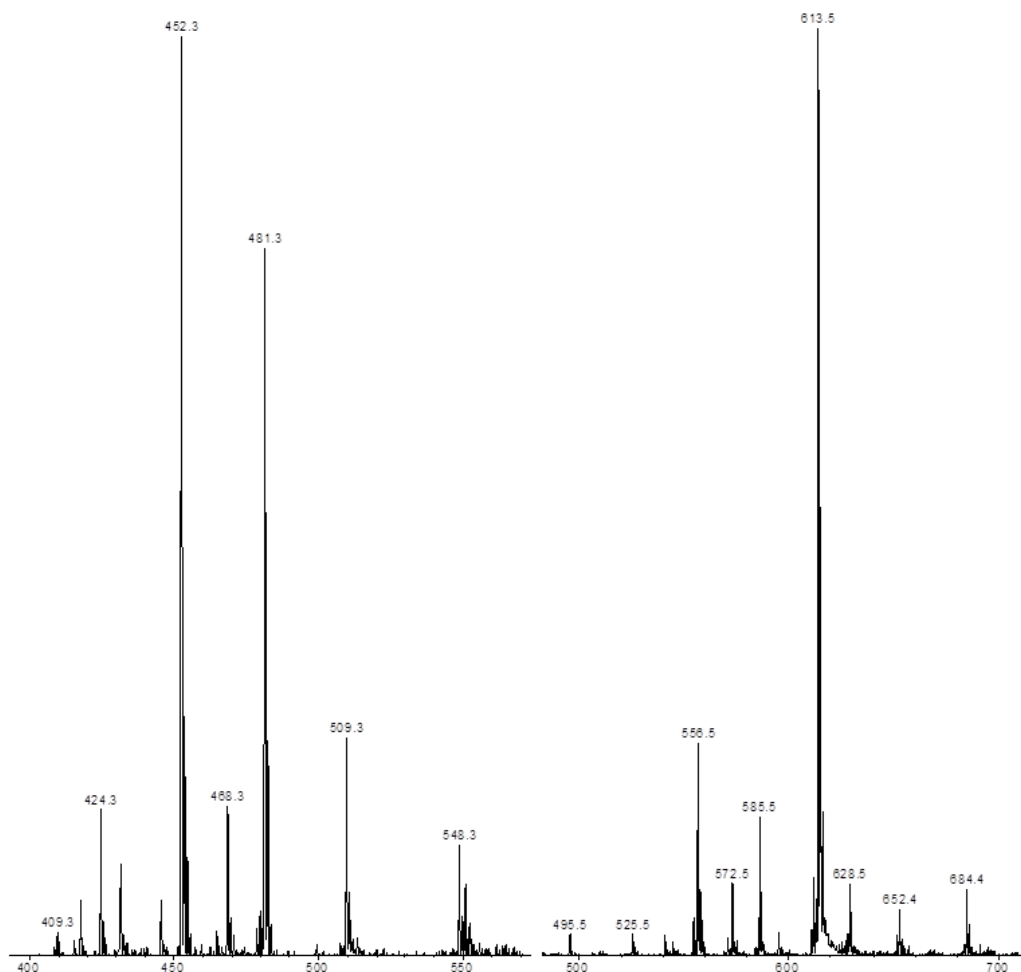
Figure 59: ESI-MS of complexes **21e** (left) and **21h** (right)

Complex **21e** shows a similar behaviour as complex **21d**, however it cleaves off the CO ligand much faster. In the full scan the most abundant at *m/z* 452.3 refers to the [Fe(PNP^{Et}-*i*Pr)]$^+$ **[M-(CO)$_2$]$^+$** fragment. The signal at *m/z* 509.3 refers to [Fe(PNP^{Et}-*i*Pr)(CO)$_2$]$^+$ **[M]$^+$** and the signal at *m/z* 481.3 to [Fe(PNP^{Et}-*i*Pr)(CO)]$^+$ **[M-CO]$^+$**.

The most abundant signal for complex **21h** appears at *m/z* 613.5 and corresponds to [Fe(PNP-Cy)(CO)$_2$]$^+$ **[M]$^+$** an iron(I) species. The signal at *m/z* 585.5 refers to [Fe(PNP-Cy)(CO)]$^+$ **[M-CO]$^+$** where on CO ligand is dissociated.

6.2 Synthesis of iron(I) complexes

For studying complexes for catalysis and their reactivity one possibility is to treat them with bases to obtain a more reactive species. In this survey to study the reactivity of our FePNP pincer carbonyl compounds the blue complex *trans*-[Fe(PNP-*i*Pr)(CO)(Cl)$_2$] was treated with KO*t*Bu to synthesize a reactive species for catalysis or to deprotonate the complex. Unfortunately no reactive species was isolated, the solution turned forest green and a brown precipitate was formed. After filtering the suspension over Celite an Fe(I) complex [Fe(PNP-*i*Pr)(CO)$_2$]$^+$ **22a** was isolated in 48% yield. The compound is very good soluble in all common solvents (e.g., THF, CH$_2$Cl$_2$, Et$_2$O, benzene, pentane), is very air sensitive and decomposes within seconds when exposed to air. Upon oixidation, the color changes from green to brown both in solution and in the solid state. The synthesis of **22a** is shown in Scheme 29.
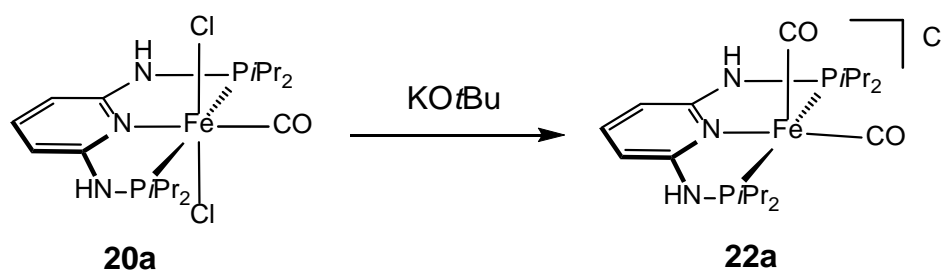
Scheme 29: Synthesis of the Fe(I) complex **22a**

To improve the yield the reaction was performed under CO atmosphere, however nothing changed.

Due to its paramagnetic nature NMR spectroscopy could not be performed, but FT-IR spectroscopy in THF solution was possible. The spectrum shows two bands for the ν_{CO} vibrations at 1957 and 1885 cm^{-1}. Furthermore, single crystals could be grown and X-ray diffraction was performed. The molecular structure of **22a** is shown in Figure 60 with selected bond length and bond angles given in the caption.

The complexes **20c** and **20k** bearing a ring modified ligand were also reacted with KO*t*Bu, the reaction mixture turned green and the corresponding Fe(I) complexes **22c** and **22k** were isolated. The recorded IR spectra in THF solution are similar to **22a**.
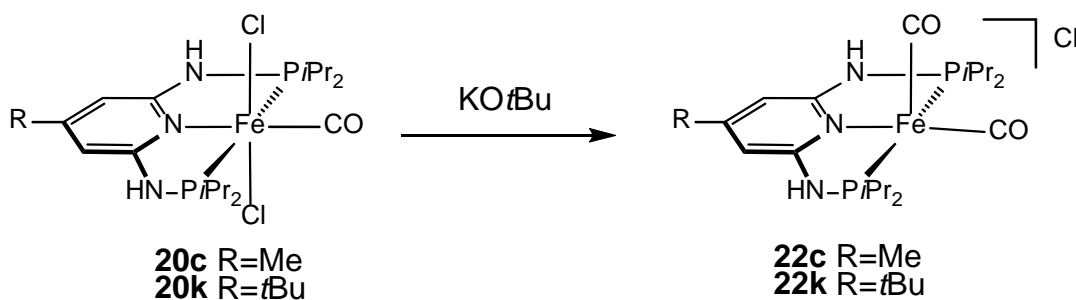
Scheme 30: Synthesis of Fe(I) complexes
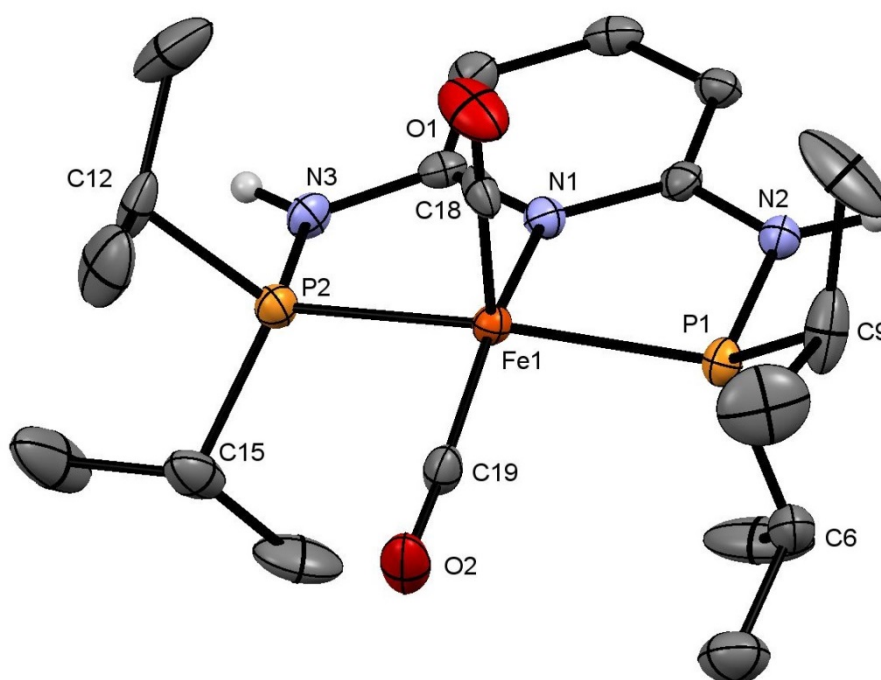
Figure 60: Molecular Structure of **22a** [Fe(PNP-*i*Pr)(CO)₂]Cl, showing 50% thermal ellipsoids (hydrogens and Cl counterion omitted for clarity); Selected bond lengths (Å) and bond angles (deg): Fe1-P1 2.208, Fe-P2 2.209, Fe1-N1 1.995, Fe1-C18 1.789, Fe1-C19 1.762, N1-Fe1-C18 104.2(1), N1-Fe1-C19 158.4(2), C18-Fe1-C19 97.3(2), P1-Fe1-P2 160.30(4), Fe1-C18-O1 178.1(3), Fe1-C19-O2 177.5(4)

The geometry of this complex can be best described as square pyramidal. Compared to the Fe(0) dicarbonyl complexes, the Fe-C-O angle is nearly perfect 180 °.

The compounds **20d** and **20e** bearing N-alkylated PNP-*i*Pr ligands were treated using the same reaction conditions. Interestingly no Fe(I) complexes were isolated, the solution turned red and after workup the Fe(0) complexes discussed in Chapter 6.1 were isolated in moderate yield (lower than 50%). The reaction is depicted in Scheme 31. Obviously the NH moiety is crucial for the formation of Fe(I) complexes.
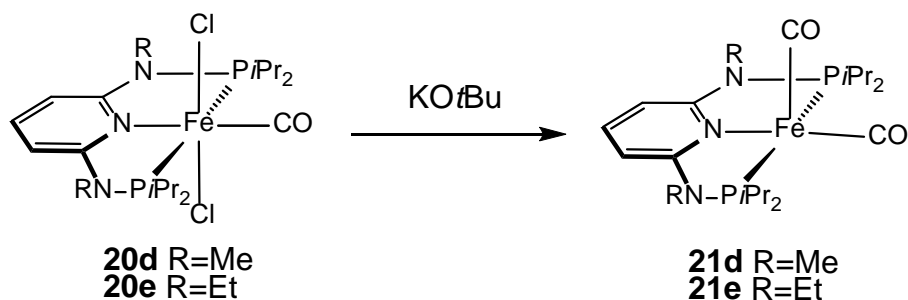
Scheme 31: Reaction of complexes bearing N-alkylated PNP pincer ligands with KO*t*Bu

Furthermore, complexes **20f** and **20g** bearing small phosphines were reacted with KO*t*Bu but unfortunately no Fe(I) complexes were isolated. The solution turned red and a brown precipitate was formed. After workup the Fe(0) complexes **21f** and **21g** were isolated. The reaction is shown in Scheme 32.
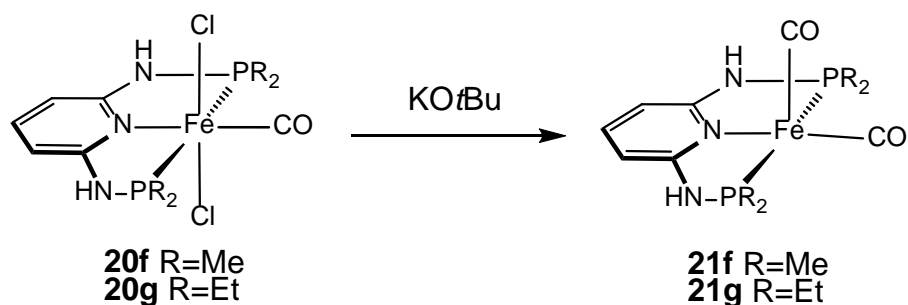
Scheme 32: Reaction of Fe pincer carbonyl complexes with small phosphines with KO*t*Bu

Surprisingly the [Fe(PNP-Cy)(CO)(Cl)$_2$] complex reacts to both, the Fe(I) and Fe(0) species, depending on the configuration of the starting material Treating the blue *trans*-**20h** complex the neutral Fe(I) compound **22h** [Fe(PNP-Cy)(CO)$_2$] is isolated, as revealed by X-ray diffraction, the ligand is deprotonated and a neutral Fe(I) species is formed. Complex *trans*-**20h** isomerizes to the red *cis*-**20h** compound when stirred in Et$_2$O during workup. Treating this solution with KO*t*Bu the reaction mixture turns red and the red Fe(0) complex **21h** is isolated. The reactions of **20h** are depicted in Scheme 33. Milstein also reported the formation of the Fe(0) complex when reacting the [Fe(PNP^{CH2}-*i*Pr)(CO)(Br)$_2$] with KO*t*Bu.[58]
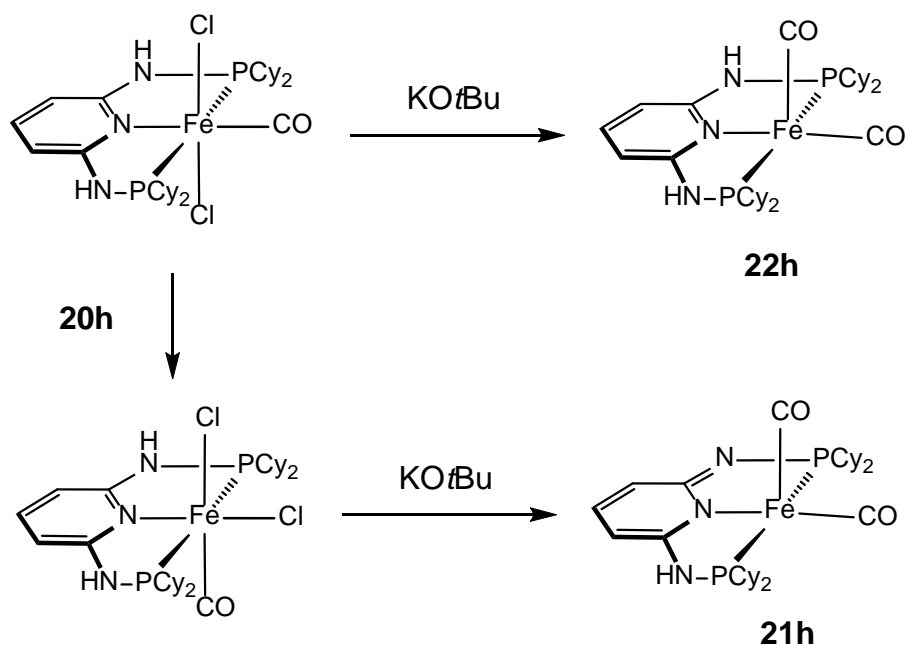
Scheme 33: Reactions of complex **20h** [Fe(PNP-Cy)(CO)(Cl)$_2$] with KO*t*Bu

Single crystals suitable for X-ray diffraction of **22h** were grown by slow evaporation of a saturated solution of the complex in EtOH. The molecular structure of **22h** is depicted in Figure 61 with selected bond length and bond angles given in the caption. The structure is square pyramidal as similar to **22a**.
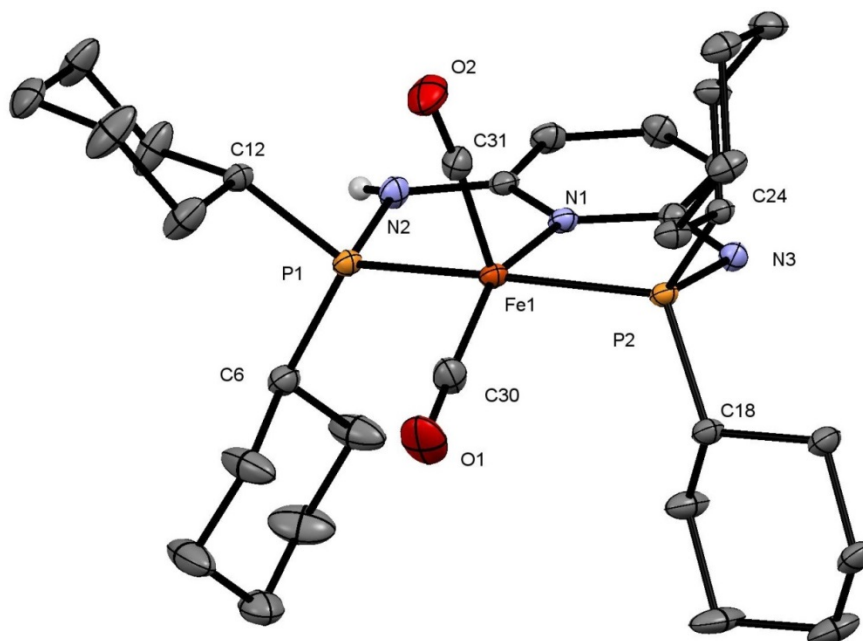
Figure 61: Molecular structure of **22h** showing 50% thermal ellipsoids (hydrogens and solvent molecules are omitted for clarity); Selected bond lengths (Å) and bond angles (deg): Fe1-P1 2.212, Fe-P2 2.229, Fe1-N1 1.995, Fe1-C30 1.770, Fe1-C31 1.800, N1-Fe1-C30 155.30(8), N1-Fe1-C31 108.21(7), C30-Fe1-C31 96.38(9), P1-Fe1-P2 161.63(2), Fe1-C30-O1 178.0(2), Fe1-C31-O2 175.4(2)

Figure 62 shows the packing of **22h**, clearly indication that one N-H is deprotonated during the reaction. The molecule is stabilized by two solvent molecules, forming hydrogen bonds. The deprotonated moiety forms a hydrogen bond the H of the EtOH molecule; the other moiety forms the bond to the O of the alcohol.
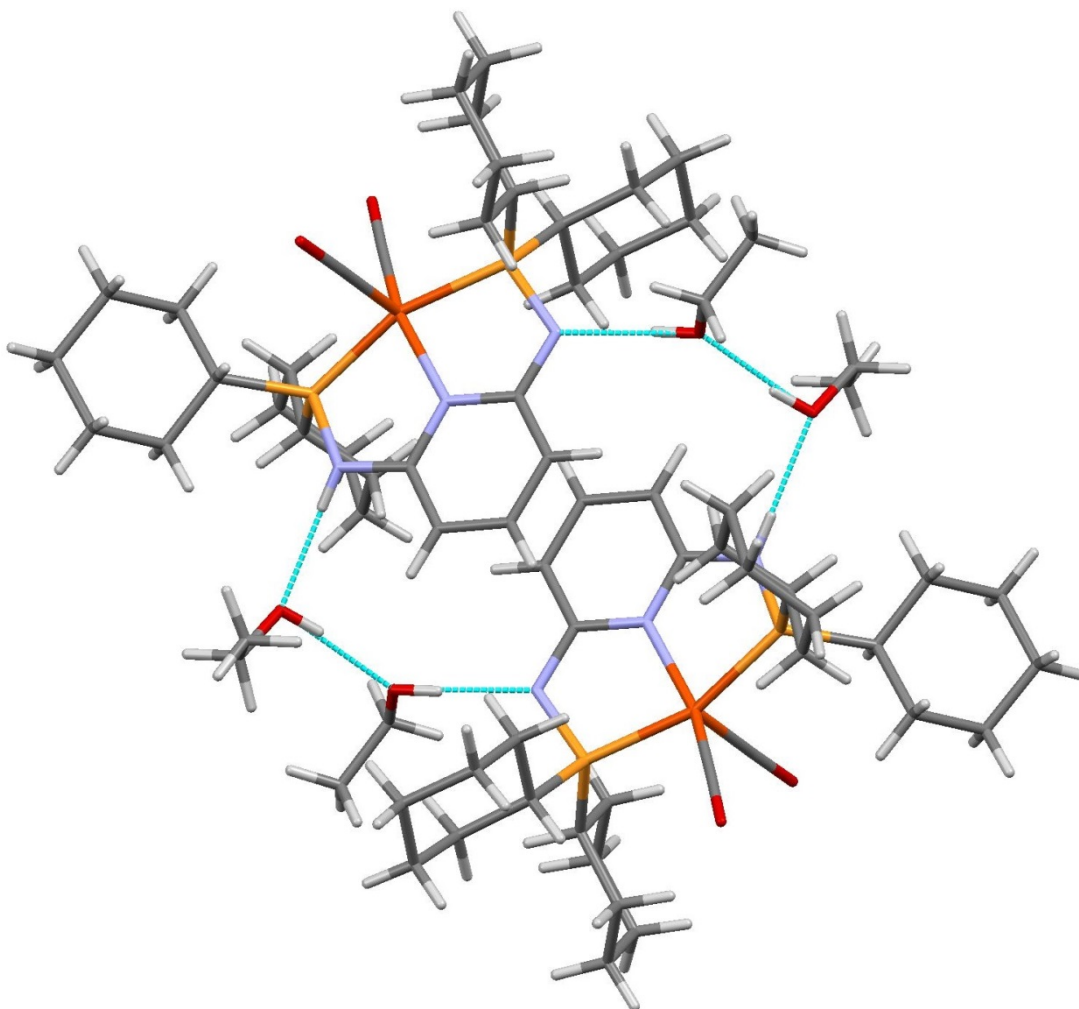
Figure 62: Hydrogen bonds in the packing of **22h**

Interestingly when exposing a solution of the complexes **21b** and **21i** [Fe(PNP-R)(CO)$_2$] with R = *t*Bu, Ad) the color changes from deep red to turquoise within seconds, the same color as the corresponding Fe(I) complexes with R = *i*Pr and Cy. Evaporating the solvent and subsequent IR spectroscopy indicated that the oxidized compounds are the Fe(I) species **22b** and **22i** [Fe(PNP-R)(CO)$_2$]$^+$. The nature of the counterion remains unclear because no crystal could be grown so far. The IR-ATR spectra of R = *t*Bu and R = Ad show CO bands, for **22h** ν_{CO} is 1945 and 1878 cm^{-1} and **22b** ν_{CO} is 1936 and 1869 cm^{-1} respectively. These Fe(I) compounds with bulky phosphines are far more stable than complexes **22a** and **22h** and can be handled at air. They decompose

after several hours at air and the color changes to blue. The reaction of **21b** and **21i** to the new Fe(I) complexes is shown in Scheme 34.
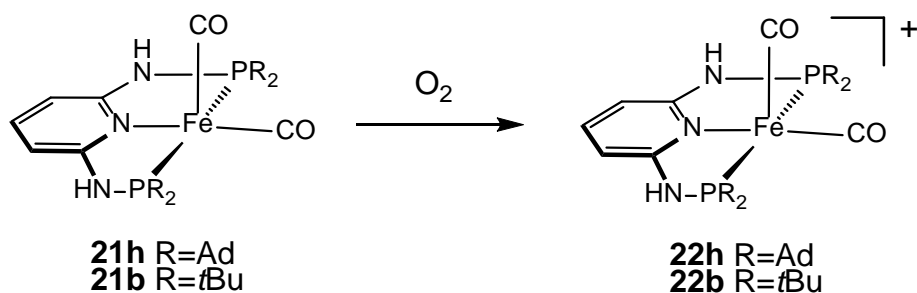
Scheme 34: Oxidation of Fe(0) complexes **21h** and **21b**

The formation of the Fe(I) species is supported by a Mössbauer spectra of a partially oxidized sample of complex **21b**. The spectra of two different samples where the upper one shows more of the Fe(I) species are depicted in Figure 63, the corresponding data is shown in Table 13.
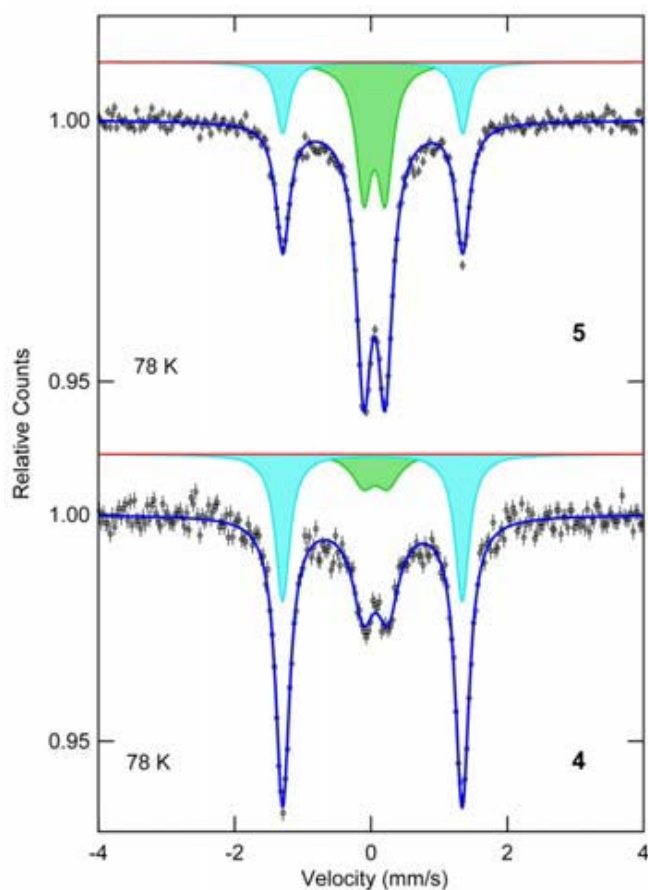
Figure 63: Mössbauer of partially oxidized complex **21b**, blue: Fe(0), green Fe(I)

Table 13: Mössbauer data for partially oxidized **21b**

Label	T(K)	Site	IS (mm.s^{-1})	ΔE_q: QS (mm.s^{-1})	I(%)
4	78	blue	0.021(1)	2.635(3)	68.5
		green	0.067(7)	0.36(1)	31.5
5	78	blue	0.026(2)	2.642(4)	31.7
		green	0.051(1)	0.313(2)	68.3

The blue species can be assigned as the iron(0) compound **21b**. The isotopic shift and the quadrupole splitting are similar to **21a** and **21e** discussed before being δ = 0.03 mms^{-1} and ΔE_q = 2.64 mms^{-1}. The observed second green species has parameters δ = 0.07 mms^{-1} and ΔE_q = 0.36 mms^{-1}. The recorded data can be compared with the reported [Fe(^{iPr}PDI)(CO)$_2$]BAr^F complex with values δ = 0.17 mms^{-1} and ΔE_q = 0.62 mms^{-1} by Chirik.[72] As it is described in this report the δ value increases in the oxidation of the neutral compound, while the quadrupole splitting decreases. Comparing these two compounds is not straight forward because the used PDI ligand is highly redox active.

In a second approach, following a methodology developed by Chirik,[72] the Fe(0) complex **21a** was oxidized with the ferrocenium salt [FeCp$_2$]PF$_6$ affording the Fe(I) species **22aPF$_6$**. Dissolving 1 equiv of **21a** in THF and adding 1.05 equiv [FeCp$_2$]PF$_6$, the reaction mixture turns green after 5 minutes and **22aPF$_6$** is obtained in 89% yield (see Scheme 35). Ferrocene can easily be removed by washing the product with pentane. With this synthetic protocol the N-alkylated complexes **21d** and **21e** were tested in this oxidation reaction, but unfortunately the desired product was not synthesized. When using 1 equiv. of ferrocenium salt, the reaction mixture stays read, and the IR shows starting material and yet an unknown Fe(II) species. Further the complexes **21b** bearing the bulky PNP-*t*Bu ligand and **21h** with the PNP-Cy ligand were oxidized to afford **22h** and **22b**.

21a R=*i*Pr, R'=H
21b R=*t*Bu, R'=H
21h R=Cy, R'=H

22a R=*i*Pr, R'=H
22b R=*t*Bu, R'=H
22h R=Cy, R'=H
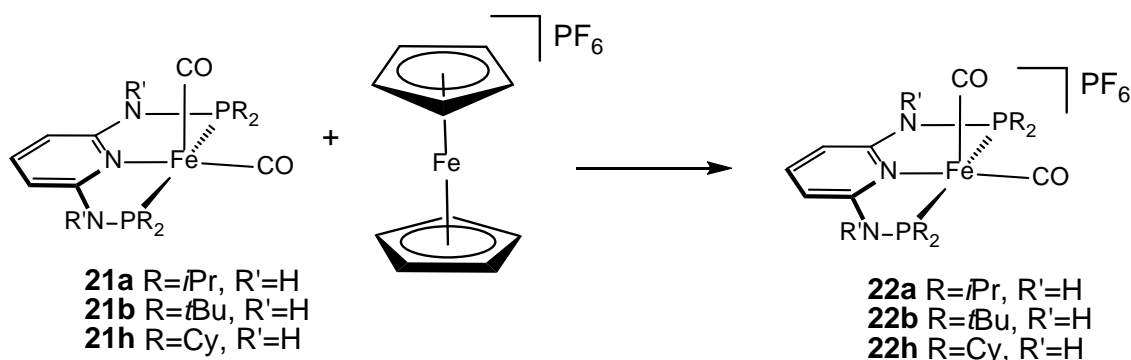
Scheme 35: Oxidation of Fe(0) complexes

Table 14 summarizes the spectroscopic data of the Fe(I) complexes measured in solution using THF as a solvent.

Table 14: Spectroscopic data of Fe(I) complexes, a) ATR

Fe(I)	ν_{co}	ν_{co}
PNP-*i*Pr	1952	1885
PNP-*t*Bu[(a)]	1945	1878
PNP-Ad[(a)]	1936	1869
PNP-Cy	1949	1884

Figure 64 shows the calculated single occupied molecular orbital and the spin density of **22a**. The electron is located in the (SOMO) at the metal center indicating a low-spin 17 electron (d^7) complex. The unpaired spin is exclusively located at the iron center as can be seen from a spin density plot.
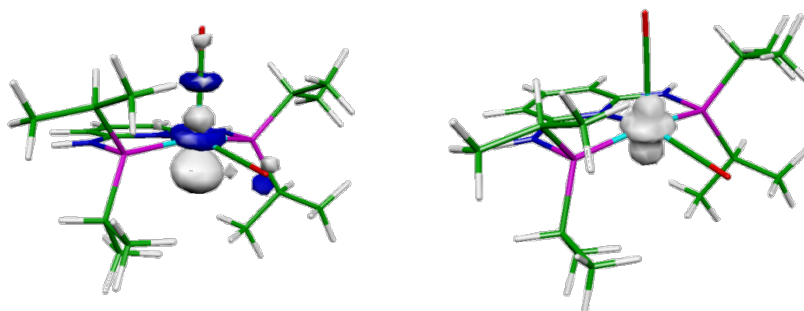
Figure 64: Calculated SOMO and spin density of **22a**

To date only a few Fe(I) PNP pincer complexes were reported. Caulton[75] and Chirik[72] described iron(I) PNP and NNN pincer complexes with (tBu$_2$PCH$_2$SiMe$_2$)$_2$N (PNP) and bis(imino)pyridine (NNN) ligands. Their syntheses is very similar, however, utilizing different starting materials. The [Fe((tBu$_2$PCH$_2$SiMe$_2$)$_2$N)] complex is synthesized by reducing the halide species and purging the reaction mixture with carbon monoxide. The starting material for the bis(imino)pyridine complex is the already reduced [Fe(bis(imino)pyridine)(CO)$_2$] complex, which is described as an Fe(II) compound because of the redox active ligand. This compound was reacted with Na/Hg and 15-crown-5 to afford the Fe(I) complex. Both complexes have similar IR ν_{co} frequencies and can be compared with our complexes being 1943, 1879 cm^{-1} and 1935, 1863 cm^{-1} respectively.

The magnetic moment for complexes **22a** and **22h** was determined in solution by using the Evans method.[100,101] The complexes were dissolved in 1mL of CH_2Cl_2 and the solution was put in a capillary fitting and NMR tube and measured immediately, because of their sensitivity towards oxidation. The magnetic moments are summarized in Table 15. The results refer to one unpaired electron (μ_{eff} = 1.73) and indicates a 17-electron low-spin d^7 complex. Chirik and Caulton reported similar results for Fe(I) pincer complexes.[75,102]

Table 15: Magnetic moments of Fe(I) complexes

	μ_{eff}
PNP-*i*Pr	1.929
PNP-Cy	1.710

The Fe(I) complexes **22a** and **22h** turned out to be reactive towards CH_2Cl_2 and formed the corresponding mono and bis carbonyl complexes. This may be an explanation for the low magnetic moment measured for complex **22h**.

Fluoride abstraction from the PF$_6$ anion and formation of an iron(II)-fluoride complex

The formation of a Fe-F bond by fluoride abstraction was reported in the literature when using BF_4^- as a counterion.[103] The decomposition of BF_4^- is well understood and studied[104,105] but for PF_6 only a few examples are known to literature.[106–108]

To study the fluoride abstraction of the PF_6^- ion complex **21e** was treated with 2 equiv of ferrocenium salt in THF. During this reaction the expected Fe(I) compound is not formed, but a Fe(II) complex. After workup and removing the formed ferrocene complex **23** was isolated as an off white solid in 87 % yield. The synthesis is shown in Scheme 36.
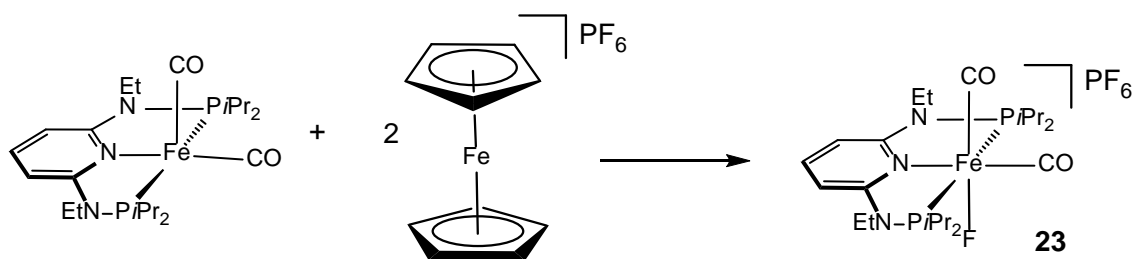
Scheme 36: Synthesis of **23**

Complex **23** was characterized by multinuclear NMR, IR and ESI-MS. The IR spectrum shows two intensive bands for the ν_{CO} at 2047 and 1987 cm^{-1}. The ^{31}P{^{1}H} NMR shows a doublet at 163 ppm for the ligand with a J_{PF} coupling constant of 26.6 Hz.

Performing ESI-MS, the full scan shows an intensive signal at *m/z* 528 which refers to the fragment [Fe(PNP^{Et}-*i*Pr)(CO)$_2$F]$^+$ **M$^+$**. Trapping the signal and performing MS2 shows a second fragment at m/z 472 which corresponds to [Fe(PNP^{Et}-*i*Pr)F]$^+$ **[M-(CO)$_2$]$^+$** after loss of both CO molecules.

Figure 65: MS2 of **23**

7. Conclusion

To conclude several new Fe PNP pincer complexes and new PNP pincer ligands based on 2,6-diamino pyridine were synthesized and characterized by various techniques as well as the reactivity of the new complexes was studied.

In Chapter 3 the synthesis of the new N-alkylated PNP ligands is elucidated. Further the new ring substituted ligands (on the para position) and the synthesis of the PNP-Ad ligand from pure adamantane and PCl_3 is described.

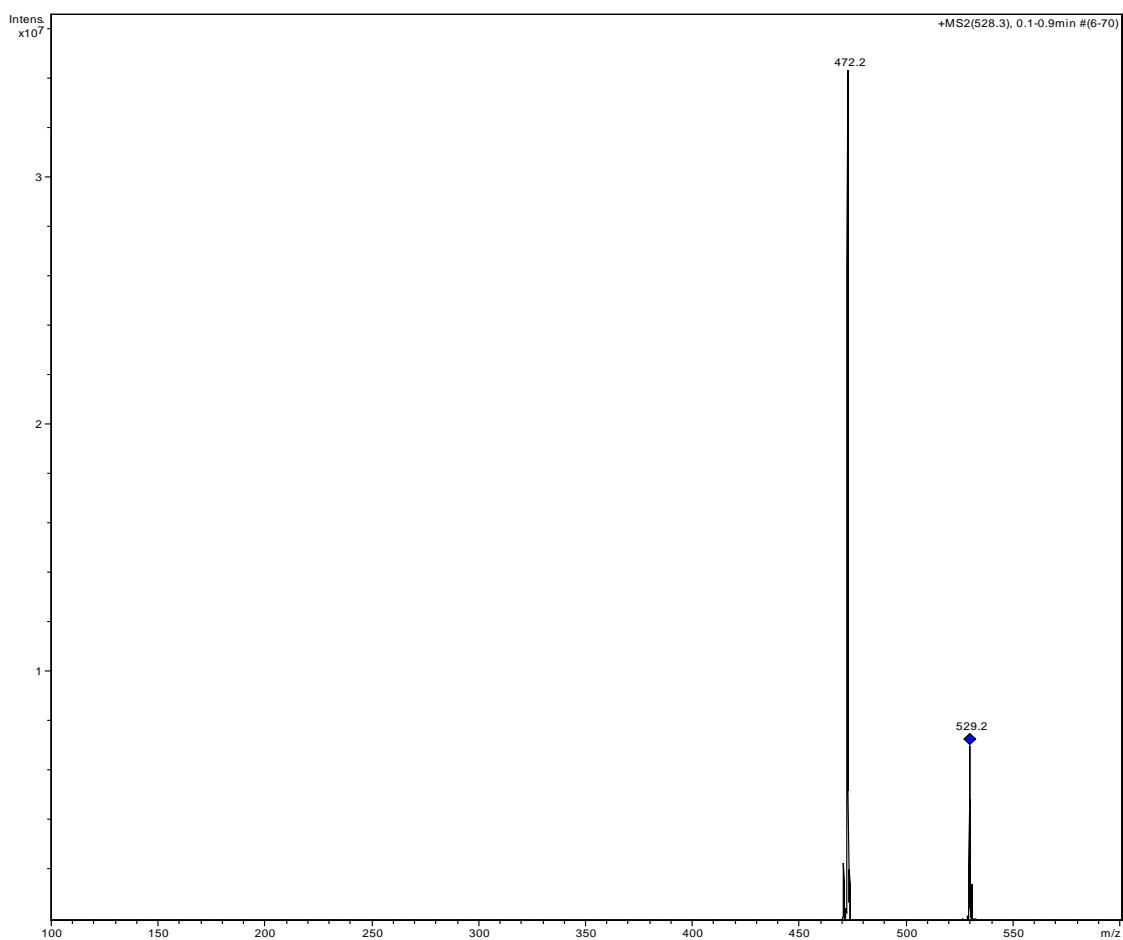Chapter 4 focuses on Fe(II) complexes with PNP-Ph ligands. A series of octahedral Fe(II) complexes of the type $[Fe(\kappa^3\text{-}P,N,P\text{-PNP})(\kappa^2\text{-}P,N\text{-PNP})X]^+$ (X = Cl, BF_4) where the PNP-Ph pincer ligands are coordinated in $\kappa^3\text{-}P,N,P\text{-}$ and $\kappa^2\text{-}P,N\text{-}$fashion, respectively. These complexes adopt a strongly distorted octahedral geometry as established by X-ray crystallography. Obviously related to these distortions is their reactivity undergoing, upon halide dissociation, a facile rearrangement reaction to give the dicationic complexes $[Fe(\kappa^3\text{-}P,N,P\text{-PNP})_2]^+$ where now both PNP ligands are bound in $\kappa^3\text{-}P,N,P\text{-}$fashion. Further the reactivity of these new complexes towards CO was investigated and both the mono-CO and the cationic bis-CO complexes were successfully synthesized and characterized. The mono-CO complexes showed a lability of the CO ligand at elevated temperatures. The heteroleptic $[Fe(PNP\text{-Ph})(PN\text{-Ph})Cl]BF_4$ showed no reaction towards CO.

Further in Chapter 5 the heterolytic cleavage of dihydrogen by reacting the *bis*-carbonyl Fe(II) complex *trans*-$[Fe(PNP\text{-}i\text{Pr})(CO)_2Cl]^+$ reacted with Zn as reducing agent under a dihydrogen atmosphere to yield the Fe(II) hydride complex in 97% isolated yield. A crucial step in this reaction is the reduction of the acidic NH protons of the PNP-*i*Pr ligand to release H_2 and to form the coordinatively unsaturated intermediate $[Fe(PNP^H\text{-}i\text{Pr})(CO)_2]^+$ bearing a dearomatized pyridine moiety. A second method for the hydride synthesis is described in the subsequent chapter by reacting a Fe(0) complex with HBF_4. The reaction mechanism was studied by DFT calculation and deuterium labelling experiments.

The last Chapter describes the synthesis and characterization of Fe(0) and Fe(I) complexes. The new Fe(0) complexes show unique structural features, these complexes show unusually bent Fe-C-O bond angles. Using IR these complexes could be identified as Fe(0) complex. NMR spectroscopy was only possible at -80°C. Performing ESI-MS experiments showed the lability of the CO ligands. Astoundingly Fe(0) complexes featuring bulky substituents seem to be oxidized to Fe(I) complexes by air. This reaction has still to be investigated in detail. In a second

approach the Fe(I) species could be synthesized by oxidizing the Fe(0) complexes with a ferrocenium salt. The Fe(0) and Fe(I) complexes were extremely air sensitive and could only be handled in a glove box. The compounds were characterized by IR spectroscopy in solution and the measuring magnetic moment with Evans method was determined. The oxidation with the ferrocenium salt showed striking differences between NH and N-alkylated ligands. The N-H bridged complexes were oxidized to the Fe(I) compounds where the complexes bearing N-alkylated ligands were oxidized to a Fe(II) complex.

8. Experimental part

8.1 List of abbreviations

Ad	adamantyl
$AlCl_3$	aluminum trichloride
AN/CH_3CN	acetonitrile
BArF	tetrakis[(3,5-trifluoromethyl)phenyl]borate
n-BuLi	n-butylithium
CCl_4	carbon tetrachloride
CO	carbon monoxide
$CHCl_3$	chloroform
DAP	2,6-diaminpyridin
DMSO	dimethyl sulfoxide
Et	ethyl
EtOH	ethanol
Et_2O	diethylether
HBF_4	tetrafluoro boronic acid
HCl	hydrochloric acid
KC_8	potassium graphite
$LiAlH_4$	lithium aluminium hydride
MW	molecular weight
Na/Hg	sodium amalgam
NEt_3	triethylamine
NHC	N-hetrolytic carbene
PCl_3	phosphorus trichloride
Ph	phenyl
*i*Pr	isopropyl
PE	light petrol
RT	room temperature
SQP	square pyramidal
TBP	trigonal bipyramidal
THF	tetrahydrofurane

8.2 General

All manipulations were performed under an inert atmosphere of argon by using Schlenk techniques or in an MBraun inert-gas glovebox. The solvents were purified according to standard procedures[109]. The deuterated solvents were purchased from Aldrich and dried over 4 Å molecular sieves. The ligands N,N'-bis(diphenylphosphino)-2,6-diaminopyridine (PNP-Ph) (**1a**), *N*-diphenylphosphino-2-aminopyridine (PN-Ph), N,N'-bis(diisopropylphosphino)-2,6-diaminopyridine (PNP-*i*Pr) (**1b**), N,N'-bis(ditertbutylphosphino)-2,6-diaminopyridine (PNP-*t*Bu) (**1e**) and N,N'-bis(diisopropylphosphino)-N,N'-dimethylpyridine-2,6-diamine (PNP^{Me}-*i*Pr) (**1k**) were synthesized according to literature[76,110,33]. The complexes *trans*-[Fe(PNP-*i*Pr)(CO)$_2$Cl]^{SbF6} (**15**), [Fe(PNP-*i*Pr)Cl$_2$] (**19a**), [Fe(PNP-*i*Pr)COCl$_2$] (**20a**), [Fe(PNP-*t*Bu)Cl$_2$] (**19b**) and [Fe(PNP^{Me}-*i*Pr)Cl$_2$] (**19d**) were prepared according to literature[26,33,27]. Complexes [Fe(PNP-Me)(CO)Cl$_2$] (**20f**) and [Fe(PNP-Et)(CO)Cl$_2$] (**20g**) were used as received from my colleague. Potassium graphite (KC$_8$) was synthesized according to literature[111]. ^{1}H, ^{13}C{^{1}H}, and ^{31}P{^{1}H} NMR spectra were recorded on Bruker AVANCE-250, AVANCE-300 DPX, and AVANCE-400 spectrometers. ^{1}H and ^{13}C{^{1}H} NMR spectra were referenced internally to residual protio-solvent, and solvent resonances, respectively, and are reported relative to tetramethylsilane (δ = 0 ppm). ^{31}P{^{1}H} NMR spectra were referenced externally to H$_3$PO$_4$ (85%) (δ = 0 ppm). FT-IR spectroscopy was performed using a Bruker Tensor 27 spectrometer.

All mass spectrometric measurements were performed on an Esquire 3000^{plus} 3D-quadrupole ion trap mass spectrometer (Bruker Daltonics, Bremen, Germany) in positive-ion mode by means of electrospray ionization (ESI). Mass calibration was done with a commercial mixture of perfluorinated trialkyl-triazines (ES Tuning Mix, Agilent Technologies, Santa Clara, CA, USA). All analytes were dissolved in methanol "hypergrade for LC-MS Lichrosolv" quality (Merck, Darmstadt, Germany) to form a concentration of roughly 1 mg/mL. Direct infusion experiments were carried out using a Cole Parmer model 74900 syringe pump (Cole Parmer Instruments, Vernon Hills, IL, USA) at a flow rate of 2 µL/min. Full scan and MS/MS (low energy CID)-scans were measured in the range m/z 100-1100 with the target mass set to m/z 1000. Further experimental conditions include: drying gas temperature: 150°C; capillary voltage: -4 kV; skimmer voltage: 40 V; octapole and lens voltages: according to the target mass set. Helium was used as buffer gas for full scans and as collision gas for MS/MS-scans in the low energy CID mode. The activation and fragmentation width for tandem mass spectrometric (MS/MS, CID) experiments was set to 6 Da to cover the main isotope cluster for fragmentation. The corresponding fragmentation amplitude ranged from 0.4 to 0.6 V in order to keep a precursor ion intensity of low abundance in the resulting MS/MS spectrum. All mass

calculations are based on the lowest mass (i.e. most abundant) iron isotope ([56]Fe-isotope). Mass spectra and CID spectra were averaged during data acquisition time of 1 to 2 min and one analytical scan consisted of five successive micro scans resulting in 50 and 100 analytical scans, respectively, for the final full scan mass spectrum or MS/MS spectrum.

## 8.3 Computational details and X-Ray structure determinations

All calculations were performed using the GAUSSIAN 09 software package[112] on the Phoenix Linux Cluster of the Vienna University of Technology. The optimized geometries were obtained with the B3LYP functional[113], without symmetry constraints. That functional includes a mixture of Hartree-Fock[114] exchange with DFT[115] exchange-correlation, given by Becke's three parameter functional with the Lee, Yang and Parr correlation functional, which includes both local and non-local terms. The basis set used for the geometry optimizations consisted of the Stuttgart/Dresden ECP (SDD) basis set to describe the electrons of iron, and a standard 6-31g** basis set for all other atoms.

Single point energy calculations were performed using the M06 functional and a standard 6-311++G(d,p) basis set, on the geometries optimized at the B3LYP/b1 level. The M06 functional is a hybrid meta-GGA functional developped by Truhlar and Zhao, and it was shown to perform very well for the kinetics of transition metal molecules, providing a good description of weak and long range interactions. Solvent effects (THF) were considered in the M06/6-311G(d,p)//B3LYP/b1 energy calculations using the Polarizable Continuum Model (PCM) initially devised by Tomasi and coworkers with radii and non-electrostatic terms of the SMD solvation model, developed by Truhler *et al*.

X-ray diffraction data were collected at T = 100 K in a dry stream of nitrogen on Bruker Kappa APEX II diffractometer using graphite-monochromatized Mo-$K\alpha$ radiation (λ = 0.71073 Å) and fine sliced φ- and ω-scans. Data were reduced with the program SAINT-Plus and corrections for absorption and detector effects were applied with the program SADABS. The structure was solved with direct methods and refined with the SHELX program package[116]. All refinements were against F^2 data. Non-hydrogen atoms were refined anisotropically. The H atoms connected to C atoms were placed in calculated positions and thereafter refined as riding on the parent atoms. H atoms connected to N atoms were mostly located in difference Fourier maps and freely refined. Molecular graphics were generated with the program MERCURY[117].

8.4 Ligand precursors

Di(1-adamantyl)chlorophosphine (4)
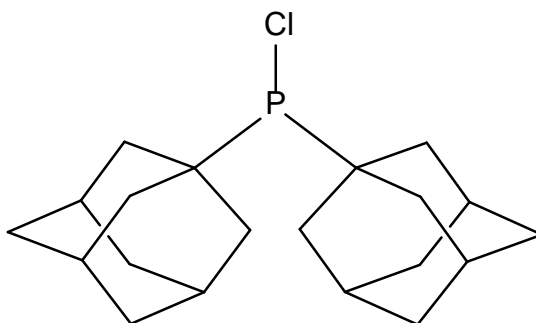
10 g (73.4 mmol) Adamantane, 10.5 g (78.7 mmol) aluminium(III)chloride and 40 ml (458.4 mmol) phosphorus(III)chloride were mixed in a round bottom flask and refluxed overnight. The excess of PCl_3 was removed under reduced pressure until a viscous substance remained. 300 ml of chloroform were added and the suspension was hydrolyzed with an ice/water mixture. Separation of the layers, drying the organic layer with amhydrous $NaSO_4$ and evaporating the solvent gave di-1-adamanylphosphinc chloride **(2)** which was used without further purification in the next step. Yield: 92 %

5 g (14.1 mmol) of **2** were dissolved in THF and cooled with a liquid nitrogen/iPrOH mixture down to -78°C and 1.2 g (31.6 mmol) $LiAlH_4$ were slowly added. After the reaction mixture reached RT it was stirred overnight, cooled down to -10°C and hydrolyzed with 1M HCl. The layers were separated, the organic layer was dried with anhydrous $NaSO_4$ and the solvent was evaporated to give pure di-1-adamantylphosphine **(3)** which was used without further purification. Yield: 98.6 %, 4.2 g 3, 13.9 mmol
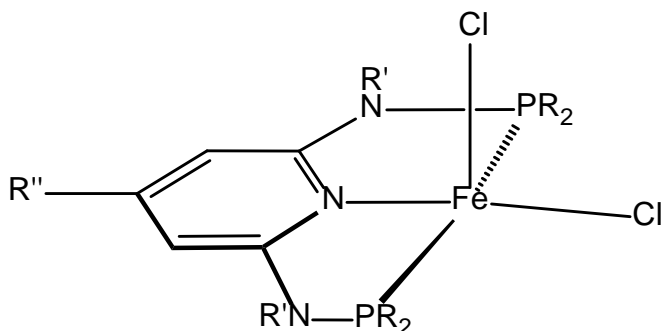
4.2 g **3** were dissolved in CCl_4 and refluxed for 24h. After evaporation of the solvent pure **4** was afforded. Yield: 100 % 4.65 g white solid. Anal Calc. for $C_{20}H_{30}ClP$ (MW: 336,88) C, 71.31; H, 8.98.

^{1}H NMR (δ, CDCl$_3$, 20°C): 2.30 – 1.57 (m).

^{31}P{^{1}H}NMR (δ, CDCl$_3$. 20°C): 149.8

8.5 Metal precursors

General procedure for complexes [Fe(PNP-R)Cl₂] (R = pMe-*i*Pr 19c), (R = N^Et-*i*Pr 19e), (R = Cy 19h), (R = Ad 19i)

19c R=*i*Pr, R'=H, R"=Me
19e R=*i*Pr, R'=Et, R"=H
19h R=Cy, R'=H, R"=H
19i R=Ad, R'=H, R"=H

Anhydrous FeCl₂ (254 mg, 2mmol) and ligand (2.2 mmol) were stirred in THF (10 ml) for 4h and the reaction mixture turned yellow. The solvent was removed under reduced pressure and the remaining yellow solid was washed with three times with Et₂O (15 ml) and dried under vacuum. Yield 85-94 %.

General procedure for complexes *trans*-[Fe(PNP-R)(CO)Cl₂] (R = pMe-*i*Pr 20c), (R = p*t*Bu-*i*Pr 20k), (R = NMe-*i*Pr 20d), (R = NEt-*i*Pr 20e), (R=Cy 20h)
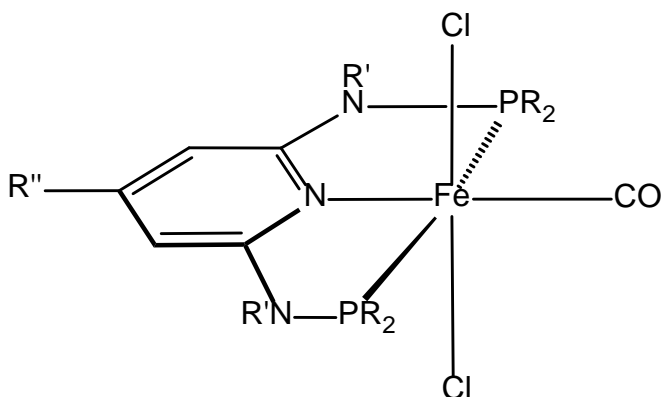
20c R=*i*Pr, R'=H, R"=Me
20k R=*i*Pr, R'=H, R"=*t*Bu
20d R=*i*Pr, R'=Me, R"=H
20e R=*i*Pr, R'=Et, R"=H
20h R=Cy, R'=H, R"=H

The yellow complexes [Fe(PNP-R)Cl₂] (usually 200 mg) were dissolved in THF (15 ml) and gaseous CO was bubbled through the solution. The color changed to blue or purple and the reaction mixture was stirred for 4h. The solvent was evaporated, the compounds were washed with Et₂O (15 ml) and dried under vacuum. When stirring blue ***trans*-20h** with Et₂O the color changes to red and ***cis*-20h** is formed. All the complexes were isolated in quantitative yields.

8.6 Ligands

N,N'-Bis(diethylphosphino)-2,6-diaminopyridine (PNP-Et) (1c)
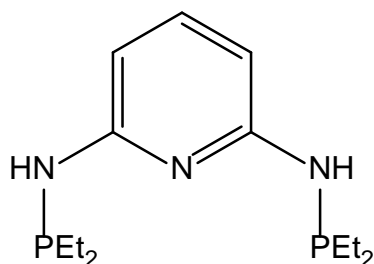
A suspension of 2,6-diaminopyridine (590 mg , 5.4 mmol) in toluene (15 mL) was cooled to 0°C and NEt_3 (1.5 mL, 10.8 mmol) was added. Then a solution of Et_2PCl (1.34 g, 10.8 mmol) in toluene (10 mL) was added slowly via a dropping-funnel. The mixture was then allowed to reach room temperature and stirred for 12 h. The mixture was filtrated over Celite and washed with toluene (5 mL). After removal of the solvent under reduced pressure, a pale red oil was obtained which afforded white crystals in the freezer at -20°C. Yield: 1.46 g (96 %). Anal Calc. for $C_{13}H_{25}N_3P_2$ (MW: 285.31): C, 54.73; H, 8.83; N, 14.73.

^{1}H NMR (δ, $CDCl_3$, 20°C): 7.25 (t, J_{HP} = 8.4 Hz, 1H, py^4), 6.37 (d, J_{HP} = 8.1 Hz, 2H, py^{3,5}), 4.26 (d, J_{HP} = 9.3 Hz, 2H, NH) 1.55 (dq, J_{HH} = 7.4 Hz, J_{HP} = 14.3 Hz, 8H, CH_2), 1.05 (dt, J_{HH} = 7.6 Hz, J_{HP} = 15.3 Hz, 12H, CH_3).

^{13}C{^{1}H} NMR (δ, $CDCl_3$, 20°C): 158.7 (d, J_{CP} = 18.1 Hz, py),139.2 (s, py), 98.1 (d, J_{CP} = 17.7 Hz, py), 23.6 (d, J_{CP} = 11.9 Hz, CH_2), 8.5 (d, J_{CP} = 13.0 Hz, CH_3).

^{31}P{^{1}H} NMR (δ, $CDCl_3$, 20°C): 33.2.

N,N'-Bis(dicyclohexylphosphino)-2,6-diaminopyridine (PNP-Cy) (1d)
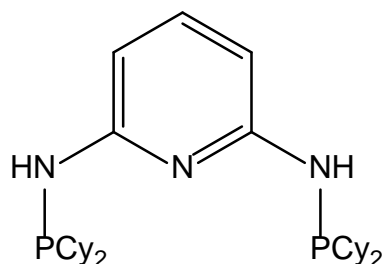
A suspension of 2,6-diaminopyridine (390 mg, 3.6 mmol) in toluene (10 ml) was cooled to 0°C before addition of NEt_3 (2 ml, 14.4 mmol). A solution of Cy_2PCl (1.68 g, 7.2 mmol) in toluene (10 ml) was slowly added via a dropping-funnel. After the addition, the mixture was allowed to reach RT and then stirred at 50-60°C for 36 h. The mixture was filtrated over celite and the solid was washed with 10 ml toluene. The yellow solution is evaporated to dryness. Yield 1.80 g (>99 %) pale yellow solid, Anal Calc. for $C_{29}H_{49}N_3P_2$ (MW: 501.67). C, 69.43; H, 9.84; N, 8.38

^1H NMR (δ, $CDCl_3$, 20°C): 7.26 (m, 1H, py^4), 6.37 (d, J_{HP} = 8.0 Hz, 2H, $py^{3,5}$), 4.26 (s, 2H, NH), 1.77-1.23 (m, 44H).

$^{13}C\{^1H\}$ NMR (δ, $CDCl_3$, 20°C): 158.8 (s, $py^{2,6}$), 139.8 (s, py^4), 97.9 (d, J_{CP} = 19.5 Hz, $py^{3,5}$), 35.9 (d, J_{CP} = 11.5 Hz, CH), 28.8 (d, J_{CP} = 17.5), 27. (d, J_{CP} = 11.4), 26.9 (d, J_{CP} = 11.7), 26.8 (s), 26.7 (s), 26.3 (s).

$^{31}P\{^1H\}$ NMR (δ, $CDCl_3$, 20°C): 41.3 (s).

N,N'-Bis(diadamantylphosphino)-2,6-diaminopyridine (PNP-Ad) (1f)
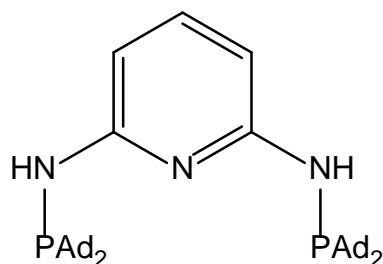
A suspension 2,6-diaminopyridine (200 mg, 1.8 mmol) in THF (50 ml) was cooled to -78°C and a solution of 2.5M n-BuLi in THF (1.5 ml) was added drop wise using a syringe and a rubber septum. After the reaction mixture reached RT it stirred for another 16h and cooled to .78°C. 4 (1.3 g, 3.9 mmol) was dissolved in 40 ml THF and added using a dropping-funnel. After the reaction mixture reached RT it was refluxed overnight. The mixture was filtrated over celite and the yellow solution was evaporated to dryness. Product was not clean; purification and

reaction have still to be improved. Yield yellow solid, Anal Calc. for $C_{45}H_{65}N_3P_2$ (MW: 709.98), C, 76.13; H, 9.23; N, 5.92.

^{1}H NMR (δ, CDCl$_3$, 20°C) 7.35 – 7.12 (m, 1H, py), 6.55 – 6.37 (m, py), 4.68 (d, J = 11.3 Hz, NH), 2.51 – 2.24 (m, Ad), 2.24 – 2.02 (m, Ad), 2.02 – 1.87 (m, Ad), 1.87 – 1.57 (m, Ad).

^{31}P{^{1}H} NMR (δ, CDCl$_3$, 20°C) 67.79 (s).

N,N'-bis(diisopropylphosphino)-4-methylpyridine-2,6-diamine (PNP-pMe-*i*Pr) (1g)
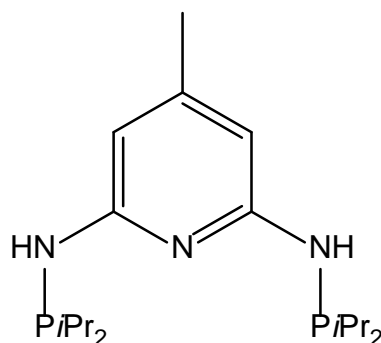
4-methylpyridine-2,6-diamine (500 mg, 4 mmol) was dissolved in toluene and NEt$_3$ (1.2 ml, 8.6 mmol) was added. The mixture was cooled down to 0°C using an ice bath and chlorodiisopropylphosphine (1.3 ml, 8.2 mmol) was added drop wise using a syringe. The cooling bath was removed and after reaching room temperature the reaction mixture was stirred at 80°C for 12h. The precipitate was filtered off and the solvent was evaporated. For further purification the compound can be recrystallized using toluene/hexane 1:1. Yield: 981 mg (69 %) off white powder, Anal Calc. for $C_{18}H_{35}N_3P_2$ (MW: 355.45) C, 60.82; H, 9.93; N, 11.82.

^{1}H NMR (δ, CDCl$_3$, 20°C) 6.34 (s, 2H, py), 4.88 (bs, 2H, NH), 2.18 (s, 3H, CH$_3$), 1.87 – 1.60 (m, 4H, *i*Pr), 1.15 – 0.92 (m, 24H, *i*Pr).

^{31}P{^{1}H} NMR (δ, CDCl$_3$, 20°C) 55.65.

^{13}C{^{1}H} NMR (δ, CDCl$_3$, 20°C) 156.59 (d, J = 21.9 Hz), 153.94 (s), 99.14 (d, J = 19.7 Hz), 26.27 (d, J = 11.4 Hz), 21.80 (d, J = 15.3 Hz), 18.46 (d, J = 19.7 Hz), 17.18 (d, J = 7.9 Hz).

N,N'-bis(diphenylphosphino)-4-methylpyridine-2,6-diamine (PNP-pMe-Ph) (1h)
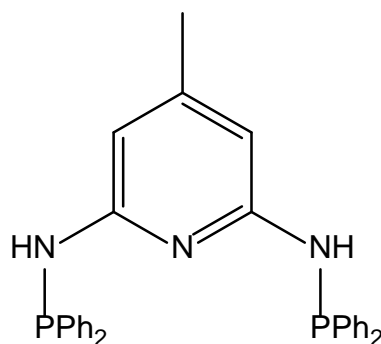
This compound was synthesized according to **1g** using 4-methylpyridine-2,6-diamine (500 mg, 4 mmol, 1 eq) and chlorodiphenylphosphine (1.5 ml, 8.2 mmol). Yield: 1.42 g (72%) off white solid, Anal Calc. for $C_{30}H_{27}N_3P_2$ (MW: 491.51) C, 73.31; H, 5.54; N, 8.55.

^{1}H NMR (δ, CDCl$_3$, 20°C) 7.85 − 7.75 (m, 2H, py), 7.52 − 7.43 (m, 6H, py. ph), 7.43 − 7.31 (m, 14H, ph), 5.02 (s, J = 8.2 Hz, 2H, NH), 2.20 (s, 3H, CH$_3$).

^{31}P{^{1}H} NMR (δ, CDCl$_3$, 20°C) 25.36 (s).

^{13}C NMR (δ, CDCl$_3$, 20°C) 139.70 (d, J = 11.1 Hz), 135.42 (s), 131.29 (d, J = 20.9 Hz), 130.40 − 126.69 (m), 100.15 (s, J = 16.8 Hz), 21.39 (s).

N,N'-bis(diisopropylphosphino)-4-tertbutylpyridine-2,6-diamine (PNP-p*t*Bu-*i*Pr) (1i)
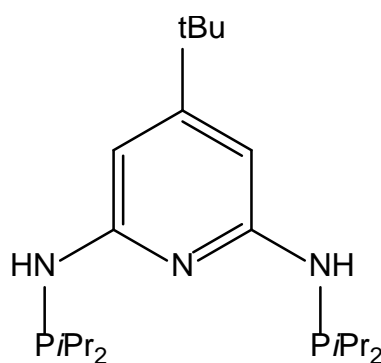
This compound was synthesized according to **1g** using 4-tertbutylpyridine-2,6-diamine (2 g, 12.1 mmol), NEt$_3$ (3.4 ml, 24.5 mmol) and chlorodiisopropylphosphine (3.9 ml, 24.3 mmol). Yield: 4.2 g (87 %), Anal Calc. for $C_{21}H_{41}N_3P_2$ (MW: 397.53) C, 63.45; H, 10.40; N, 10.57

^{1}H NMR (δ, CDCl$_3$, 20°C) 6.48 (d, J = 2.7 Hz, 2H, py), 4.49 (s, 2H, NH), 1.91 − 1.59 (m, 4H, *i*Pr), 1.24 (s, 9H, *t*Bu), 1.15 − 0.97 (m, 24H, *i*Pr).

^{31}P{^{1}H} NMR (δ, CDCl$_3$, 20°C) 59.85 (s).

$^{13}C\{^1H\}$ NMR (δ, CDCl$_3$, 20°C) 158.66 (d, J = 21.0 Hz), 95.79 (d, J = 19.1 Hz), 35.04 (s), 30.54 (s), 26.42 (d, J = 11.5 Hz), 18.69 (d, J = 19.5 Hz), 17.16 (d, J = 7.9 Hz).

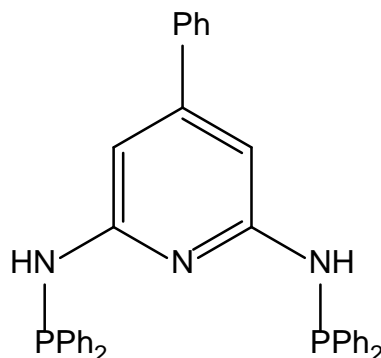**N,N'-bis(diphenylphosphino)-4-phenylpyridine-2,6-diamine (PNP-pPh-Ph) (1j)**

This compound was synthesized according to **1g** using 4-phenylpyridine-2,6-diamine (1g, 5.4 mmol), NEt$_3$ (1.5 ml, 11 mmol) and chlorodiphenylphosphine (2 ml, 11 mmol). Yield: 2.5 g (83 %) beige solid, Anal Calc. for C$_{35}$H$_{29}$N$_3$P$_2$ (MW: 553.59) C, 75.94; H, 5.28; N, 7.59

^1H NMR (δ, CDCl$_3$, 20°C) 7.86 − 7.67 (m, 2H, py), 7.66 − 7.52 (m, 5h, py, ph), 7.52 − 7.19 (m, 24H, ph), 6.80 (d, J = 1.5 Hz, 2H, ph), 5.44 (s, 2H, NH).

$^{31}P\{^1H\}$ NMR (δ, CDCl$_3$, 20°C) 38.15 (s).

N,N'-bis(diisopropylphosphino)-N,N'-diethylpyridine-2,6-diamine (PNP^{Et}-iPr) (1l)
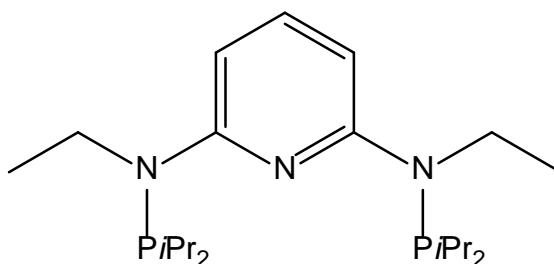
A solution of 2,6–N,N'-diethylaminopyridine (500 mg, 3 mmol) in toluene (50 ml) was cooled down to -78°C and a solution of 2.5M n-BuLi in THF (1,2 ml, 3 mmol) was added using a syringe. The reaction mixture was allowed to reach RT and it was stirred for another 4h. The mixture was colled down to -40°C and chlorodiisopropylphosphine (0.5 ml, 3 mmol) was added. After the reaction mixture reached RT it was refluxed overnight. The mixture was cooled down to -78°C and a solution of 2.5M n-BuLi in THF (1,2 ml, 3 mmol) was added using a syringe. The reaction mixture was allowed to reach RT and it was stirred for another 4h. The mixture was colled down to -40°C and chlorodiisopropylphosphine (0.5 ml, 3 mmol) was added. After the reaction mixture reached RT it was refluxed overnight. The reaction mixture

was allowed to reach RT and it was quenched with water. The organic layer was dried with anhydrous $NaSO_4$ and the solvent was evaporated. Yield: 1.1 g (90%) yellow oil. Anal Calc. for $C_{21}H_{41}N_3P_2$ (MW: 397.53) C, 63.45; H, 10.40; N, 10.57.

^1H NMR (δ, $CDCl_3$, 20°C) 7.26 (t, J = 8.0 Hz, 1H, py), 6.50 (s, 2H, py), 3.85 – 3.42 (m, 4H, CH_2), 2.73 – 1.81 (m, 4H, iPr), 1.56 – 0.53 (m, 30H, iPr, CH_3).

$^{31}P\{^1H\}$ NMR (δ, $CDCl_3$, 20°C) 91.1 (bs).

N,N'-bis(diphenylphosphino)-N,N'-dimethylpyridine-2,6-diamine (PNP^{Me}-Ph) (1m)
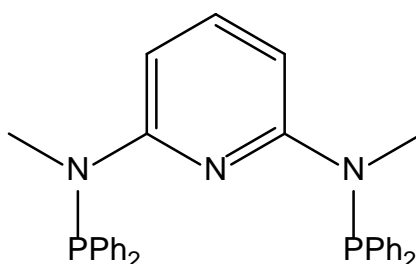
This compound was synthesized according to **1l** using 2,6–N,N'-dimethylaminopyridine (300 mg, 2.2 mmol), two times n-BuLi solution (0.9 ml, 2.2 mmol) and two times chlorodiiphenylphosphine (0.4 ml, 2.2 mmol). Yield: 0.9 g (81%) yellow solid, Anal Calc. for $C_{31}H_{29}N_3P_2$ (MW: 505.54) C, 73.65; H, 5.78; N 8.31.

^1H NMR (δ, $CDCl_3$, 20°C): 7.38-7.44 (m, 21H, py, ph), 6.87(d, J = 7.4 Hz, 2H, ph), 2.89 (s, 6H, CH_3).

$^{31}P\{^1H\}$ NMR (δ, $CDCl_3$, 20°C): 62.5 (s)

$^{13}C\{^1H\}$ NMR (δ, $CDCl_3$, 20°C): 159.6 (d, J = 27.4 Hz), 138.4 (t, J = 3.0 Hz), 137.5 (d, J = 16.0 Hz), 132.2 (d, J = 20.8 Hz), 129.2 (s), 128.5 (d, J = 5.9 Hz), 99.9 (d, J = 21.2 Hz), 34.1 (d, J = 8.6 Hz).

8.7 Fe(II) complexes featuring κ^3, κ^2 bound PNP-Ph based ligands

[Fe(κ^3-*P,N,P*-PNP-Ph)(κ^2-*P,N*-PNP-Ph)Cl]$^+$ (2)
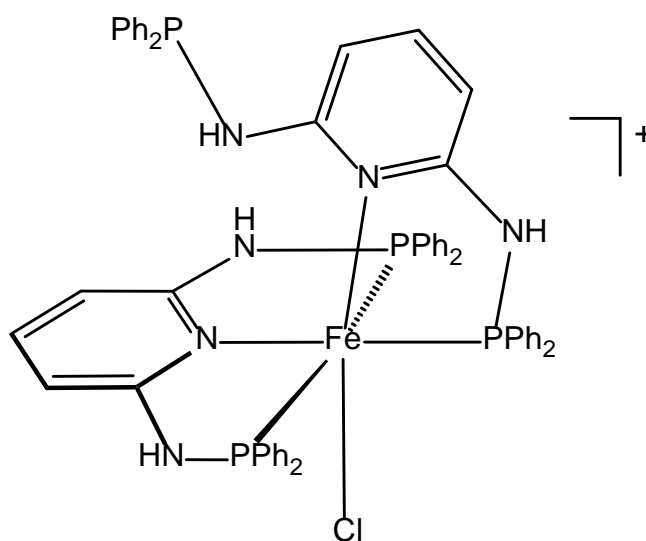
2BF$_4$: To a suspension of anhydrous FeCl$_2$ (127 mg, 1 mmol) in THF (10 mL) PNP-Ph (**1a**) (960 mg, 2.00 mmol) and AgBF$_4$ (195 mg, 1.0 mmol) was added and the mixture was stirred for 4h. The solvent was removed under reduced pressure and the remaining green solid was dissolved in CH$_2$Cl$_2$. The white precipitate (AgCl) was removed by filtration over celite and the solution was evaporated under reduced pressure. The remaining green solid was washed twice with diethyl ether (10 mL) and dried under vacuum. Yield: 1.10 g. (97%) green solid. Anal Calc. for C$_{58}$H$_{50}$BClF$_4$FeN$_6$P$_4$ (1133.07): C, 58.18; H, 4.30; N, 6.90. Found: C: 59.12; H, 4.51; N, 6.73.

2Cl: This complex was prepared in similar fashion to 2 with anhydrous FeCl$_2$ (127 mg, 1 mmol) and PNP-Ph (**1a**) (980 mg, 2.05 mmol). The reaction mixture was stirred in THF (10mL) for 4h and the solvent was then removed under reduced pressure. The green solid was washed with 10 mL of diethy ether (three times) and dried under vacuum. Yield: 1.06 g (98 %) green solid Anal Calc. for C$_{58}$H$_{50}$Cl$_2$FeN$_6$P$_4$ (MW: 1081.72): C, 64.40; H, 4.66; N, 7.77. All spectral data for **2Cl** were identical with those of **2BF$_4$**

^{1}H NMR (CD$_2$Cl$_2$, 20°C, δ): 6.2-8.7 (m, 50H, py, ph, NH).

^{31}P{^{1}H} (CD$_2$Cl$_2$, 20°C, δ): A$_2$B spin system, δ_A = 108.7 (2P), δ_B = 100.9 (1P), J$_{PP}$ = 50.0 Hz (shifts and J$_{PP}$ determined from simulation), 47.0 (s, 1P)

^{13}C{^{1}H} NMR (CD$_2$Cl$_2$, 20°C, δ) 163.55 (s), 140.63 (s), 138.03 (s), 135.98 (s), 133.69 – 131.60 (m), 130.83 – 127.33 (m), 100.51 (s).

[Fe(κ³-P,N,P-PNP-Ph)₂](Cl)₂ (3)
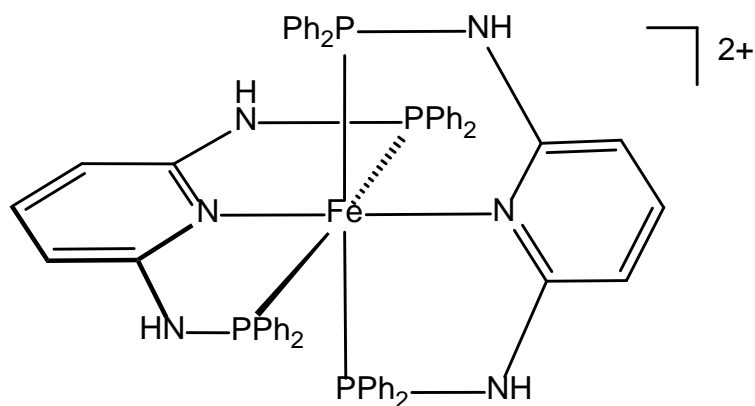
A solution of complex **2Cl** (50mg, 0.046 mmol) in 5 ml of CH_3CN was stirred for 15 min, whereupon the color changed from green to red. The solvent was evaporated and the remaining red solid was washed with diethyl ether and dried in vacuum. Yield: 45 mg (90 %) red solid. All spectral data for **3** were identical with those of the authentic sample reported previously[25].

[Fe(κ³-*P,N,P*-PNP^Me-Ph)(κ²-*P,N*-PN^NHMe-Ph)Cl]BF₄ (4)
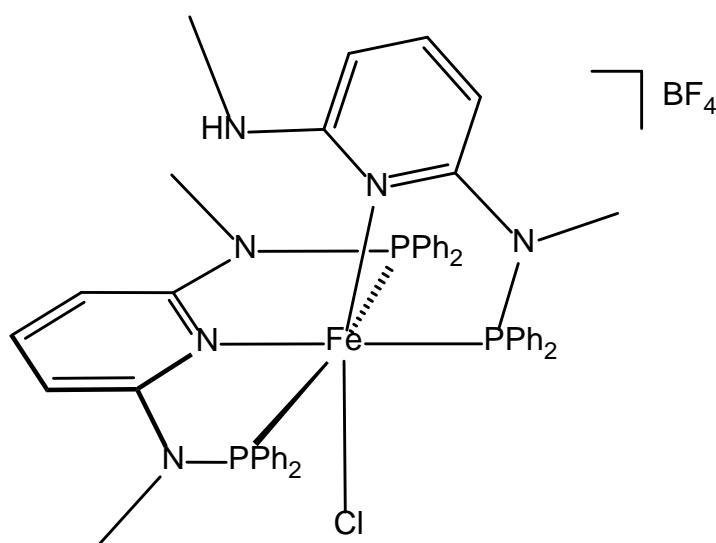
This compound was synthesized according to **2BF₄** using anhydrous $FeCl_2$ (127 mg, 1.0 mmol) in THF (10 ml) PNP^Me-Ph (**1m**) (1.02 g, 2.00 mmol) and AgBF₄ (195 mg, 1.0 mmol). Yield: 950 mg (94%) green solid. Crystals of **4** were grown by slow diffusion of diethyl ether into a solution of THF. Anal Calc. for $C_{50}H_{49}BClF_4FeN_6P_3$ (1005.00): C, 59.76; H, 4.91; N, 8.36. Found: C, 59.83; H, 4.86; N, 8.31.

¹H NMR (δ, CD_2Cl_2, 20°C): 6.80-8.10 (m, 41H, py, Ph), 2.97 (bs, 9H, C*H₃*).

^{31}P{^{1}H} (δ, CD$_2$Cl$_2$, 20°C): A$_2$B spin system, δ$_A$ = 128.1 (2P), δ$_B$ = 122.6 (1P), J$_{PP}$ = 45.5 Hz (shifts and J$_{PP}$ determined from simulation).

^{13}C{^{1}H} NMR (δ, CD$_2$Cl$_2$, 20°C) 164.67 (s), 162.22 (s), 161.38 (s), 142.48 (s), 138.99 (s), 133.53 (s), 132.42 – 127.28 (m), 100.52 (s).

[Fe(κ^3-*P,N,P*-PNP-pMe-Ph)(κ^2-*P,N*-PN^{NH}-pMe-Ph)Cl]BF$_4$ (5)
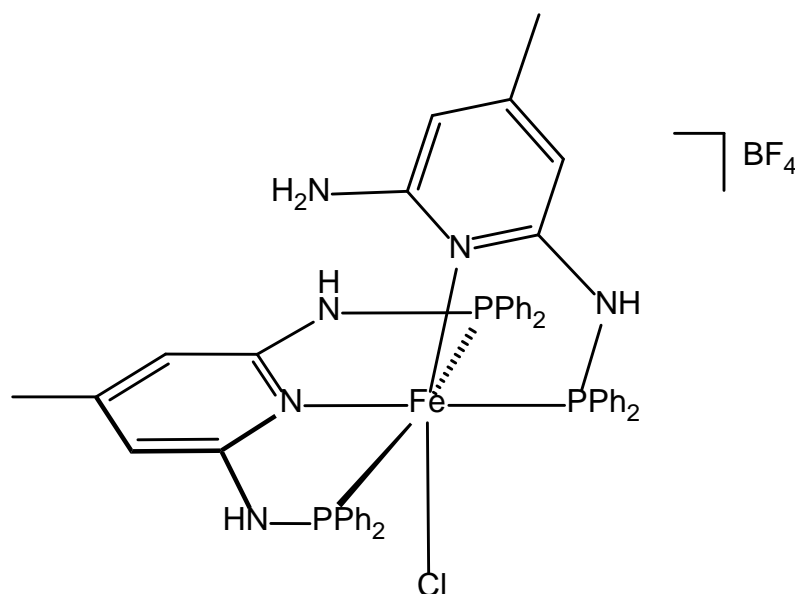
This compound was synthesized according to **2BF$_4$** using anhydrous FeCl$_2$ (127 mg, 1.0 mmol) in THF (10 ml) PNP-pMe-Ph (**1h**) (1 g, 2.00 mmol) and AgBF$_4$ (195 mg, 1.0 mmol). Yield: 910 mg (93%) green solid. Anal Calc. for C$_{48}$H$_{45}$BClF$_4$FeN$_6$P$_3$ (MW: 976.95) C, 59.01; H, 4.64; N, 8.60

^{1}H NMR (δ, CD$_2$Cl$_2$, 20°C): 8.26 – 6.50 (m, ph), 5.36 (s, NH), 3.71 (s), 1.85 (s).

^{31}P{^{1}H} (δ, CD$_2$Cl$_2$, 20°C): A$_2$B spin system, δ$_A$ = 97.2 (2P), δ$_B$ = 89.5 (1P), J$_{PP}$ = 55 Hz (shifts and J$_{PP}$ determined from simulation).

^{13}C{^{1}H} NMR (δ, Acetone, 20°C): 163.23 (s), 152.63 (s), 132.95 (s), 131.67 (s), 130.56 – 127.02 (m).
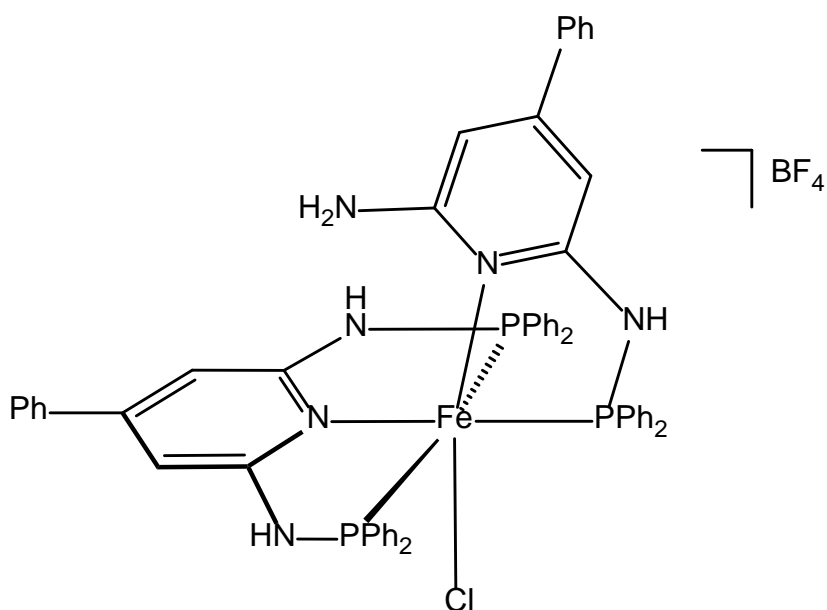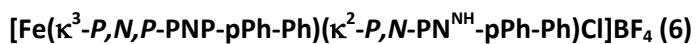
[Fe(κ³-*P,N,P*-PNP-pPh-Ph)(κ²-*P,N*-PN^NH-pPh-Ph)Cl]BF₄ (6)

This compound was synthesized according to **2BF₄** using anhydrous $FeCl_2$ (127 mg, 1.0 mmol) in THF (10 ml) PNP-pMe-Ph (**1j**) (1 g, 2.00 mmol) and $AgBF_4$ (195 mg, 1.0 mmol). Yield 985 mg (89%) green solid. Anal Calc. for $C_{58}H_{49}BClF_4FeN_6P_3$ (MW: 1101.09) C, 63.27; H, 4.49; 5.07; N, 7.63.

^1H NMR (δ, Acetone, 20°C) 8.51 – 6.05 (m), 5.82 (s), 3.00 (s)

$^{31}P\{^1H\}$ (δ, Acetone, 20°C): A_2B spin system, δ_A = 106.9 (2P), δ_B = 101.5 (1P), J_{PP} = 50 Hz (shifts and J_{PP} determined from simulation).

$^{13}C\{^1H\}$ NMR (δ, Acetone, 20°C) 134.84 – 125.11 (m).

Fe[(κ³-*P,N,P*-PNP--Ph)(κ²-*P,N*-PN-Ph)Cl]BF₄ (7)
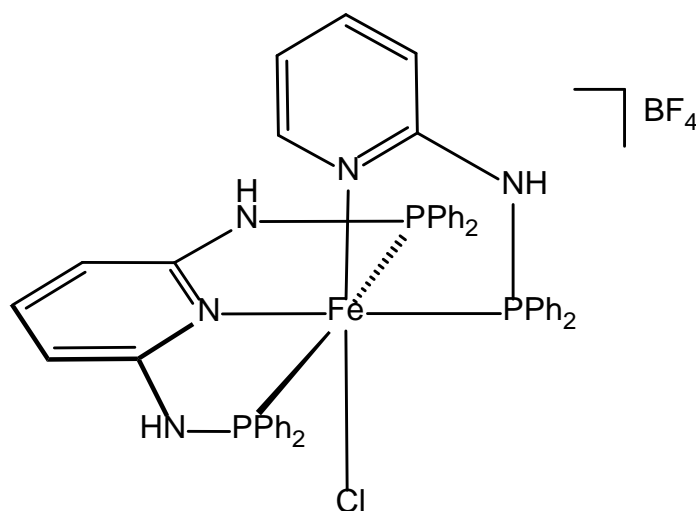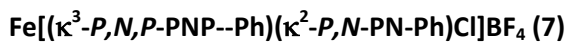
To a suspension of FeCl₂ (127mg, 1mmol) in THF (10 ml) PNP-Ph (**1a**) (480mg, 1mmol), PN-Ph (280mg, 1mmol) and NaBF₄ (110mg, 1mmol) were added and stirred for 4h. The mixture became green immediately. The white precipitate war filtered off over celite and the solution was evaporated under reduced pressure. The green powder was washed twice with diethyl ether (10ml) affording **7** as a green solid. Single crystals suitable for X-ray diffraction could be grown by Et₂O diffusion into a saturated solution of **7** in THF… Yield 900 mg (96%) green solid. Anal Calc. for C₄₆H₄₀BClF₄FeN₅P₃ (MW: 933.88): C: 59.11, H: 4.32, N: 7.5.

^{1}H NMR (δ, d_6-Acetone, 20°C): 8.67 (s, 2H, py), 7.81 (s), 7.37 (s), 7.26 − 7.00 (m), 7.00 − 6.73 (m).

^{31}P{^{1}H} (δ, Acetone, 20°C): A₂B spin system, δ_A = 112.5 (2P, PNP-Ph), δ_B = 111.85 (1P, PN-Ph), J_{PP} = 50.5 Hz (shifts and J_{PP} determined from simulation).

^{13}C{^{1}H} NMR (δ, Acetone, 20°C) δ 164.88 (s), 163.04 (s), 150.57 (s), 140.54 (s), 136.04 (s), 133.35 (s), 130.26 − 129.24 (m), 129.14 − 128.61 (m), 128.28 − 127.72 (m), 127.49 (s), 115.30 (s), 99.78 (s).

8.8 Fe(II) carbonyl complexes bearing PNP-Ph based ligands

Fe(PNP-Ph)COCl₂ (8)
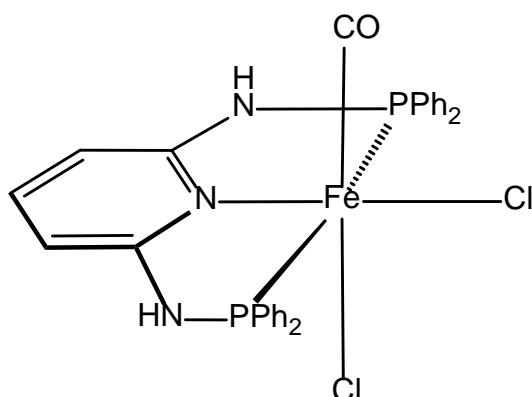
Procedure 1: Compound **2Cl** (200 mg, 0.185 mmol) was dissolved in THF (10 ml), CO was bubbled through the solution and the color changed from green to red after 30 minutes. The solution was stirred overnight and a red precipitate was formed. The solvent was evaporated under reduced pressure and the compound was washed with 3 times with ether (10 ml) and dried under vacuum. Yield: 117 mg (98%). **Procedure 2:** To a suspension of anhydrous FeCl₂ (100 mg, 0.787 mmol) in THF (10 ml) PNP-Ph (**1a**) (380 mg, 0.790 mmol) was added and CO gas was immediately bubbled through the solution. The mixture was stirred for 4 h. The red suspension was evaporated to dryness and the red solid was washed three times with Et₂O (15 ml) and dried under vacuum. Yield: 463 mg (93%) red solid. Anal Calc. for $C_{30}H_{25}Cl_2FeN_3OP_2$ (MW: 632.24): C, 56.99; H, 3.99; N, 6.65

^{1}H NMR (δ, CD_2Cl_2, 20°C) 9.38 (s, 1H), 8.30 – 8.23 (m, 1H), 8.13 (s, 1H), 7.98 (s, 2H), 7.84 (s, 2H), 7.51 (s, 2H), 7.40 (s, J = 6.8 Hz, 7H), 6.37 (s, J = 6.5 Hz, 1H).

^{31}P{^{1}H} NMR (δ, CD_2Cl_2, 20°C) δ 88 (s).

^{13}C{^{1}H} NMR (δ, CD_2Cl_2, 20°C) 216.92 (t, J = 29.0 Hz, CO), 162.33 (t, J = 9.3 Hz), 132.78 (t, J = 5.5 Hz), 130.39 (t, J = 5.9 Hz), 130.05 (s), 128.28 (t, J = 4.4 Hz), 127.63 (t, J = 5.2 Hz), 99.40 (s).

IR (ATR, cm^{-1}): 1985 (ν_{CO}).

[Fe(PNP-Ph)*trans*-(CO)₂Cl]BF₄ (9)
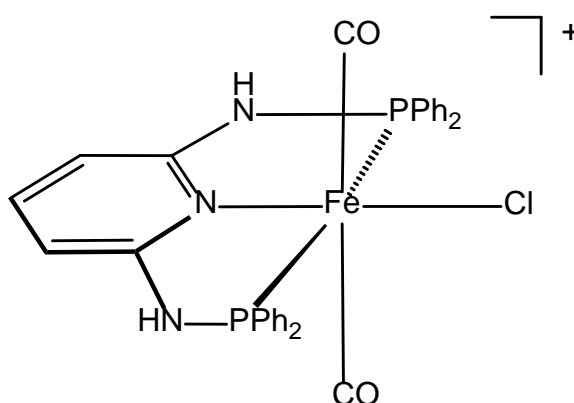
Complex **8** (200 mg, 0.316 mmol) was dissolved in THF (10 ml), CO gas was bubbled through the solution and AgBF₄ (62 mg, 0.316 mmol) was added. After 4h the red solution was filtered over celite and the solvent was evaporated. The red powder was washed with Et₂O (20 ml) and dried under vacuum. Yield 180 mg (85 %) red solid. Anal Calc. for $C_{34}H_{33}ClFeN_3O_2P_2$ (MW: 668.9): C, 61.05; H, 4.97; N, 6.28.

^{1}H NMR (δ, Acetone, 20°C) 8.89 (s, 1H), 8.22 (s, 2H), 8.01 (s, 2H), 7.45 (s, 3H), 7.39 (s, 4H), 6.44 (d, *J* = 6.6 Hz, 1H).

^{31}P{^{1}H} NMR (δ, Acetone, 20°C) 85 (s).

^{13}C{^{1}H} NMR (δ, Acetone, 20°C) 207.19 (t, *J* = 25.8 Hz), 161.34 (s), 141.84 (s), 133.75 (s, *J* = 27.2 Hz), 132.10 (s), 130.18 (s, *J* = 5.2 Hz), 129.20 (s, *J* = 5.3 Hz), 102.15 (s).

IR (ATR, cm^{-1}): 2031 (ν_{CO}).

Fe(PNP^Me-Ph)COCl₂ (11)
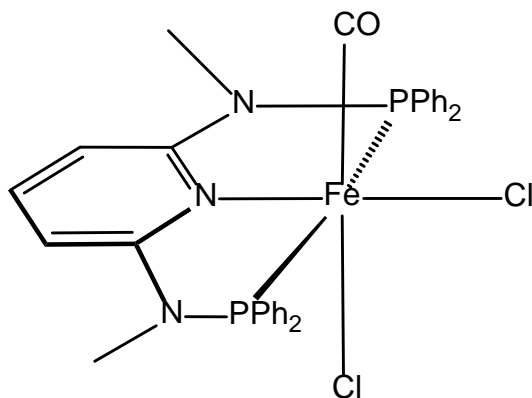
This complex was synthesized according to **8** using anhydrous FeCl₂ (100 mg, 0.787 mmol) and **1m** (410 mg, 0.811 mmol). Yield: 473 mg (91%) red powder. Anal Calc. for C₃₂H₂₉Cl₂FeN₃OP₂ (MW: 660.3) C, 58.21; H, 4.43; N, 6.36.

^{1}H NMR (δ, CD₂Cl₂, 20°C): 8.22 (s, 1H), 7.92 – 7.10 (m, 7H), 6.33 (s, 1H), 3.35 (s, 1H).

^{31}P{^{1}H} NMR (δ, CD₂Cl₂, 20°C) 115.10 (s).

^{13}C{^{1}H} NMR (δ, CD₂Cl₂, 20°C) 216.39 (t, J = 28.9 Hz, CO), 163.50 (t, J = 10.5 Hz), 135.03 (s), 134.91 – 134.48 (m), 131.12 (s), 130.81 (s), 129.57 (s), 129.35 (s), 129.12 (s), 128.78 (s), 127.88 (s), 100.25 (s), 37.81 (s).

IR (ATR, cm^{-1}): 1961 (ν_{CO}).

[Fe(PNP^Me-Ph)*trans*-(CO)₂Cl]BF₄ (12)
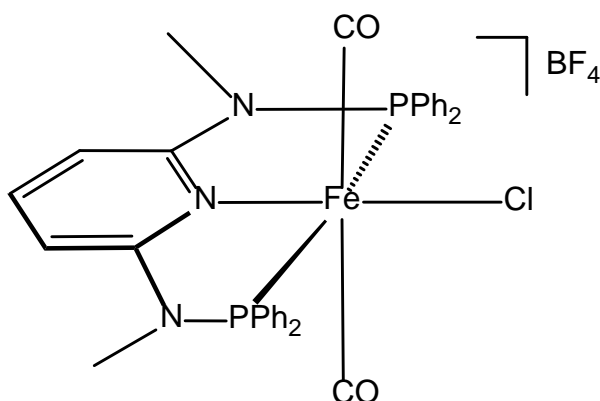
This complex was synthesized like **9** using **11** (200 mg, 0.303 mmol) and AgBF₄ (60 mg, 0.308 mmol) as starting material. Yield: 165 mg (78%) red powder. Anal Calc. for C₃₆H₃₇ClFeN₃O₂P₂ (MW: 696.95) C, 62.04; H, 5.35; N, 6.03.

^{1}H NMR (δ, CD₂Cl₂, 20°C) 8.61 – 6.99 (m, 10H), 1.20 (s, J = 5.6 Hz, 1H).

$^{31}P\{^1H\}$ NMR (δ, CD_2Cl_2, 20°C) 111.24 (s).

$^{13}C\{^1H\}$ NMR (δ, CD_2Cl_2, 20°C) 206.89 (t, J = 25.4 Hz), 133.07 (s), 131.82 (s, J = 23.2 Hz), 130.14 (s), 130.08 – 128.18 (m), 15.30 (s).

IR (ATR, cm^{-1}): 2012 (ν_{CO}).

Fe(PNP-pMe-Ph)COCl$_2$ (13)
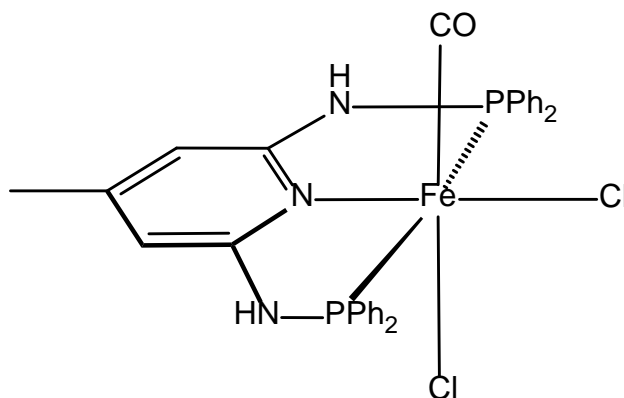
This complex was synthesized according to **8** using anhydrous FeCl$_2$ (100 mg, 0.787 mmol) and **1h** (400 mg, 0.814 mmol). Yield: 380 mg (75 %) red powder. Anal Calc. for C$_{31}$H$_{27}$Cl$_2$FeN$_3$OP$_2$ (MW: 646.27) C, 57.61; H, 4.21; N, 6.50.

^1H NMR (δ, DMSO, 20°C) 8.69 – 6.35 (m, ph, py), 3.49 (s, CH$_3$).

^{31}P NMR (δ, DMSO, 20°C) 87.5 (s).

IR (ATR, cm^{-1}): 1974 (ν_{CO}).

[Fe(PNP-pMe-Ph)(CO)₂Cl]BF4 (14)
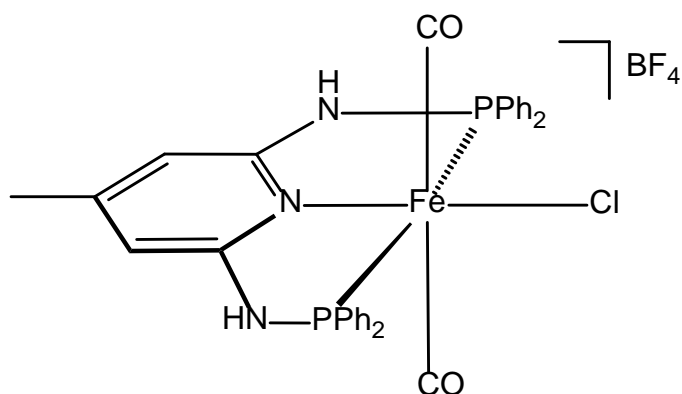
This complex was synthesized like **9** using **13** (200 mg, 0.310 mmol) and AgBF$_4$ (60 mg, 0.310 mmol) as starting material. Yield: 188 mg (84 %) red powder. Anal Calc. for C$_{32}$H$_{27}$BClF$_4$FeN$_3$O$_2$P$_2$ (MW: 725.63) C, 52.97; H, 3.75; N, 5.79.

^{1}H NMR (δ, Acetone, 20°C) 8.66 – 6.31 (m, ph. py), 5.26 (s, NH), 3.50 (s, CH3).

^{31}P{^{1}H} NMR (δ, Acetone, 20°C) 85.8 (s).

^{13}C{^{1}H} NMR (δ, CD$_2$Cl$_2$, 20°C) 207.64 (t, J = 25.8 Hz, CO), 162.02 (d, J = 81.9 Hz), 153.85 (t, J = 60.7 Hz), 138.39 – 123.31 (m, ph, py), 21.23 (s, CH$_3$).

IR (ATR, cm^{-1}): 2038 (ν_{CO}).

8.9 Fe (II) complexes with PNP-*i*Pr ligands

***trans*-[Fe(PNP-*i*Pr)(CO)₂Cl]SbF₆ (15-d₂)**
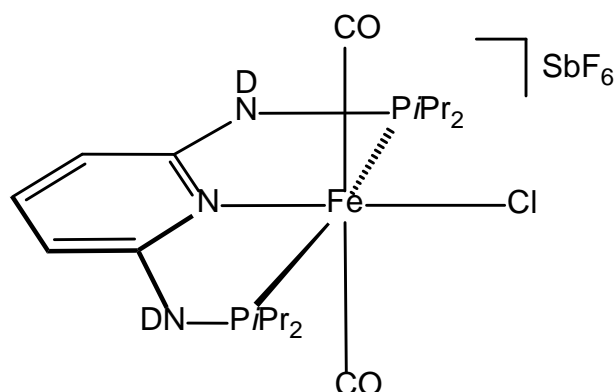
This complex was prepared in analogous fashion to **15** utilizing the N-deuterated ligand PNP-*i*Pr. **1b-d₂** (150 mg, 0.319 mmol) was treated with AgSbF₆ (110 mg, 0.319 mmol) in THF (15 mL) under CO atmosphere for 2h. The former was obtained by treatment of PNP-*i*Pr with D_2O in CH_2Cl_2. After drying over $NaSO_4$ and filtration under argon, the solvent was removed under vacuum, giving the N- deuterated ligand PNP-*i*Pr in essentially quantitative yield. The pink solution was filtered and the solvent was evaporated. The resulting residue was washed twice with Et_2O (15 mL) and dried under vacuo. Yield: 176 mg (76%).

¹H-NMR (δ, acetone-d₆, 20°C): 7.40 (s, 1H, py⁴), 6.32 (s, 2H, py³,⁵), 3.40 (bs, 4H, C*H*(CH₃)₂), 1.64 (bs, 24H, CH(C*H*₃)₂).

¹³C{¹H} NMR (δ, acetone-d₆, 20°C): 212.2 (t, $^2J_{CP}$ = 24.6 Hz, *C*O), 161.9 (d, $^2J_{CP}$ = 6.2 Hz, py) 161.9 (d, $^2J_{CP}$ = 6.5 Hz, py), 141.9 (s, py⁴), 100.4 (bs, py³,⁵), 32.0 (d, $^1J_{CP}$ = 12.4 Hz, *C*H(CH₃)₂), 31.9 (d, $^1J_{CP}$ = 12.3 Hz, *C*H(CH₃)₂), 17.8 (s, CH(*C*H₃)₂), 17.6 (s, CH(*C*H₃)₂).

³¹P{¹H} NMR (δ, acetone-d₆, 20°C): 107.2.

IR (ATR, cm⁻¹): 2015 cm (ν$_{CO}$), 1957 cm (ν$_{CO}$).

cis-[Fe(PNP-*i*Pr)₂(CO)₂H]SbF₆ (17a)
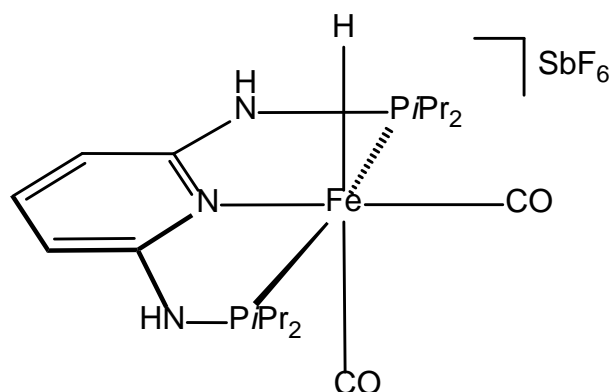
A solution of complex **1** (200 mg, 0.276 mmol) in THF (10 mL) was stirred in the presence of Zn powder (100 mg, 1.530 mmol) under a hydrogen atmosphere (1bar) for 2h. After that time the unreacted Zn powder was removed by filtration and the solution was filtrated through Celite. The solvent was evaporated under reduced pressure and the pale yellow solid was collected on a glass frit, washed with *n*-pentane, and dried under vacuum. Yield: 185 mg (97%). Anal Calc. for $C_{19}H_{34}F_6FeN_3O_2P_2Sb$: C, 33.07; H, 4.97; N, 6.09%. Found: C, 33.15; H, 4.86; N, 6.12%.

Reaction of [Fe(PNP-*i*Pr)₂(CO)₂] (21) with HBF₄ to form (17)

To a solution of **21** (80 mg, 0.181 mmol) in THF (10 mL) HBF₄ (24.3 µL, 0.181 mmol, 54% in Et₂O) was added at room temperature. After stirring the solution for 1h, solid materials were removed by filtration, and the solvent was evaporated under reduced pressure. The pale yellow solid was collected on a glass frit, washed with *n*-pentane, and dried under vacuum. Yield: 88 mg (90%).

^{1}H NMR (δ, CD₂Cl₂, 20°C): 7.35 (t, 1H, J = 7.7 Hz, py[4]), 6.78 (s, 2H, NH), 6.34 (d, 1H, J = 8.0, py[3]), 2.90 - 2.20 (m, 4H, CH(CH₃)₂), 1.60 - 1.00 (m, 24H, CH(CH_3)₂), -7.47 (t, 1H, $^2J_{HP}$ = 47.7 Hz).

^{13}C{^{1}H} NMR (δ, CD₂Cl₂, 20°C): 212.2 (t, J_{CP} = 20.2 Hz, CO), 207.5 (t, J_{CP} = 11.8 Hz, CO), 159.6 (d, J = 7.4 Hz, py), 159,5 (d, J = 7.4 Hz, py), 140.7 (s, py[4]), 99.3 (t, J = 2.4 Hz, py[3,5]), 32.3 (t, J = 13.7 Hz, CH(CH₃)₂), 30.8 (t, J = 15.2 Hz, CH(CH₃)₂), 18.0 (s, CH(CH₃)₂), 17.9 (s, CH(CH₃)₂), 17.5 (s, CH(CH₃)₂), 17.2 (s, CH(CH₃)₂).

^{31}P{^{1}H} NMR (δ, CD₂Cl₂, 20°C): 162.8.

IR (ATR, cm^{-1}): 2027 (ν_{CO}), 1969 (ν_{CO}).

trans-[Fe(PNP^{Me}-*i*Pr)(CO)$_2$Cl]SbF$_6$ (18)
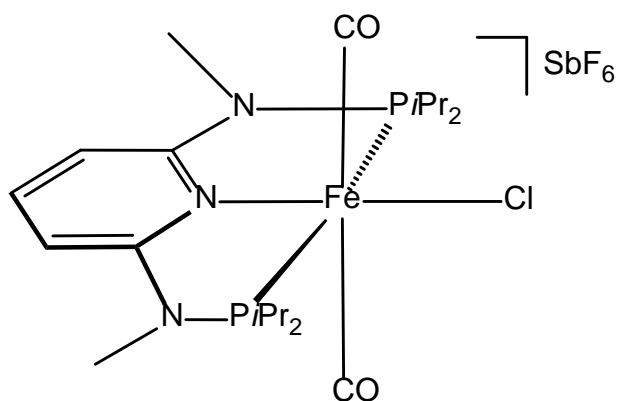
This complex was prepared analogously to **15-d$_2$** with **1k** (250 mg, 0.504 mmol) and AgSbF$_6$ (173 mg, 0.504 mmol) as starting materials. Yield: 299 mg (82%). Anal Calc. for C$_{21}$H3$_7$ClF$_6$FeN$_3$O$_2$P$_2$Sb (MW: 752.54) C, 33.52; H, 4.96; N, 5.58.

^{1}H-NMR (δ, CD$_2$Cl$_2$, 20°C): 7.63 (bs, 1H, py^4), 6.22 (d, *J* = 7.6 Hz, 2H, py^{3,5}), 3.30 (bs, 4H, C*H*(CH$_3$)$_2$), 3.18 (bs, 6H, NC*H$_3$*), 1.60 (bs, 24H, CH(C*H$_3$*)$_2$).

^{13}C{^{1}H} NMR (δ, CD$_2$Cl$_2$, 20°C): 211.5 (t, $^2J_{CP}$ = 24.1 Hz, *C*O), 163.0 (d, $^2J_{CP}$ = 7.2 Hz, py), 162.9 (d, $^2J_{CP}$ = 6.3 Hz, py), 142.1 (s, py^4), 100.0 (s, py^{3,5}), 35.3 (s, N*C*H$_3$), 32.0 (d, $^1J_{CP}$ = 11.1 Hz, *C*H(CH$_3$)$_2$), 31.9 (d, $^1J_{CP}$ = 11.0 Hz, *C*H(CH$_3$)$_2$), 18.5 (s, CH(*C*H$_3$)$_2$), 17.7 (s, CH(*C*H$_3$)$_2$).

^{31}P{^{1}H} NMR (δ, CD$_2$Cl$_2$, 20°C): 130.7.

IR (ATR, cm^{-1}): 2004 (ν$_{CO}$), 1980 (ν$_{CO}$).

Reaction of [Fe(PNP-*t*Bu)₂(CO)₂] (21b) with HBF₄ (17b)
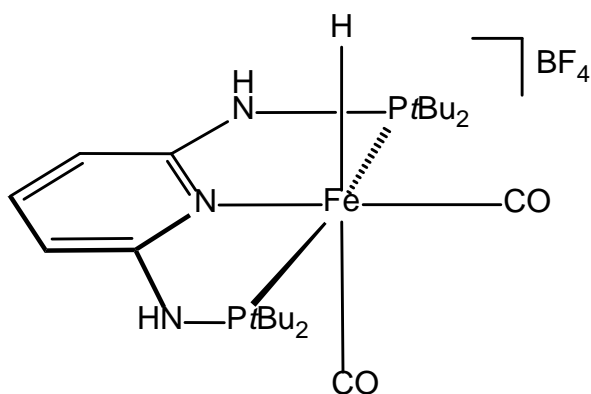
Complex **21b** (20 mg, 0.039 mmol) was dissolved in CD_2Cl_2 in an NMR tube and HBF₄ in Et₂O was added. The solution became clear immediatly and meassuring ¹H NMR proove the formation of the hydride **17h**.

¹H NMR (δ, CD_2Cl_2, 20 °C): -6.8 ppm, (t, J_{HP}=51.2Hz)

8.10 Fe(0) and Fe(I) complexes

[Fe(PNP-*i*Pr)₂(CO)₂] (21a)
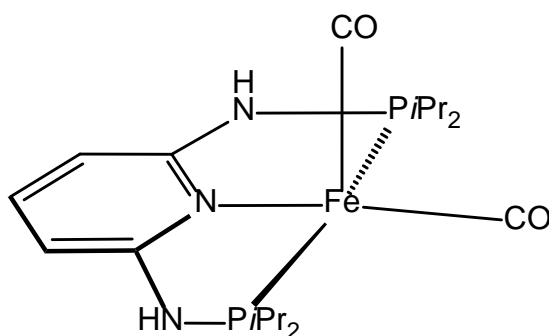
Complex **19a** (200 mg, 0.439 mmol) was added to a suspension of freshly prepared 5% Na/Hg (1.0 g, 2.174 mmol) in THF (10 mL) and CO was bubbled through the reaction mixture for 30 minutes, whereupon the solution changed from yellow to orange-red. The solution was decanted away from the amalgam and filtered through basic alumina. The filtrate was collected and the solvent was removed under vacuum. Complex **21a** was isolated as an orange solid. Yield: 88 mg (95%). Alternatively, complex **21a** was also obtained in a similar yield by using 2.5 equivs of KC₈ (149 mg, 1.098 mmol) instead of Na/Hg as reducing reagent. Anal Calc. for $C_{19}H_{33}FeN_3O_2P_2$ (MW: 453.28) C, 50.35; H, 7.34; N, 9.27%. Found: C, 50.19; H, 7.40; N, 9.30%.

^{1}H NMR (δ, THF-d$_8$, -80°C): 6.97 (s, 2H, py^{3,5}), 6.86 (t, J = 7.1 Hz, 1H, py^4), 5.93 (d, J = 7.8 Hz, 2H, N*H*), 2.40 (s, 4H, C*H*(CH₃)₂), 1.28 (dd, J = 14.1, 6.8 Hz, 24H, CH(C*H₃*)₂).

^{13}C{^{1}H} NMR (δ, THF-d$_8$, -80°C): 219.5 (t, J = 27.8 Hz, *C*O), 160.5 (s, py^{2,6}), 132.7 (s, py^4), 94.7 (s, py^{3,5}), 28.4 (d, J = 14.7 Hz, *C*H(CH₃)₂), 16.4 (d, J = 14.1 Hz; CH(*C*H₃)₂).

^{31}P{^{1}H} NMR (δ, THF-d$_8$, -80°C): 173.8.

IR (THF, cm^{-1}): 1872 (ν_{CO}), 1822 (ν_{CO}).

[Fe(PNP-*t*Bu)₂(CO)₂] (21b)
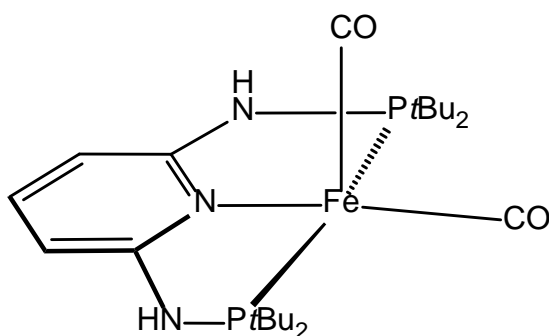
This complex was prepared according to **21a** using **19b** (200 mg, 0.381 mmol) and KC₈ (170 mg, 1.259 mmol) as starting materials. This complex is extremely air sesnsitve and decomposes within seconds when exposed to air, in solutiono as well as in solid state. Yield 181 mg (91 %) red solid. Anal Calc. for $C_{23}H_{41}FeN_3O_2P_2$ (MW: 509.39) C, 54.23; H, 8.11; N, 8.25.

IR (THF, cm⁻¹): 1865 (ν_{CO}), 1814 (ν_{CO}).

[Fe(PNP-pMe-*i*Pr)₂(CO)₂] (21c)
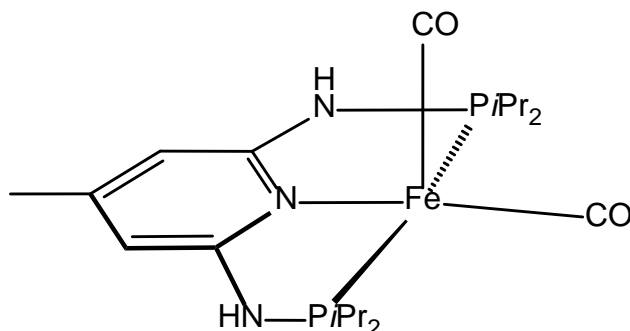
This complex was prepared according to **21a** using **19c** (200 mg, 0.415 mmol) and KC₈ (200 mg, 1.479 mmol) as starting materials. Yield 174 mg (90 %) yellow solid. Anal Calc. for $C_{20}H_{35}FeN_3O_2P_2$ (MW: 467.31) C, 51.40; H, 7.55; Fe, 11.95; N, 8.99.

IR (THF, cm⁻¹): 1870 (ν_{CO}), 1819 (ν_{CO}).

[Fe(PNP^Me-*i*Pr)₂(CO)₂] (21d)
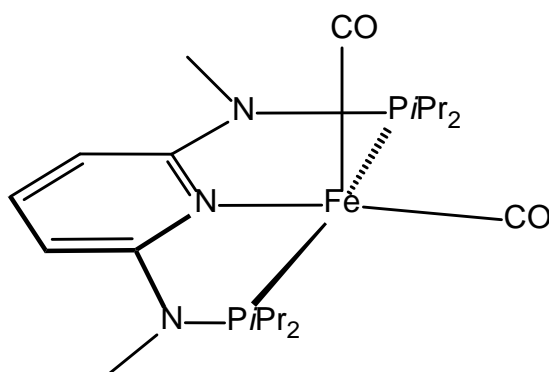
This complex was prepared according to **21a** using **19d** (200 mg, 0.403 mmol) and KC₈ (200 mg, 1.479 mmol) as starting materials. Yield 190 mg (98 %) orange solid. **Procedure 2:** Complex **20d** (100 mg, 0.190 mmol) was dissolved in THF (10 ml) and 45 mg KO*t*Bu (43 mg, 0.380 mmol) was added. The reaction mixture turned red. After filtration over celite the solvent was evaporated and the remaining red solid was washed with anhydrous pentane and dried in vacuum. Yield: 41 mg (47 %). Anal Calc. for $C_{21}H_{37}FeN_3O_2P_2$ (MW: 481.34) C, 52.40; H, 7.75; N, 8.73

^{1}H NMR (δ, C₆D₆, 20°C) δ 6.94 (tt, *J* = 8.1, 1.4 Hz, 1H, py⁴), 5.55 (d, *J* = 8.1 Hz, 2H, py³,⁵), 2.40 (s, 6H, NMe), 2.37 – 2.25 (m, 4H, *i*Pr), 1.36 (dd, *J* = 16.4, 7.4 Hz, 12H, *i*Pr), 1.11 (dd, *J* = 13.9, 7.0 Hz, 12H, *i*Pr).

^{31}P{^{1}H} NMR (δ, C₆D₆, 20°C) δ 181.7 (s).

^{13}C{^{1}H} NMR (δ, C₆D₆, 20°C) δ 219.63 (t, *J* = 28.0 Hz, CO), 161.24 (t, *J* = 10.6 Hz, py²,⁶), 132.77 (s, py⁴), 94.93 (t, *J* = 3.4 Hz, py³,⁵), 32.28 (d, *J* = 3.0 Hz, NMe), 29.61 (t, *J* = 11.0 Hz, *i*Pr), 17.49 (s, *i*Pr), 16.88 (t, *J* = 3.3 Hz, *i*Pr).

IR (THF, cm^{-1}): 1869 (ν_{CO}), 1819 (ν_{CO}).

IR (ATR, cm^{-1}): 1856 (ν_{CO}), 1802 (ν_{CO}).

[Fe(PNP^{Et}-*i*Pr)₂(CO)₂] (21e)
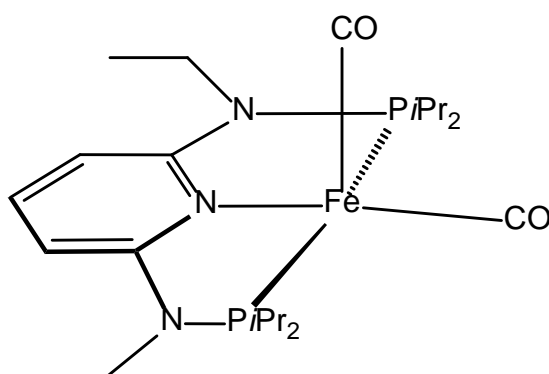
This complex was prepared according to **21a** using **19e** (200 mg, 0.381 mmol) and KC$_8$ (200 mg, 1.479 mmol) as starting materials and according to **21d** using **20e** respectiveley. Yield 183 mg (94 %) orange solid. Anal Calc. for C$_{23}$H$_{41}$FeN$_3$O$_2$P$_2$ (MW: 509.39): C, 54.23; H, 8.11; Fe, 10.96; N, 8.25.

^{1}H NMR (δ, C$_6$D$_6$, 20°C) δ 6.89 (t, *J* = 8.1 Hz, 1H, py^4), 5.59 (d, *J* = 8.1 Hz, 2H, py^{3,5}), 2.98 (qd, *J* = 6.9, 4.6 Hz, 4H, NEt), 2.26 (td, *J* = 7.1, 3.8 Hz, 4H, *i*Pr), 1.42 (dd, *J* = 16.5, 7.1 Hz, 12H, *i*Pr), 1.17 (dd, *J* = 14.2, 7.0 Hz, 12H, *i*Pr), 0.86 (t, *J* = 7.0 Hz, 6H, NEt).

^{31}P{^{1}H} NMR (δ, C$_6$D$_6$, 20°C) δ 183.7 (s).

^{13}C{^{1}H} NMR (δ, C$_6$D$_6$, 20°C) δ 219.90 (t, *J* = 27.5 Hz, CO), 160.63 (t, *J* = 10.8 Hz, py^{2,6}), 132.17 (s, py^4), 95.82 (t, *J* = 3.5 Hz, py^{3,5}), 40.10 (s, NEt), 30.05 (t, *J* = 11.0 Hz, *i*Pr), 17.84 (s, *i*Pr), 17.28 (t, *J* = 3.5 Hz, *i*Pr), 12.90 (s, NEt).

IR (THF, cm^{-1}): 1869 (ν$_{CO}$), 1818 (ν$_{CO}$).

IR (ATR, cm^{-1}): 1858 (ν$_{CO}$), 1801 (ν$_{CO}$).

[Fe(PNP-Me)₂(CO)₂] (21f)
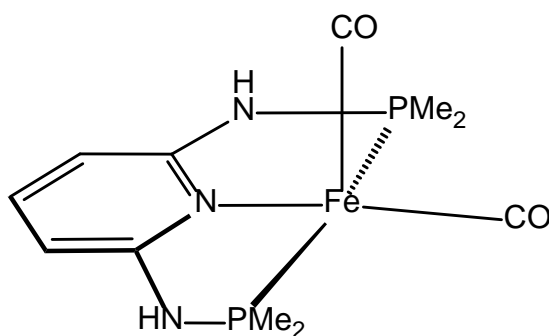
This complex was prepared according to **21a** using **20f** (200 mg, 0.562 mmol) and KC$_8$ (210 mg , 1.553 mmol) as starting materials and according to **21d** using **20f** respectiveley. Yield 130 mg (68 %) yellow solid. Anal Calc. for C$_{11}$H$_{17}$FeN$_3$O$_2$P$_2$ (MW: 341.07) C, 38.74; H, 5.02; N, 12.32.

IR (THF, cm^{-1}): 1877 (ν_{CO}),1826 (ν_{CO}).

[Fe(PNP-Et)₂(CO)₂] (21g)
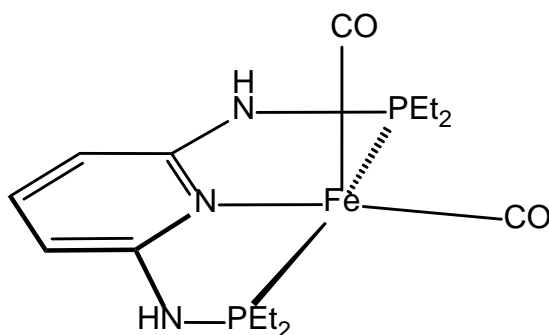
This complex was prepared according to **21a** using **20g** (200 mg, 0.504 mmol) and KC$_8$ (200 mg, 1.479 mmol) as starting materials and according to **21d** using **20g** respectiveley. Yield 144 mg (72 %) yellow solid. Anal Calc. for C$_{15}$H$_{25}$FeN$_3$O$_2$P$_2$ (MW: 397.18) C, 45.36; H, 6.34; Fe, 14.06; N, 10.58.

IR (THF, cm^{-1}): 1872 (ν_{CO}),1821 (ν_{CO}).

[Fe(PNP-Cy)₂(CO)₂] (21h)
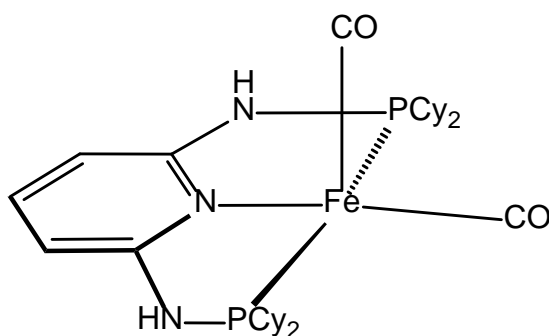
Procedure1: This complex was prepared according to **21a** using **19h** (200 mg, 0.318 mmol) and KC$_8$ (150 mg, 1.110 mmol) as starting materials. Yield 170 mg (87 %) orange solid. **Procedure 2**: Complex **cis-20h** (100 mg, 0.152 mmol) was dissolved in THF (10 ml) and KOtBu (35 mg, 0.304 mmol) was added. The color changes to orange. After filtration over celite the solvent was evaporated and the remaining red solid was washed with anhydrous pentane and dried in vacuum. Yield 39 mg (42 %) orange solid. Anal Calc. for C$_{31}$H$_{49}$FeN$_3$O$_2$P$_2$ (MW: 613.254): C, 60.69; H, 8.05; N, 6.85.

IR (THF, cm^{-1}): 1834(1862) (ν_{CO}), 1782(1813) (ν_{CO}).

[Fe(PNP-Ad)₂(CO)₂] (21i)
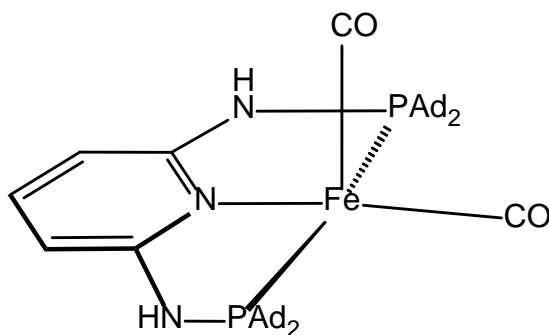
This complex was prepared according to **21a** using **19i** (200 mg, 0.239 mmol) and KC$_8$ (120 mg, 0.888 mmol) as starting materials. Yield 165 mg (84 %) red solid. Anal Calc. for C$_{47}$H$_{65}$FeN$_3$O$_2$P$_2$ (MW: 821.85) C, 68.69; H, 7.97; N, 5.11.

[Fe(PNP-*i*Pr)(CO)$_2$]$^+$ (22a)
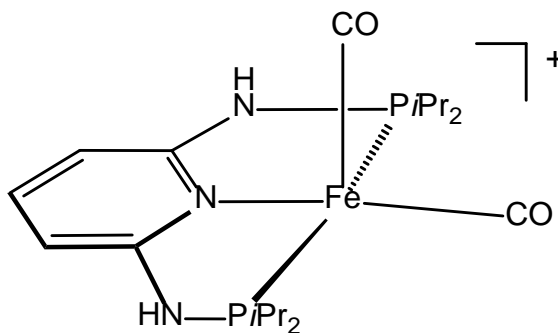
Procedure 1 (22aCl): Complex **20a** (200 mg, 0.403 mmol) was dissolved in THF (10 ml) and KO*t*Bu (90 mg, 0.806 mmol) was added. The reaction mixture was stirred for 4h and the color changed to green and a brown precipitate was formed. The solvent was evaporated and the flask was transferred into a glovebox. The green compound was dissolved in Et$_2$O and filtered over celite. After evaporating the solvent the green compound was quickly washed with n-pentane (10 ml) and dried under vacuum. Yield: 80 mg (41 %) green solid. Anal Calc. for C$_{19}$H$_{33}$ClFeN$_3$O$_2$P$_2$ (MW: 488.73) C, 46.69; H, 6.81; N, 8.60.

Procedure 2 (22aPF$_6$): In a glove box complex **21a** (60 mg, 0.132 mmol) was dissolved in THF and [FeCp$_2$]PF$_6$ (44 mg, 0.132 mmol) was added to the solution. After 10 min. the solution turned green and it was allowed to stir for another 50 min. The solvent was evaporated and the remaining green solid washed twice with pentane (10ml) to remove the remaining ferrocene. The compound was dried under vacuum. Yield 75 mg (95 %) green solid. Anal Calc. for C$_{19}$H$_{33}$F$_6$FeN$_3$O$_2$P$_3$ (MW: 598.25) C, 38.15; H, 5.56; N, 7.02.

IR (THF, cm^{-1}): 1952 (ν_{CO}), 1885 (ν_{CO}).

Magnetic moment (Evans): μ_{eff} = 1.93

[Fe(PNP-Cy)(CO)₂]⁺ (22h)
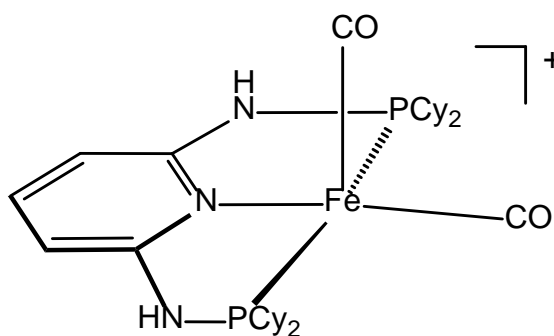
22hCl: This compound was prepared according to **22a** using **20h** (200 mg, 0.33 mmol) and KOtBu (73 mg, 0.66 mmol) as starting materials.

22hPF6: This compound was prepared according to **22aPF6** using **21h** (30 mg, 0.049 mmol) and [FeCp₂]PF₆ (17 mg, 0.051) as starting materials. Yield 35 mg (93 %) green solid. Anal Calc. for $C_{31}H_{49}F_6FeN_3O_2P_3$ (MW: 758.51) C, 49.09; H, 6.51; N, 5.54.

IR (THF, cm⁻¹): 1949 (ν_{CO}), 1884 (ν_{CO}).

Magnetic moment (Evans): μ_{eff} = 1.71

[Fe(PNP-tBu)(CO)₂]PF6 (22b)
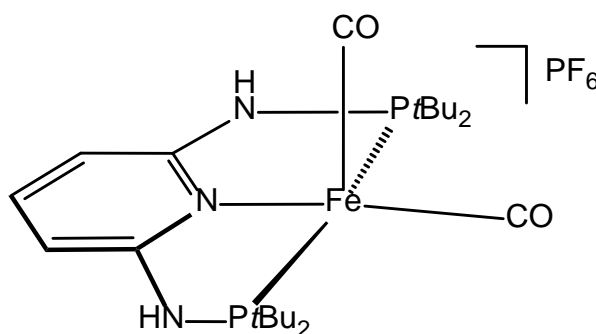
This compound was prepared according to **22bPF6** using **21b** (51 mg, 0.1 mmol) and [FeCp₂]PF₆ (33 mg, 0.1 mmol) as starting materials. Yield 60 mg (92 %) green solid. Anal Calc. for $C_{23}H_{41}F_6FeN_3O_2P_3$ (MW: 654.36) C, 42.22; H, 6.32; N, 6.42

IR (THF, cm⁻¹): 1944 (ν_{CO}), 1878 (ν_{CO}).

Magnetic moment (Evans): μ_{eff} = 1.1 (due to ferrocene impurities)

8.11 Crystallographic data

Table 16: Details for the crystal structure determination of **1g**, **2**·2THF·Et$_2$O and **4**

	1g	**2·2THF·Et$_2$O**	**4**
Empirical formula	C$_{18}$H$_{35}$N$_3$P$_2$	C$_{70}$H$_{76}$BClF$_4$FeN$_6$O$_3$P$_4$	C$_{50}$H$_{49}$BClF$_4$FeN$_6$P$_3$
MW [g/mol]	355.4	1351.41	1005.00
Crystal size [mm]	0.70 x 0.28 x 0.04	0.44 x 0.25 x 0.15	0.46 x 0.40 x 0.19
Color, shape	colorless, plate	green	green, trapezoidal
Crystal system	orthorhombic	triclinic	monoclinic
Space group	Pbca	P-1	P 2$_1$/n
a [Å]	14.3394(12)	14.0627(4)	14.5198(17)
b [Å]	10.0089(16)	15.4356(5)	21.308(3)
c [Å]	29.562(9)	15.5238(5)	15.1462(18)
α [°]	90	77.733(2)	90
β [°]	90	81.791(2)	99.710(4)
γ [°]	90	85.786(2)	90
V [Å^3]	4242.9(9)	3255.77	4618.92
Z	8	2	4
ρ$_{calc}$ [g/cm^3]	1.113	1.378	1.4448
T [K]	100	100	100
μ [mm^{-1}] (Mo K$_\alpha$)	0.21	0.435	0.549
F(000)	1552	1412	2080
Θ$_{max}$ [°]	2.5-30	1.86-27	2.3-32.5
no. of reflns. measd.	149837	38325	275623
no. of unique rflns.	6241	14099	16825
no. of reflns. I > 2σ(I)	4614		13286
no. of params.	216	766	599
R [F^2 > 2σ(F^2)]	0.031	0.0550	0.031
R$_{int}$	0.066	0.0305	0.0383
wR (F^2)	0.046	0.1557	0.0482
GooF		1.102	2.09
Diff. Four. peaks (min/max) [eÅ^{-3}]	-0.21/0.29	-1.02/1.43	-0.34/0.49

Table 17: Details for the crystal structure determination of **7**·2THF, **8**·2DMSO Et$_2$O and **9**

	7·2THF	**8**·2DMSO·Et$_2$O	**9**
Empirical formula	C$_{54}$H$_{56}$BClF$_4$FeN$_5$P$_3$O$_2$	C$_{38}$H$_{47}$Cl$_2$FeN$_3$O$_4$P$_2$S$_2$	C$_{31}$H$_{25}$ClF$_6$FeN$_3$O$_2$P$_2$Sb
MW [g/mol]	1078.09	862.60	860.53
Crystal size [mm]	0.41 x 0.33 x 0.03	0.44 x 0.20 x 0.15	0.38 x 0.18 x 0.06
Color, shape	clear green		red
Crystal system	orthorhombic	triclinic	triclinic
Space group	Pbca	P-1	P-1
a [Å]	17.9705(9)	9.5606(2)	8.4371(3)
b [Å]	18.5536(8)	14.3875(3)	12.1634(4)
c [Å]	30.0107(14)	15.3193(3)	16.3808(6)
α [°]	90	90.049(1)	78.054(2)
β [°]	90	107.494(1)	84.361(2)
γ [°]	90	92.298(1)	84.351(2)
V [Å^3]	10006.1	2007.95(7)	1631.42(10)
Z	8	2	2
ρ_{calc} [g/cm^3]	1.4308	1.427	1.752
T [K]	100	100	100
μ [mm^{-1}] (Mo K$_\alpha$)	0.514	0.736	1.522
F(000)	4480	900	852
Θ_{max} [°]	2.3-30.1	1.97-30	2.33-30
no. of reflns. measd.	334449	30228	41391
no. of unique rflns.	15995	11597	9452
no. of reflns. I > 2σ(I)	11652		
no. of params.	652	478	424
R [F^2 > 2σ(F^2)]	0.0315	0.0421	0.0373
R$_{int}$	0.0557	0.0403	0.0362
wR (F^2)	0.0341	0.0978	0.0893
GooF	1.67	1.016	1.051
Diff. Four. peaks (min/max) [eÅ^{-3}]	-0.36/0.45	-0.457/0.840	-1.01/1.88

Table 18: Details for the crystal structure determination of **17**, **21**·CH$_2$Cl$_2$ and **21b**

	17	**21a**·CH$_2$Cl$_2$	**21b**
Empirical formula	C$_{19}$H$_{34}$F$_6$FeN$_3$O$_2$P$_2$Sb	C$_{20}$H$_{35}$Cl$_2$ FeN$_3$O$_2$P$_2$	C$_{25.25}$H$_{45.5}$FeN$_3$O$_{2.75}$P$_2$
MW [g/mol]	690.0	538.2	553
Crystal size [mm]	0.11 × 0.08 × 0.04	0.43 × 0.18 × 0.02	0.48 x 0.33 x 0.15
Color, shape	clear red block	clear colorless plate	dark red block
Crystal system	monoclinic	triclinic	triclinic
Space group	P2$_1$/c	P1	P-1
a [Å]	10.8864(5)	9.330(6)	12.9438(3)
b [Å]	14.8347(7)	14.762(9)	14.2817(3)
c [Å]	16.8177(8)	18.911(12)	18.8732(4)
α [°]	90	90.517(14)	70.5715(10)
β [°]	94.269(2)	93.27(2)	75.6235(10)
γ [°]	90	93.48(2)	65.0841(9)
V [Å^3]	2708.5(2)	2595(3)	2960.04(11)
Z	4	4	4
ρ_{calc} [g/cm^3]	1.692	1.377	1.2404
T [K]	100	100	100
μ [mm^{-1}] (Mo K$_\alpha$)	1.714	0.931	0.646
F(000)	1384	1128	1178
θ_{max} [°]	1.83–33.52	1.08-32.67	2.5-30
no. of reflns. measd.	65235	96393	97920
no. of unique rflns.	9061	17322	17355
no. of reflns. I > 2σ(I)	6349	13893	15213
no. of params.	316	576	631
R [F^2 > 2σ(F^2)]	0.0501	0.0422	0.0245
R$_{int}$	0.0412	0.0271	0.0298
wR (F^2)	0.0609	0.0566	0.0380
GooF	2.87	2.64	2.3
Diff. Four. peaks (min/max) [eÅ^{-3}]	-1.24 / 2.21	-1.03 / 1.48	-0.35/0.44

Table 19: Details for the crystal structure determination of **21b** and **22a**

	21e	**22a**	**22h**
Empirical formula	$C_{20}H_{30}FeN_3O_2P_2$	$C_{19}H_{33}ClFeN_3O_2P_2$	$C_{35}H_{60}FeN_3O_4P_2$
MW [g/mol]	462.3	488.73	704.7
Crystal size [mm]			0.63 x 0.51 x 0.06
Color, shape			translucent blue
Crystal system	monoclinic		monoclinic
Space group	P 1 21/c 1		P 1 21/c 1
a [Å]	31.781(3)	10.6741(3)	15.7694(6)
b [Å]	18.262(3)	14.5773(5)	24.4686(14)
c [Å]	18.012(5)	14.7472(5)	9.6449(10)
α [°]	90	90	90
β [°]	90.004(2)	90	93.946(3)
γ [°]	90	90	90
V [Å^3]	10454(3)	2294.66(13)	3712.7(5)
Z	16	4	4
ρ_{calc} [g/cm^3]	1.1745	1.411	1.2603
T [K]	100	100	100
μ [mm^{-1}] (Mo K$_\alpha$)	0.717		0.532
F(000)	4352	960	1516
Θ_{max} [°]	0.64-30.17	1.96-27.19	1.29-34.9
no. of reflns. measd.	450669		15978
no. of unique rflns.	30833	4977	11757
no. of reflns. I > 2σ(I)	25467	4255	9507
no. of params.	1080	270	418
R [F^2 > 2σ(F^2)]	0.0769	0.0485	0.0627
R$_{int}$	0.0802	0.0630	0.0888
wR (F^2)	0.0778	0.0921	0.0704
GooF	3.81	1.077	2.66
Diff. Four. peaks (min/max) [eÅ^{-3}]	-0.75/2.09		-0.85/1.03

Bibliography

[1]   W. V. Dahlhoff, S. M. Nelson, *J. Chem. Soc. A Inorganic, Phys. Theor.* **1971**, 2184.

[2]   G. Vasapollo, P. Giannoccaro, C. F. Nobile, A. Sacco, *Inorganica Chim. Acta* **1981**, *48*, 125–128.

[3]   B. D. Steffey, A. Miedaner, M. L. Maciejewski-Farmer, P. R. Bernatis, A. M. Herring, V. S. Allured, V. Carperos, D. L. DuBois, *Organometallics* **1994**, *13*, 4844–4855.

[4]   C. Hahn, M. Spiegler, E. Herdtweck, R. Taube, *Eur. J. Inorg. Chem.* **1999**, *1999*, 435–440.

[5]   C. Hahn, J. Sieler, R. Taube, *Chem. Ber.* **1997**, *130*, 939–945.

[6]   C. Hahn, A. Vitagliano, F. Giordano, R. Taube, *Organometallics* **1998**, *17*, 2060–2066.

[7]   Q. Jiang, D. Van Plew, S. Murtuza, X. Zhang, *Tetrahedron Lett.* **1996**, *37*, 797–800.

[8]   M. V. Andreocci, G. Mattogno, R. Zanoni, P. Giannoccaro, G. Vasapollo, *Inorganica Chim. Acta* **1982**, *63*, 225–231.

[9]   A. Sacco, G. Vasapollo, C. F. Nobile, A. Piergiovanni, M. A. Pellinghelli, M. Lanfranchi, *J. Organomet. Chem.* **1988**, *356*, 397–409.

[10]   R. A. T. M. Abbenhuis, I. del Río, M. M. Bergshoef, J. Boersma, N. Veldman, A. L. Spek, G. van Koten, *Inorg. Chem.* **1998**, *37*, 1749–1758.

[11]   N. Rahmouni, J. A. Osborn, A. De Cian, J. Fischer, A. Ezzamarty, *Organometallics* **1998**, *17*, 2470–2476.

[12]   R. Sablong, J. A. Osborn, *Tetrahedron Lett.* **1996**, *37*, 4937–4940.

[13]   R. Sablong, C. Newton, P. Dierkes, J. A. Osborn, *Tetrahedron Lett.* **1996**, *37*, 4933–4936.

[14]   L. Barloy, S. Y. Ku, J. A. Osborn, A. De Clan, J. Fischer, *Polyhedron* **1997**, *16*, 291–295.

[15]   J. Zhang, G. Leitus, Y. Ben-David, D. Milstein, *J. Am. Chem. Soc.* **2005**, *127*, 10840–1.

[16]   J. Zhang, M. Gandelman, L. J. W. Shimon, H. Rozenberg, D. Milstein, *Organometallics* **2004**, *23*, 4026–4033.

[17]   D. Hermann, M. Gandelman, H. Rozenberg, L. J. W. Shimon, D. Milstein, *Organometallics* **2002**, *21*, 812–818.

[18]   D. H. Gibson, C. Pariya, M. S. Mashuta, *Organometallics* **2004**, *23*, 2510–2513.

[19]   H. Katayama, C. Wada, K. Taniguchi, F. Ozawa, *Organometallics* **2002**, *21*, 3285–3291.

[20]   * Guochen Jia, and Hon Man Lee, I. D. Williams, C. P. L. and, Y. Chen, **1997**.

[21]   G. Müller, M. Klinga, M. Leskelä, B. Rieger, I. Eine, R. Von, *Zeitschrift für Anorg. und Allg. Chemie* **2002**, *628*, 2839–2846.

[22]   J. Ansell, M. Wills, *Chem. Soc. Rev.* **2002**, *31*, 259–268.

[23]   W. Schirmer, U. Flörke, H.-J. Haupt, *Zeitschrift für Anorg. und Allg. Chemie* **1987**, *545*, 83–97.

[24]   W. Schirmer, U. Flörke, H.-J. Haupt, *Zeitschrift für Anorg. und Allg. Chemie* **1989**, *574*, 239–255.

[25]   D. Benito-Garagorri, E. Becker, J. Wiedermann, W. Lackner, M. Pollak, K. Mereiter, J. Kisala, K. Kirchner, *Organometallics* **2006**, *25*, 1900–1913.

[26]   D. Benito-Garagorri, M. Puchberger, K. Mereiter, K. Kirchner, *Angew. Chem. Int. Ed. Engl.* **2008**, *47*, 9142–5.

[27]   D. Benito-Garagorri, L. G. Alves, M. Puchberger, K. Mereiter, L. F. Veiros, M. J. Calhorda, M. D. Carvalho, L. P. Ferreira, M. Godinho, K. Kirchner, *Organometallics* **2009**, *28*, 6902–6914.

[28]   D. Benito-Garagorri, L. G. Alves, L. F. Veiros, C. M. Standfest-Hauser, S. Tanaka, K. Mereiter, K. Kirchner, *Organometallics* **2010**, *29*, 4932–4942.

[29]   L. G. Alves, G. Dazinger, L. F. Veiros, K. Kirchner, *Eur. J. Inorg. Chem.* **2010**, *2010*, 3160–3166.

[30]   D. Benito-Garagorri, J. Wiedermann, M. Pollak, K. Mereiter, K. Kirchner, *Organometallics* **2007**, *26*, 217–222.

[31]   D. Benito-Garagorri, K. Mereiter, K. Kirchner, *Eur. J. Inorg. Chem.* **2006**, *2006*, 4374–4379.

[32]   S. R. M. M. de Aguiar, B. Stöger, E. Pittenauer, M. Puchberger, G. Allmaier, L. F. Veiros, K. Kirchner, *J. Organomet. Chem.* **2014**, *760*, 74–83.

[33]   O. Oztopcu, C. Holzhacker, M. Puchberger, M. Weil, K. Mereiter, L. F. Veiros, K. Kirchner, *Organometallics* **2013**, *32*, 3042–3052.

[34]   H. Nakazawa, M. Itazaki, *Iron Catalysis*, Springer Berlin Heidelberg, Berlin, Heidelberg, **2011**.

[35]   P. Bhattacharya, H. Guan, **n.d.**, 37–41.

[36]   J. N. Harvey, R. Poli, K. M. Smith, **2003**, *239*, 347–361.

[37]   J. N. Harvey, *Phys. Chem. Chem. Phys.* **2007**, *9*, 331–43.

[38]   D. Benito-Garagorri, I. Lagoja, L. F. Veiros, K. a Kirchner, *Dalton Trans.* **2011**, *40*, 4778–92.

[39]   B. C. J. Moulton, B. L. Shaw, **1975**, 1020–1024.

[40] M. Kranenburg, Y. E. M. Van Der Burgt, P. C. J. Kamer, P. W. N. M. Van Leeuwen, **1995**, 3081–3089.

[41] M. a. Zuideveld, B. H. G. Swennenhuis, M. D. K. Boele, Y. Guari, G. P. F. van Strijdonck, J. N. H. Reek, P. C. J. Kamer, K. Goubitz, J. Fraanje, M. Lutz, et al., *J. Chem. Soc. Dalt. Trans.* **2002**, 2308.

[42] B. L. Small, M. Brookhart, A. M. A. Bennett, C. Hill, N. Carolina, **1998**, *7863*, 4049–4050.

[43] S. C. Bart, E. Lobkovsky, P. J. Chirik, *J. Am. Chem. Soc.* **2004**, *126*, 13794–13807.

[44] A. M. Tondreau, E. Lobkovsky, P. J. Chirik, *Org. Lett.* **2008**, *10*, 2789–92.

[45] R. J. Trovitch, E. Lobkovsky, E. Bill, P. J. Chirik, **2008**, 1470–1478.

[46] S. K. Russell, J. M. Darmon, E. Lobkovsky, P. J. Chirik, *Inorg. Chem.* **2010**, *49*, 2782–92.

[47] A. M. Tondreau, C. C. H. Atienza, K. J. Weller, S. a Nye, K. M. Lewis, J. G. P. Delis, P. J. Chirik, *Science* **2012**, *335*, 567–70.

[48] S. K. Russell, E. Lobkovsky, P. J. Chirik, *J. Am. Chem. Soc.* **2011**, *133*, 8858–61.

[49] R. P. Yu, J. M. Darmon, J. M. Hoyt, G. W. Margulieux, Z. R. Turner, P. J. Chirik, *ACS Catal.* **2012**, *2*, 1760–1764.

[50] R. B. Bedford, M. Betham, D. W. Bruce, A. a Danopoulos, R. M. Frost, M. Hird, *J. Org. Chem.* **2006**, *71*, 1104–10.

[51] A. M. Tondreau, J. M. Darmon, B. M. Wile, S. K. Floyd, E. Lobkovsky, P. J. Chirik, *Organometallics* **2009**, *28*, 3928–3940.

[52] S. C. Bart, K. Chłopek, E. Bill, M. W. Bouwkamp, E. Lobkovsky, F. Neese, K. Wieghardt, P. J. Chirik, *J. Am. Chem. Soc.* **2006**, *128*, 13901–12.

[53] P. J. Chirik, K. Wieghardt, *Science* **2010**, *327*, 794–5.

[54] S. Hosokawa, J. Ito, H. Nishiyama, *Organometallics* **2010**, *29*, 5773–5775.

[55] T. Inagaki, A. Ito, J.-I. Ito, H. Nishiyama, *Angew. Chem. Int. Ed. Engl.* **2010**, *49*, 9384–7.

[56] B. K. Langlotz, H. Wadepohl, L. H. Gade, *Angew. Chem. Int. Ed. Engl.* **2008**, *47*, 4670–4.

[57] K. Kamata, A. Suzuki, Y. Nakai, H. Nakazawa, *Organometallics* **2012**, *31*, 3825–3828.

[58] R. Langer, G. Leitus, Y. Ben-David, D. Milstein, *Angew. Chem. Int. Ed. Engl.* **2011**, *50*, 2120–4.

[59] R. Langer, M. a Iron, L. Konstantinovski, Y. Diskin-Posner, G. Leitus, Y. Ben-David, D. Milstein, *Chemistry* **2012**, *18*, 7196–209.

[60] T. Zell, B. Butschke, Y. Ben-David, D. Milstein, *Chemistry* **2013**, *19*, 8068–72.

[61] D. Srimani, Y. Diskin-Posner, Y. Ben-David, D. Milstein, *Angew. Chem. Int. Ed. Engl.* **2013**, *52*, 14131–4.

[62] E. Alberico, P. Sponholz, C. Cordes, M. Nielsen, H.-J. Drexler, W. Baumann, H. Junge, M. Beller, *Angew. Chem. Int. Ed. Engl.* **2013**, *52*, 14162–6.

[63] C. Bornschein, S. Werkmeister, B. Wendt, H. Jiao, E. Alberico, W. Baumann, H. Junge, K. Junge, M. Beller, *Nat. Commun.* **2014**, *5*, 4111.

[64] P. O. Lagaditis, P. E. Sues, J. F. Sonnenberg, K. Y. Wan, A. J. Lough, R. H. Morris, *J. Am. Chem. Soc.* **2014**, *136*, 1367–80.

[65] P. Bhattacharya, J. a. Krause, H. Guan, *Organometallics* **2011**, *30*, 4720–4729.

[66] H. Zhao, H. Sun, X. Li, **2014**.

[67] D. Peng, Y. Zhang, X. Du, L. Zhang, X. Leng, M. D. Walter, Z. Huang, *J. Am. Chem. Soc.* **2013**, *135*, 19154–66.

[68] L. Zhang, D. Peng, X. Leng, Z. Huang, *Angew. Chem. Int. Ed. Engl.* **2013**, *52*, 3676–80.

[69] J. V Obligacion, P. J. Chirik, *Org. Lett.* **2013**, *15*, 2680–3.

[70] R. J. Trovitch, E. Lobkovsky, P. J. Chirik, *Inorg. Chem.* **2006**, *45*, 7252–7260.

[71] E. M. Pelczar, T. J. Emge, K. Krogh-Jespersen, A. S. Goldman, *Organometallics* **2008**, *27*, 5759–5767.

[72] A. M. Tondreau, C. Milsmann, E. Lobkovsky, P. J. Chirik, *Inorg. Chem.* **2011**, *50*, 9888–95.

[73] T. Zell, P. Milko, K. L. Fillman, Y. Diskin-Posner, T. Bendikov, M. a Iron, G. Leitus, Y. Ben-David, M. L. Neidig, D. Milstein, *Chemistry* **2014**, *20*, 4403–13.

[74] A. a Danopoulos, D. Pugh, H. Smith, J. Sassmannshausen, *Chemistry* **2009**, *15*, 5491–502.

[75] P. C. H. Sime, M. J. Ingleson, B. C. Fullmer, D. T. Buschhorn, H. Fan, M. Pink, J. C. Huffman, K. G. Caulton, *Inorg. Chem.* **2007**, *47*, 407–409.

[76] D. Benito-Garagorri, K. Kirchner, *Acc. Chem. Res.* **2008**, *41*, 201–213.

[77] M. Su, S. L. Buchwald, *Angew. Chem. Int. Ed. Engl.* **2012**, *51*, 4710–3.

[78] J. R. Goerlich, R. Schmutzler, *Phosphorus. Sulfur. Silicon Relat. Elem.* **1995**, *102*, 211–215.

[79] M. Mastalir, **n.d.**, *0727105*.

[80] B. Stöger, M. Weil, B. Bichler, W. Eder, K. Kirchner, *Acta Crystallogr. Sect. E Struct. Reports Online* **2014**, *70*, o889–o890.

[81]   G. J. P. Britovsek, M. Bruce, V. C. Gibson, B. S. Kimberley, P. J. Maddox, S. Mastroianni, S. J. Mctavish, C. Redshaw, G. A. Solan, S. Stro, et al., **1999**, 8728–8740.

[82]   B. Bichler, C. Holzhacker, B. Sto, M. Puchberger, L. F. Veiros, K. Kirchner, **2013**.

[83]   R. Langer, Y. Diskin-Posner, G. Leitus, L. J. W. Shimon, Y. Ben-David, D. Milstein, *Angew. Chem. Int. Ed. Engl.* **2011**, *50*, 9948–52.

[84]   G. Müller, M. Klinga, M. Leskelä, B. Rieger, I. Eine, R. Von, **2002**, 2839–2846.

[85]   B. W. V Dahlhoff, S. M. Nelson, **1971**.

[86]   P. Giannoccaro, G. Vasapollo, C. F. Nobile, A. Sacco, *Inorganica Chim. Acta* **1982**, *61*, 69–75.

[87]   S. Pavlik, K. Mereiter, M. Puchberger, K. Kirchner, *Organometallics* **2005**, *24*, 3561–3575.

[88]   D. M. Roddick, *Organometallic Pincer Chemistry*, Springer Berlin Heidelberg, Berlin, Heidelberg, **2013**.

[89]   E. Poverenov, D. Milstein, **2013**, *40*, DOI 10.1007/978-3-642-31081-2.

[90]   E. Poverenov, D. Milstein, in *Organomet. Pincer Chem. SE - 2* (Eds.: G. van Koten, D. Milstein), Springer Berlin Heidelberg, **2013**, pp. 21–47.

[91]   T. Zell, R. Langer, M. a Iron, L. Konstantinovski, L. J. W. Shimon, Y. Diskin-Posner, G. Leitus, E. Balaraman, Y. Ben-David, D. Milstein, *Inorg. Chem.* **2013**, DOI 10.1021/ic401432m.

[92]   B. Gnanaprakasam, E. Balaraman, Y. Ben-David, D. Milstein, *Angew. Chem. Int. Ed. Engl.* **2011**, *50*, 12240–4.

[93]   T. Liu, S. Chen, M. J. O'Hagan, M. Rakowski DuBois, R. M. Bullock, D. L. DuBois, *J. Am. Chem. Soc.* **2012**, *134*, 6257–72.

[94]   P. Jaunky, H. W. Schmalle, O. Blacque, T. Fox, H. Berke, *J. Organomet. Chem.* **2005**, *690*, 1429–1455.

[95]   J. K. Burdett, J. Wiley, **n.d.**

[96]   R. Birk, H. Berke, H.-U. Hund, G. Huttner, L. Zsolnai, L. Dahlenburg, U. Behrens, T. Sielisch, *J. Organomet. Chem.* **1989**, *372*, 397–410.

[97]   F. R. Ahmed, J. L. A. Roustan, **1985**, 2526–2532.

[98]   B. L. Haymore, J. A. Ibers, *Inorg. Chem.* **1975**, *14*, 1369–1376.

[99]   R. Hoffmann, M. M. L. Chen, M. Elian, A. R. Rossi, D. M. P. Mingos, *Inorg. Chem.* **1974**, *13*, 2666–2675.

[100] I. A. Cohen, **1972**, *111*, 11201.

[101] D. H. Grant, *J. Chem. Educ.* **1995**, *72*, 39.

[102] A. M. Tondreau, S. C. E. Stieber, C. Milsmann, E. Lobkovsky, T. Weyhermüller, S. P. Semproni, P. J. Chirik, *Inorg. Chem.* **2013**, *52*, 635–46.

[103] K. S. Min, A. M. Arif, J. S. Miller, *Inorganica Chim. Acta* **2007**, *360*, 1854–1858.

[104] J. Reedijk, *Comments Inorg. Chem.* **2006**, *1*, 379–389.

[105] J. Olguín, S. Bernès, L. Gasque, *Crystals* **2012**, *2*, 1357–1365.

[106] B. F. Straub, F. Rominger, P. Hofmann, D.- Heidelberg, R. V October, **2000**, 2113–2119.

[107] J. C. Fettinger, D. W. Keogh, R. Poli, C. Park, R. V December, **1996**, 4325–4333.

[108] B. J. Thomas, J. F. Mitchell, K. H. Theopold, J. A. Leaq, **1988**, *348*, 333–342.

[109] W. L. F. Armarego, C. L. L. Chai, *Purification of Laboratory Chemicals*, Elsevier, **2009**.

[110] B. Bichler, L. F. Veiros, M. Puchberger, K. Mereiter, K. Matsubara, K. A. Kirchner, Ö. Öztopcu, *Organometallics* **2011**, *2*, 5928–5942.

[111] J. M. Killough, **1978**, *1978*.

[112] M. J. Frisch, G. W. Trucks, H. B. Schlegel, G. E. Scuseria, M. A. Robb, J. R. Cheeseman, G. Scalmani, V. Barone, B. Mennucci, G. A. Petersson, et al., **n.d.**

[113] C. Lee, W. Yang, R. G. Parr, *Phys. Rev. B* **1988**, *37*, 785–789.

[114] K. B. Wiberg, *J. Comput. Chem.* **1986**, *7*, 379–379.

[115] J.-L. Calais, *Int. J. Quantum Chem.* **1993**, *47*, 101–101.

[116] G. M. Sheldrick, *Acta Crystallogr. A.* **2008**, *64*, 112–22.

[117] C. F. Macrae, I. J. Bruno, J. A. Chisholm, P. R. Edgington, P. McCabe, E. Pidcock, L. Rodriguez-Monge, R. Taylor, J. van de Streek, P. A. Wood, *J. Appl. Crystallogr.* **2008**, *41*, 466–470.

Curriculum Vitae

Bernhard Bichler

Contact Information and Personal:

Address:

Spörlingasse 3/8

1060 Wien

Date and place of birth: 19.05.1985 in Oberpullendorf

e-mail: bernhard.bichler@tuwien.ac.at

Studies:

Dec. 2011 – Nov 2014:	Project Assistant at TU Vienna in the research group of Prof. Karl Kirchner, started working on PhD thesis
	Thesis title: The Synthesis, Characterization and Reactivity of new Iron PNP Pincer Complexes
Jan. 2011:	Dipl. Ing (M. Sc) in Technical Chemistry, Vienna University of Technology
	Thesis title: Syntheses, Characterization, Ligand Dynamics and Catalysis of new Palladium Allyl Complexes
Sep. 2009:	started work for my diploma thesis at the IAS with Prof. Kirchner's working group
Feb. 2005 - Jan. 2011:	Diploma Study in Technical Chemistry at the Vienna University of Technology
Oct. 2003 – Jan. 2004:	Diploma Study in Technical Physics at the Vienna University of Technology

Internships:

Sep. 2006:	intern at the OMV laboratories
Jul./Aug. 2008:	internship at a laboratory in the Austrian Research Centers Seibersdorf
Oct. 2009 – Jan. 2011:	Teaching Assistant at the TU Vienna
Feb. 2007:	internship at the IAS with an organic chemistry working group for 2 weeks
Aug. - Sep. 2008:	internship at the IAS with an inorganic chemistry working group for 4 weeks

| Feb. 2009: | internship with an organic chemistry working group for 4 weeks. |

Community Service:

Feb. 2004 – Jan. 2005:   Paramedic at the Red Cross

Languages:

German: Mother tongue

English: Fluent

French: Intermediate

List of Publications

1. "Synthesis, Structure, and Ligand Dynamics of Cationic [Pd(η^3-allyl)(E-N-chelate)]$^+$ (E = P, O, S, Se) Complexes", B. Bichler; M. Puchberger, L. F. Veiros, Ö. Öztopcu, K. Mereiter, K. Matsubara and K. A. Kirchner, *Organometallics* **2011**, *30* (21), 5928–5942.

2. "Heterolytic Cleavage of Dihydrogen by an Iron(II) PNP Pincer Complex *via* Metal-Ligand Cooperation", B. Bichler, B. Stöger, M. Puchberger and K. A. Kirchner, *Organometallics*, **2013**, *32* (15), 4114–4121.

3. "*Crystal structure of N,N-bis(diisopropylphosphanyl)-4-methylpyridine-2,6-diamine*", B. Stöger, M. Weil, B. Bichler, W. Eder and K. Kirchner, *Acta Crystallographica Section E: Structure Reports*, **2014,** *E70,* 889-890.

4. "An iron(II) complex featuring κ^3 and labile κ^2-bound PNP pincer ligands – striking differences between CH_2 and NH spacers", B. Bichler, M. Glatz, B. Stöger, K. Mereiter, L. F. Veiros, and K. Kirchner, ***Dalton Trans.***, **2014,** *43***,** 14517-14519.

5. "Iron(II) complexes featuring κ^3- and κ^2-bound PNP pincer ligands - The significance of sterics", M. Glatz, B. Bichler, M. Mastalir, B. Stöger, M. Weil, K. Mereiter, E. Pittenauer, G. Allmaier, L. F. Veiros, and K. Kirchner, ***Dalton Trans.***, **2015, 44**, 281-294.